

Journal of Materials Chemistry A

Accepted Manuscript



This is an *Accepted Manuscript*, which has been through the Royal Society of Chemistry peer review process and has been accepted for publication.

Accepted Manuscripts are published online shortly after acceptance, before technical editing, formatting and proof reading. Using this free service, authors can make their results available to the community, in citable form, before we publish the edited article. We will replace this *Accepted Manuscript* with the edited and formatted *Advance Article* as soon as it is available.

You can find more information about *Accepted Manuscripts* in the [Information for Authors](#).

Please note that technical editing may introduce minor changes to the text and/or graphics, which may alter content. The journal's standard [Terms & Conditions](#) and the [Ethical guidelines](#) still apply. In no event shall the Royal Society of Chemistry be held responsible for any errors or omissions in this *Accepted Manuscript* or any consequences arising from the use of any information it contains.

Recent advances in dye-sensitized semiconductor systems for photocatalytic hydrogen production

Xiaohu Zhang, Tianyou Peng* and Shuaishuai Song

Photocatalytic water splitting by solar light has received tremendous attentions for the production of clean and renewable hydrogen energy from water. Some challenges still remain in improving the solar-to-hydrogen energy conversion efficiency, such as utilizing longer-wavelength photons and enhancing the photocatalytic activity and stability of H₂ production over the semiconducting materials. Dye sensitization, as a successful strategy for extending the spectral responsive region (even to near-IR light) of wide bandgap semiconductors for H₂ production, has been developed more than 30 years, but it is still lack of the corresponding specialized review up till now. This review emphasizes especially the fundamental aspects and the research advances on the heterogeneous dye-sensitized semiconductor suspension systems for visible (and even near-IR) light responsive photocatalytic H₂ production, and the commonly used dyes, semiconductors, co-catalysts and electron donors are systematically discussed. Also, a short perspective on the challenges and new directions in this field is proposed, which would be of great interests in the field of solar fuel conversion.

KEYWORDS: *dye-sensitized semiconductor, photocatalytic hydrogen production, visible light response, photoactivity, apparent quantum yield*

1. Introduction

Among various new energy technologies for supporting the global sustainable development in the future, “solar fuels” production over semiconductor by using inexhaustible solar energy hitting the earth (1.3×10^5 TW), which far exceeds the whole energy consumed by humanity per year,¹ is considered as one of the most promising choice since the pioneering work on the water splitting for H₂ production over TiO₂ photoelectrode was reported in 1972.² Generally, the so-called “solar fuels” production systems mainly mean semiconductor-based photocatalytic systems for H₂ production from water splitting and C-containing fuels (such as methane, methanol, ethanol *etc.*) production from CO₂ reduction.³⁻⁶ Especially, semiconductor-based photocatalytic water splitting systems have received more attentions because of its potential application in the direct production of clean hydrogen energy by using water and light (or ideally sunlight).⁶⁻⁹ The photon energy is converted to chemical energy with concomitant largely positive change in the Gibbs free energy ($+237 \text{ kJ mol}^{-1}$) through the water splitting. This uphill reaction is similar to the photosynthesis of green plants, and thus is regarded as an artificial photosynthesis, which is an attractive and challenging theme in the field of new energy sources.^{5,6}

It is well known that semiconductor has a band structure in which the conduction band (CB) is separated from the valence band (VB) by a bandgap.^{1,3,6-9} The band structure, including the bandgap and the positions of

College of Chemistry and Molecular Sciences, Wuhan University, Wuhan 430072, P R China.

E-mail: typeng@whu.edu.cn; Tel. & Fax: +86-27-6875-2237

VB and CB, is one of the important properties because it determines the light absorption and the redox capabilities of a semiconductor.³ In theory, the photocatalytic reaction processes proceed over semiconductors as shown in Fig. 1. When the energy of incident light is larger than that of bandgap, electrons and holes can be generated in the CB and VB of semiconductor, respectively. These photogenerated carriers may be involved in the following possible processes: 1) migrate to the surface active sites of semiconductor; 2) captured by the defect sites in bulk and/or on the surface of semiconductor, and 3) recombine and release the energy in the form of heat or photon. The last two processes are generally thought as deactivation processes because these photogenerated carriers would not contribute to the surface photocatalytic reactions.³ Namely, an efficient charge separation is one of the most important factors that determine the photoactivity. Only those photogenerated carriers that reached to the semiconductor surface can cause the redox reactions similarly to the electrolysis processes, and thus water molecules are reduced by the electrons to produce H₂ and oxidized by the holes to produce O₂ for water splitting. Although some particular surface sites of a semiconductor can act as active centers themselves (especially for oxidation reaction on oxide semiconductor), efficient photocatalytic reactions proceed only after loading co-catalysts in most cases.^{1,3,6-9}

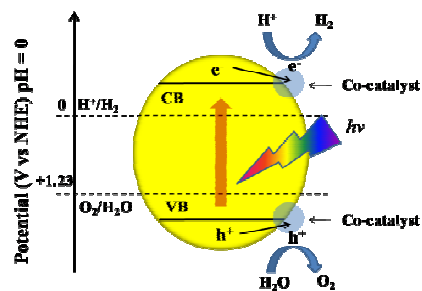


Fig. 1 Schematic illustration of photocatalytic water splitting over semiconducting photocatalyst for H₂ and O₂ production mediated by suitable redox co-catalysts.

For a water splitting reaction, the CB's bottom level of a semiconductor should be more negative than the redox potential of H⁺/H₂ (0 V vs. NHE, pH7.00), while the VB's top level should be more positive than the redox potential of O₂/H₂O (+1.23 V vs. NHE, pH7.00). Nevertheless, an appropriate band structure of photocatalyst (e.g., the bandgap straddles the potentials of water reduction and oxidation) is just a thermodynamic requirement but not a sufficient condition for the water splitting because other factors, such as photoreaction conditions, overpotentials, and the photogenerated carriers' separation/mobility/lifetime, would affect the H₂ production activity from water splitting as well.^{1,3,6-9} For example, the band edges and the phase stability of a semiconductor usually vary with the change of pH environments.⁹ In addition, the crystal structure, crystallinity, particle size, active sites and surface area of a semiconductor also significantly affect the photogenerated carriers' separation, migration, recombination, and surface chemical reactions.³⁻⁹

Since an overall water splitting over semiconductor is a tough uphill reaction with both largely positive change in the Gibbs free energy and difficult 4-electron oxidation of H₂O for O₂ production, an actual photocatalytic procedure for water splitting is usually facing some problems, such as the lack of efficient semiconductors with appropriate band structure and stability, the rapid recombination of the photogenerated carriers, and the easy surface back reaction (SBR) between the evolved H₂ and O₂.⁶⁻⁹ Furthermore, the

4-electron oxidation of H₂O for O₂ production is usually difficult to match with the performance in the 2-electron reduction of H₂O for H₂ production for economically viable solar-to-hydrogen conversion efficiency.⁵ The above problems cause the extremely insufficient visible light utilization and relatively low quantum yield of a water splitting system.

Up till now, the kinds of photocatalysts that are capable of steady overall water splitting through visible-light-driven photocatalytic process are very limited, and the efficiency of this process is still far from reaching industrial viability.^{1,7} To circumvent these problems, electron donor such as methanol (or electron acceptor such as Ag⁺) is often added to the reaction solution to measure the photoactivity for H₂ (or O₂) production.¹ These additives as sacrificial agents can work as an external driving force for the surface chemical reaction and depress the undesirable charge recombination and SBR reactions because the photogenerated holes (or electrons) can be consumed by the sacrificial agents irreversibly and rapidly.^{1,9} Especially, the photocatalytic system containing electron donor for H₂ production is the main stream in the field of water splitting because it can evade the more difficult 4-electron oxidation of H₂O for O₂ production and directly produce the clean hydrogen energy by using water and solar light.⁶⁻⁹ In addition, photoelectrochemical (PEC) route for water splitting can utilize two smaller bandgap semiconductors to absorb a greater portion of the solar spectrum, in which careful alignment of their CB and VB energy positions should be obtained so as to maintain sufficiently large photovoltage for water splitting.⁵ Nevertheless, the major bottleneck of this route is the low photoanodic performance for driving solar water oxidation.^{1,2,5,10,11} It was reported that engineering interfaces in the form of hetero-junctions and surface modifications can overcome the intrinsically limited PEC performance in well-studied photoanode materials such as hematite.^{5,10-12} For instance, Barreca and Fornasiero's group prepared Fe₂O₃-TiO₂ nano-heterostructured photoanodes on FTO glass by the initial plasma enhanced-chemical vapor deposition (PECVD) growth of Fe₂O₃ nanosystems followed by an atomic layer deposition (ALD) of TiO₂ layers, and found that the formed Fe₂O₃-TiO₂ heterojunctions exhibited higher and more stable photoanode activity compared with Fe₂O₃ alone due to the enhanced charge separation and retarded charge recombination.¹¹

Another potential route for solar-to-hydrogen energy conversion is photoreforming of organic precursors, such as biomass extracts/byproducts, into H₂ on oxide semiconductors.¹³⁻¹⁸ Different from photocatalytic and PEC water splitting, the solar energy used during the biomass photoreforming is mainly for overcoming the activation energy of the reaction because it usually is a thermodynamically favorable reaction.^{2,14} In addition, the advantage of H₂ production by the use of representative oxygenated compounds, such as methanol, ethanol, glycerol, and sugars, is energy-saving and eco-friendly as compared to other routes, such as H₂ production by pyrolysis of biomass.^{2,14,16} Anyway, the success of the above photoactivated H₂ production routes, ranging from photocatalytic and PEC water splitting to photoreforming of suitable oxygenateds, depends on the efficient use of solar spectrum and on the identification of active and stable photocatalysts.^{5,13}

Solar spectrum (AM1.5G) consists of three main components in terms of wavelengths: UV rays ($\lambda < 400$ nm), visible light ($400 \text{ nm} > \lambda < 800 \text{ nm}$), and infrared rays ($\lambda > 800 \text{ nm}$), accounting for 4%, 53%, and 43% of the total solar energy, respectively.¹ As the most popular and significant photocatalysts, TiO₂ and SrTiO₃ that are active for overall water splitting have a bandgap energy ($E_g > 3.00 \text{ eV}$), which are too large to absorb visible light;¹⁹⁻²³ while many other visible-light-responsive semiconductors (such as WO₃, BiVO₄, and Fe₂O₃)

are just active for O_2 evolution but not for H_2 production because of their CB edges are more positive than the H_2 evolution potential.^{1,24,25} Furthermore, some non-oxide materials (such as chalcogenides, (oxy)nitrides and oxysulphides) with narrow bandgap and suitable band levels are not an ideal photocatalyst for water splitting due to their stability and/or photocorrosion problems.^{1,5,7} To more effectively utilize the visible light of solar light, many strategies, such as element doping,^{3,9,20,26} exploiting narrow bandgap semiconductors or solid solutions,^{7,19,20-23,28} composite with narrow bandgap semiconductors,^{7,9,27,28} and dye sensitization,^{3,5-7,9} have been developed to improve the visible-light-driven photoactivity. Dye sensitization as an effective strategy for utilizing visible light has been studied extensively in dye-sensitized solar cells (DSSCs),^{29,30} but the H_2 production activity based on dye-sensitized semiconductors is still insufficient, and thus there is a long way to go for improving the solar-to-hydrogen conversion efficiency and stability.^{6,7,9,31-38}

In the early 1980s, Grätzel summarized three suitable light-harvesting units (Fig. 2) which serve to capture photons, convert their energy into chemical potential, and use it to split water.³³ In which, Case (a) represents a two-component system containing a sensitizer (S) and an electron relay (R). Light promotes electron transfer from S to R to produce the energy-rich radical ions (S^+) and (R^-). In several examples, the reduced relay (R^-) and oxidized sensitizer (S^+) are thermodynamically capable of water splitting.³⁴⁻³⁷ In Case (b), the sensitizer is adsorbed onto a colloidal semiconductor without electron relay. The excited sensitizer injects an electron into CB of semiconductor where it is channeled to a co-catalyst for H_2 production. A second co-catalyst, co-deposited onto the colloidal particle, mediates O_2 production from S^+ and H_2O whereby the original form of the sensitizer is regenerated.³⁸ In Case (c), an electron-hole pair is formed through bandgap excitation as shown in Fig. 1, and the photogenerated electrons contribute H_2 production while the holes give rise to O_2 evolution from water mediated by suitable co-catalyst. The light-harvesting units delineated in Case (b) and (c) have the advantage over the simple sensitizer-relay pair mentioned in Case (a) that light-induced charge separation and redox catalysis are concentrated in a very small and confined reaction space, and thus all the water splitting events can take place on a single semiconductor particle, eliminating the need for bulk phase diffusion of the reactants.³³ The light-harvesting unit of Case (b) has further advantage than that of Case (c), that is the tunable of light absorption region and ability of various adsorbed sensitizers.³³

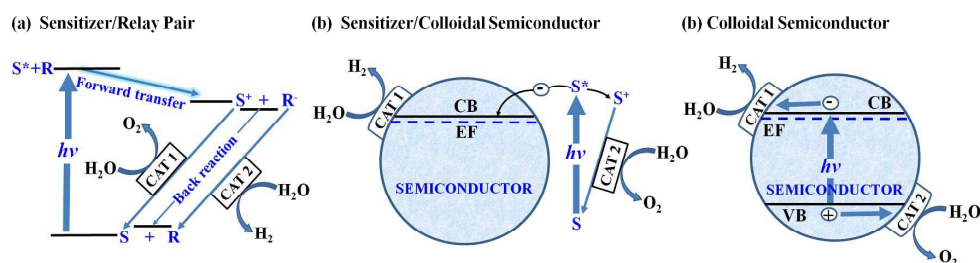


Fig. 2 Schematic illustration of light-harvesting units employed in photochemical water splitting devices. Figures reproduced with permission from ref. 33. Copyright 1981, American Chemical Society.

In 1980, Grätzel's group reported a bifunctional redox co-catalyst, composed of Pt and RuO_2 co-deposited on colloidal Nb-doped TiO_2 particles, is a highly potent mediator for water splitting by visible light in the presence of $Ru(bpy)_3^{2+}$ ($bpy = 2,2'$ -bipyridine) and methyl viologen (MV^{2+}),³⁷ in which MV^{2+} is reduced after $Ru(bpy)_3^{2+}$ is excited by visible light and then the electron is injected from the reduced MV^{2+} into TiO_2 's CB.

To rationalize the high activity of this photoredox system, they proposed a mechanism involving species adsorbed on TiO₂ surface, which leads them to explore sensitizers with an enhanced affinity through suitable functionalization for adsorption at the particle/water interface. In 1981, they described the same bifunctional redox co-catalysts composed of RuO₂ and Pt co-loaded on colloidal Nb-doped TiO₂ particles is capable of splitting water into H₂ and O₂ under visible light without MV²⁺ as electron relay, and the other component is just a sensitizer (amphiphilic surfactant derivatives of Ru(bpy)₃²⁺, see Fig. 3).³⁸ Based on their experimental observation, a photochemical mechanism was proposed as shown in Fig. 2b, that is, adsorption of the sensitizer at the particle/water interface and the excitation of the sensitizer is followed by electron injection into TiO₂'s CB. Among which, the mono C₁₂-substituted Ru-complex (Ru(bpy)₃²⁺•C₁₂) sensitized Pt/TiO₂/RuO₂ exhibits an optimal H₂ production activity of 1.5 mL h⁻¹ (O₂ remained in stoichiometric ratio to the H₂ produced) after a short induction period, which gives a quantum yield of ~5% for H₂ production under λ ≥ 400 nm light irradiation.³⁸ Also, this work can be thought as the pioneering work on the photocatalytic water splitting over dye-sensitized semiconductor.

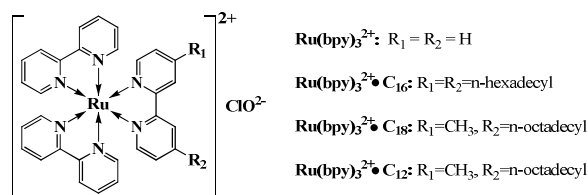


Fig. 3 Molecular structures of amphiphilic surfactant derivatives of Ru(bpy)₃²⁺ in the 1st work of water splitting over dye-sensitized semiconductor (Pt/TiO₂/RuO₂). Figure reproduced with permission from ref. 38. Copyright 1981, Nature Publishing Group.

Except for the above surfactant derivatives of Ru(bpy)₃²⁺, many other metal complexes and organic dyes, such as Ru(dcbpy)₃²⁺ (dcbpy = 4,4'-dicarboxy-2,2'-bipyridine), porphyrins, xanthenes, and even some D-π-A organic dyes, have also been utilized for H₂ production from a dye-sensitized semiconductor system. Up till now, dye sensitization has become an efficient route to improve the spectral responsive capability and visible-light-induced activity of wide bandgap semiconductors. However, a systemic review on dye-sensitized semiconductors for visible-light-induced H₂ production is still neglected to the best of our knowledge though there are numerous and informative reviews on the photocatalytic H₂ production performance of semiconductor suspension systems,^{1,3,7-9,19-23,33,39-43} homogeneous dye-sensitized systems,^{33,44-46} and PEC water splitting systems.^{1,5,6,31,47,48} This review will focus on the fundamental aspects of the heterogeneous dye-sensitized semiconductor systems for visible (and even near-IR) light driven H₂ production. Firstly, the basic working principles and systems of dye-sensitized semiconductor for heterogeneous photocatalytic H₂ production are introduced on the basis of thermodynamics, and then the criteria for evaluating photocatalytic activity for H₂ production are described. Secondly, the recent advances in the dye types and the corresponding visible-light-driven H₂ production performance over dye-sensitized semiconductors are reviewed. In addition, some new strategies for extending the spectral responsive region for H₂ production are described. Thirdly, the progress in coupling of various components in a dye-sensitized photocatalytic system, including rational nano-organization controls, energy level matching, co-catalyst and electron donor optimization, which could

affect the stability, charge transfer kinetics and mechanism of the photocatalytic application, are specifically mentioned so as to give an overview of the various problems and solutions. Finally, the future challenges and the most attractive opportunities for research advancements in these fields are also briefly explored.

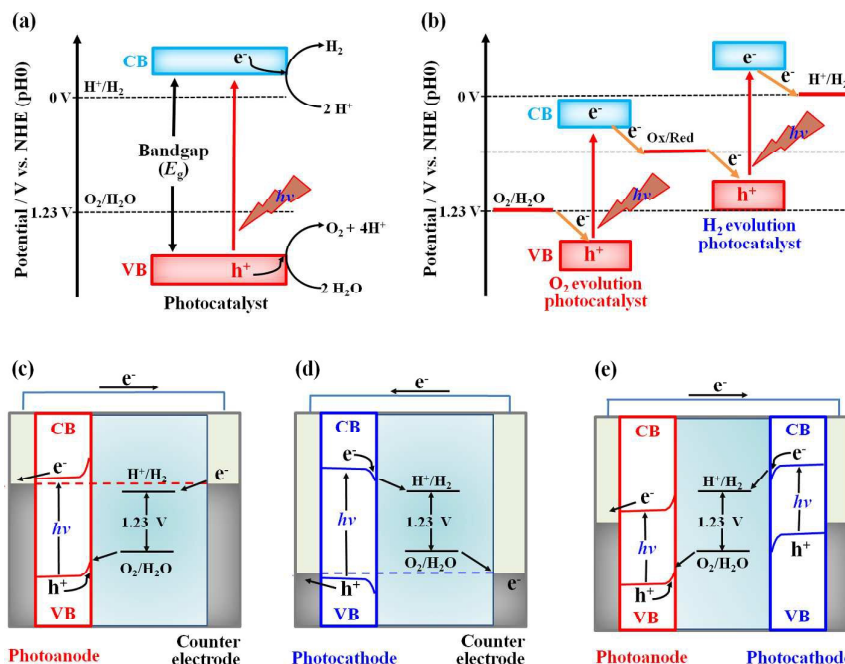


Fig. 4 Energy diagrams of photocatalytic water splitting systems based on (a) one-step excitation and (b) two-step excitation (Z-scheme); and PEC water splitting systems using (c) photoanode, (d) photocathode, and (e) photoanode/photocathode in tandem configuration. Figures reproduced with permission from ref. 1. Copyright 2014, The Royal Society of Chemistry.

2. Basic principles of dye-sensitized semiconductors

2.1 Photocatalytic H₂ production systems

In 2014, Domen's group has summarized three common photocatalytic water splitting systems (Fig. 4), that is, one-step excitation powdered photocatalyst suspension system, two-step excitation powdered photocatalyst suspension system (the so-called Z-scheme), and semiconductor electrode-based PEC system.¹ For the one-step excitation system (Fig. 4a), H₂ is readily produced when sun shines at photocatalyst powders dispersed in water (see Fig. 1). The disadvantage of this water splitting system is the necessity of separation of the produced H₂ from O₂.¹ This problem can be overcome by using a Z-scheme system (Fig. 4b), where two semiconductors can be connected in series with reversible redox shuttles. In this case, the reduction of water to H₂ and oxidation of reduced redox mediators occur on one photocatalyst concurrently with the reduction of oxidized redox mediators and oxidation of water to O₂ on the other photocatalyst.

PEC water splitting system should be more attractive because of H₂ and O₂ can produce at two different electrodes in one cell or separate cells to avoid the SBR of produced H₂ and O₂. If the Fermi level of a semiconductor is more negative (positive) than the reduction potential of an electrolyte solution, the electrolyte solution can accept (donate) electrons from (to) the semiconductor. Since the density of electrons in a semiconductor is finite and the potentials of the band positions at the interfaces can be assumed to be

pinned, the electron transfer would cause band bending, and the electric field induced by the space charge layer plays an important role in the necessary charge separation.¹ Typically, a n-type/p-type semiconductor can act as photoanode/photocathode respectively and a water splitting cell can be fabricated by accompanying with a counter electrode as shown in Fig. 4c and 4d. Alternatively, a photoanode and a photocathode can be connected in tandem as in Z-scheme water splitting cell (Fig. 4e).¹ Among which, the powdered photocatalyst suspension system is the most popular one adopted by numerous researchers because of the simplicity and advantage for large-scale application. Especially, the photocatalyst suspension system containing electron donor for H₂ production is the main trend in the field of photocatalytic water splitting because of its simplicity, wider varieties of semiconductors or composites, and higher solar-to-hydrogen conversion efficiency than that of the Z-scheme and PEC systems.^{7-9,19-23}

2.2 Photocatalytic H₂ production principles of dye-sensitized semiconductors

Generally, dye-sensitized semiconductor can be used in all water splitting systems mentioned above. For example, the first report on surfactant derivatives of Ru(bpy)₃²⁺-sensitized Pt/TiO₂/RuO₂ is a one-step excitation system;³⁸ the two-step excitation between coumarin-(NKX-2311, 2587, 2677, 2697) and carbazole-based (MK-1, MK-2) dye-sensitized Pt/H₄Nb₆O₁₇ and Pt/WO₃/IrO₂ in the presence of a I₃⁻/I⁻ shuttle is a Z-scheme system;³² while a systemic review on the designing and development of photoanodes for dye-sensitized PEC systems is given by Mallouk's group.³¹ Although many efforts have been made to promote the photoactivity of water splitting, the desired synergism for H₂ and O₂ production in one dye-sensitized system is still far from the high solar-to-hydrogen conversion efficiency.⁷ For example, the two-step excitation between NKX-2677-Pt/H₄Nb₆O₁₇ and Pt/WO₃/IrO₂ just gives a quantum yield of ~0.05% for H₂ production at 480 nm;³² the one-step excitation of Ru(bpy)₃²⁺•C₁₂-sensitized Pt/TiO₂/RuO₂ exhibits a quantum yield of ~5% under λ>400 nm light irradiation.³⁸ All these are far from the target suggested by Kudo,⁷ that is, the efficiency of water splitting into H₂ and O₂ is 30% in terms of a quantum yield at 600 nm, which would give ~5% of solar-to-hydrogen conversion efficiency.⁷

It is well known that DSSCs use a redox shuttle in organic solvent to complete the PEC circuit for the photovoltaic conversion.^{29,30} If the dye is instead coupled to a water oxidation co-catalyst, water would act as an electron source for regenerating the oxidized dye, in which the photoanode of the DSSCs would oxidize water, and proton reduction to H₂ occurs at the cathode. Since the photovoltage generated by DSSCs is not sufficient to drive overall water splitting, an external bias voltage must be applied.^{1,31} Although these dye-sensitized photoanodes could be coupled to complementary photocathode to evoke water splitting in an 8-photon, 4-electron process that is mimetic of the two coupled photosystems in plant photosynthesis, the current performance of these systems is very poor (with steady state photocurrents corresponding to only 2-3% quantum yield in visible light).³¹ On the contrary, photocatalytic H₂ production (other than overall water splitting) over dye-sensitized semiconductor suspensions containing sacrificial agent exhibited higher apparent quantum yield (AQY) than that of Z-scheme and PEC systems.^{1,49,50} For example, Pal's group reported a high AQY of ~50% over a thiophenothiazine-based dye (UP3) sensitized Pt/TiO₂ (see Fig. 5) with 10% triethanolamine (TEOA) as electron donor under λ≥400 nm light irradiation.⁵⁰ Therefore, dye-sensitized semiconductor suspension system containing sacrificial agent for H₂ production is widely investigated.^{9,49,50}

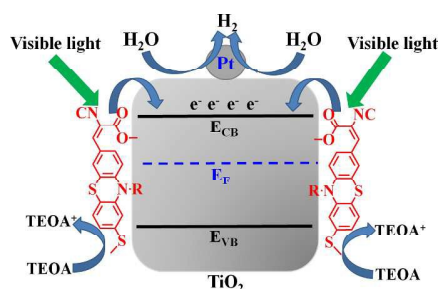


Fig. 5 Illustration of the visible-light-driven H_2 production over thiophenothiazine-based dye-sensitized Pt/TiO₂. Figure reproduced with permission from ref. 50. Copyright 2015, The Royal Society of Chemistry.

Fig. 6 illustrates the typical principle of a dye-sensitized semiconductor for visible-light-induced H_2 production from water reduction half-reaction.⁴⁹ There are four main components in this system: dye molecules (adsorbed on semiconductor), semiconductor (as electron relay and reaction matrix), H_2 production co-catalyst (such as Pt, commonly co-loaded on semiconductor) and electron donor. There are several basic procedures: 1) the excitation of dye molecules by the incident light followed by the photogenerated electron transition from its highest occupied molecular orbital (HOMO) to the lowest unoccupied molecular orbital (LUMO); 2) the injection of photogenerated electrons from the dye's LUMO to the semiconductor's CB; 3) the CB electrons further migrate to the semiconductor surface and reduce water for H_2 production; 4) the regeneration of dye molecules for cyclic utilization through sacrificing of electron donor. Among which, the H_2 production procedure commonly needs the loading of co-catalyst such as Pt, which can act as active sites, create a Schottky barrier as an efficient electron trap for accelerating the charge separation, and debase the overpotential loss for H_2 evolution.⁴⁹

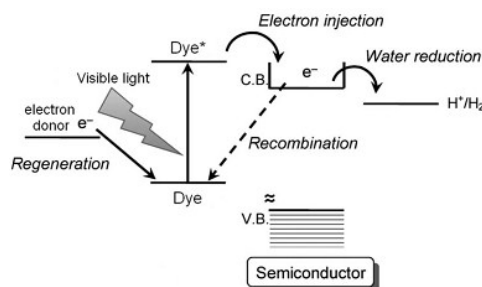


Fig. 6 Typical principle of a dye-sensitized semiconductor for visible-light-induced photocatalytic H_2 production from water reduction half-reaction. Figure reproduced with permission from ref. 49. Copyright 2008, American Chemical Society.

Expect for the above expectant positive processes, some recombination reactions (such as the self-recombination of the photogenerated carriers and the recombination of electrons coming from semiconductor's CB and the oxidation state of dye molecules after the excitation) and harmful reactions (such as the degradation of dye itself) will accompany with the whole photoreaction processes, and thus significantly affect the photocatalytic activity and stability for H_2 production in a dye-sensitized semiconductor system. Therefore, there are some basic prerequisites for an efficient H_2 production: 1) dye molecules must possess wide spectral absorption region (ideally whole vis/near-IR light region) and high

molar extinction coefficient; 2) the dye's LUMO must be more negative than the semiconductor's CB and its HOMO must be more positive than the sacrificial reagent's redox potential; 3) dye molecules should also undergo long-term visible light irradiation with considerable stability; 4) the cost of the dye must be taken into consideration when exploiting and designing a dye for solar energy conversion. Finally, the kinds of semiconductor, co-catalyst and electron donor, which are very important for the photogenerated carriers' separation and transfer, should also be considered in a photocatalytic system.

2.3 Performance evaluation of dye-sensitized semiconductor

Except for the above basic principles, there are some important technical parameters, such as photoactivity and its long-term stability, apparent quantum yield (AQY) and turnover number (TON), to evaluate the performance of various photocatalytic H₂ production systems.^{1,7,9} Among which, photoactivity for H₂ production can be directly reflected by the H₂ production amount in a special experimental condition and commonly signed as $\mu\text{mol h}^{-1}$ or $\mu\text{mol h}^{-1} \text{g}_{\text{catalyst}}^{-1}$. As a stability index, time course for H₂ production of photocatalytic system is also important for an efficient dye-sensitized semiconductor. Nevertheless, the photoactivity marked as $\mu\text{mol h}^{-1}$ or $\mu\text{mol h}^{-1} \text{g}_{\text{catalyst}}^{-1}$ usually is not very meaningful for the performance comparison among different research groups because of no acknowledged experimental setup and methods in the field of photocatalytic H₂ production up till now. Therefore, quantum yield (QY) becomes an important, acceptable and acknowledged index. Typically, the calculated QY from the H₂ production amount just represents an AQY because the real photon number absorbed by the photocatalyst is difficult to be measured in a common aqueous suspension system. Since the absorbed photon number is usually smaller than that of incident light, AQY is usually smaller than the real QY. Sometimes, solar energy conversion efficiency (ECE) and turnover number (TON) are also utilized in literatures to evaluate the photocatalytic performance. The above QY, AQY, ECE, and TON can be defined as eqns. (1-4).^{1,7,9}

$$\text{QY (\%)} = \frac{\text{Number of reacted electrons}}{\text{Number of absorbed photons}} \times 100\% \quad (1)$$

$$\text{AQY (\%)} = \frac{\text{Number of reacted electrons}}{\text{Number of incident photons}} \times 100\% \quad (2)$$

$$\text{ECE (\%)} = \frac{\text{Output energy of hydrogen evolved}}{\text{Energy of incident solar light}} \times 100\% \quad (3)$$

$$\text{TON} = \frac{2 \times \text{number of H}_2 \text{ molecules evolved}}{\text{Number of dye molecules utilized}} \quad (4)$$

3. An overview of dye types in dye-sensitized semiconductors

3.1 Dye types

Up till now, the commonly used dyes for the photocatalytic H₂ production can be roughly divided into metal complexes, organic dyes and quantum dots. Among which, metal complexes can be further divided into Ru-complexes and the other transition metal complexes. Although quantum dots (mainly InP, CdS, CdSe, CdTe, PbS *etc.*) are widely utilized in DSSCs,⁵¹⁻⁵³ and PEC water splitting,^{54,55} there is no report on the quantum dot-sensitized semiconductor suspension system for photocatalytic H₂ production. Recently, carbon

quantum dots (CQDs) and their sensitized semiconductors have garnered much interest in photocatalytic pollutant degradation and water splitting, but the corresponding investigations are insufficient and the ECE is far from satisfactory.⁵⁶⁻⁵⁹ Alternatively, those commonly used dyes can also be divided into three main types according to their spectral responsive regions, that is, visible-light-responsive, near-IR-light-responsive and vis/near-IR-light-responsive dyes (IR-light-responsive dye has not been utilized in dye-sensitized H₂ production). Currently, most dyes such as Ru-complexes, metal porphyrins, metal-free organic dyes can just response visible light in the region of ~400-600 nm,^{32,60-62} while a few dyes such as squaraine dye (VJ-S) can response the red/near-IR light near to ~800 nm.⁶³ Currently, Ru-complexes are one of the most popular dyes in dye-sensitized photocatalytic H₂ production systems, and metal-free organic dyes become the current trend because of their variety, low cost, tunable structure and spectral responsive ability. Therefore, Ru-complexes, other metal complexes and metal-free organic dyes are focused in the following sections.

3.2 Ru-complexes

(1) **Mononuclear Ru-complexes.** Up till now, Ru-complexes mainly means Ru-bi(poly)pyridyl complexes or its analogues, and mononuclear Ru-complexes are still one of the most popular dyes in dye-sensitized photocatalytic H₂ production systems since the early reports.^{33-38,64-103} The relative reports are partly listed in Table 1, and the molecular structures and literature symbols of typical Ru-complexes used for H₂ production are shown in Fig. 7.

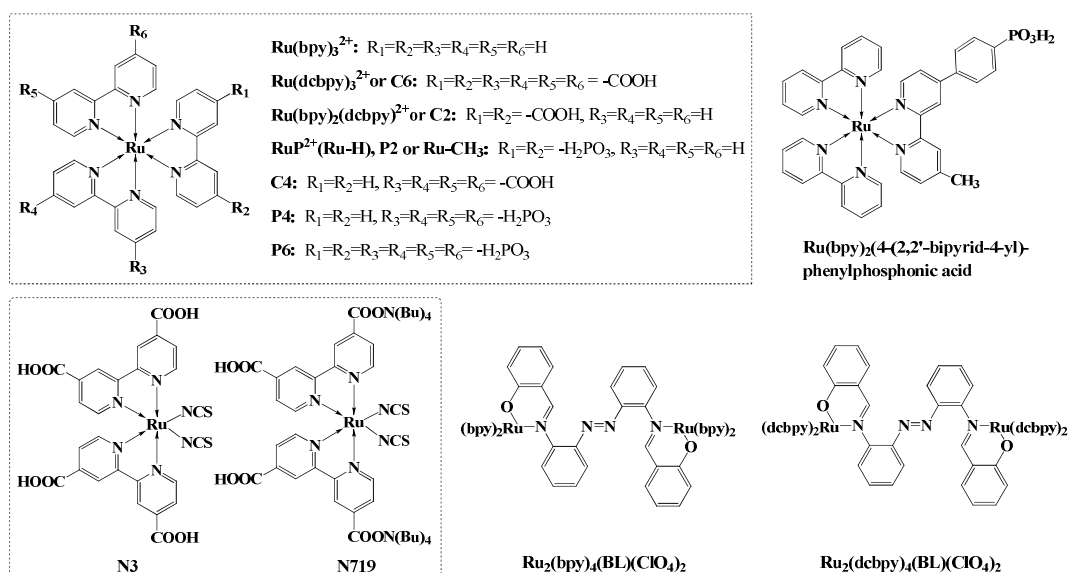


Fig. 7 Basic molecular structures of typical Ru-complexes used in the dye-sensitized semiconductor suspension systems for photocatalytic H₂ production.

As mentioned above, Grätzel's group reported the first dye-sensitized semiconductor for water splitting by using surfactant derivatives of Ru(bpy)₃²⁺ sensitized Pt/TiO₂/RuO₂ based on the mechanism shown in Fig. 2b.³⁸ Thereafter, some modified Ru(bpy)₃²⁺, such as Ru(dcbpy)₃²⁺, Ru(bpy)₂(4,4'-tridecyl-2,2'-bpy)²⁺, Ru(bpym)₃²⁺ (bpym = trisbipirimidine), Ru(dcbpy)₂(dpq)²⁺ (dpq = 2,3-bis-(2'-pyridyl)-quinoxaline), Ru(bpy)₂(4,4'-(PO₃H₂)₂bpy)²⁺, and even those commonly used Ru-complex dyes (N3 (*cis*-Ru(dcbpy)₂(NCS)₂), N719

((n-Bu₄N)₂-*cis*-Ru(dcbpy)₂(SCN)₂), and Z907 (*cis*-Ru(dcbpy)(4,4'-(dinonyl)bpy)(SCN)₂) in DSSCs, were utilized to sensitize TiO₂ for H₂ production.^{60,61,64-95} According to whether containing terminal group or not (Fig. 7), those Ru-complexes can be divided into three types, that is, Ru(bpy)₃²⁺ derivatives without terminal group,^{33-38,49,64-70} with carboxyl terminal group,^{61,71-87} and with phosphonate terminal group.^{60,88-95}

The adsorption of Ru(bpy)₃²⁺ on semiconductor results in charge injection from the metal-to-ligand charge transfer (MLCT) excited state of dye, and then causing H₂ production.^{28,49} Since the dye excited state is typically too short-lived to allow for diffusion of the dye molecules to the surface, the essential requirement for an efficient H₂ production is strong adsorption of sensitizer molecules onto semiconductor.^{49,71} Therefore, Furlong and co-workers used Ru(dcbpy)₃²⁺ bearing carboxyl anchoring groups on Pt/TiO₂ with ethylenediaminetetraacetic acid (EDTA) as sacrificial electron donor, and found that the acidity of the powdered suspension affect the dye adsorption on TiO₂, the sensitization requires the adsorption of sensitizer in addition to favorable redox potentials for electron injection from dye into TiO₂'s CB.⁷¹ Thereafter, Ru-complex dyes bearing carboxyl as anchoring groups are extensively used to sensitize platinized mesoporous TiO₂, Al₂O₃ overcoated TiO₂, niobates, titanates, titanoniobates, Ti-MCM-48, zeolite/TiO₂(or Nb₂O₅) composites, and reduced graphene oxide (RGO).⁷²⁻⁸⁸

In 1997, Mallouk's group firstly used Ru(bpy)₂(4,4'-(PO₃H₂)₂bpy)²⁺ (RuP²⁺) with phosphonate terminal group sensitized internally platinized K₄Nb₆O₁₇, and found that the strong bond between the surface and the phosphonate group of RuP²⁺ allows one to adsorb other surface species, which decrease the rate of the back electron transfer reaction between CB electrons and I₃.⁸⁹ In 2009, the same group found that RuP²⁺ with phosphonate terminal group, which is anchored by a covalent linkage to the hexaniobate nanoscrolls (NS-H₄Nb₆O₁₇) and acid-restacked calcium niobate nanosheets (R-HCa₂Nb₃O₁₀) surface, functions more efficiently than the electrostatically bound Ru(bpy)₃²⁺, because of more efficient electron injection from the excited dye to NS-H₄Nb₆O₁₇. RuP²⁺-sensitized NS-H₄Nb₆O₁₇ and R-HCa₂Nb₃O₁₀ both produce H₂ photocatalytically using EDTA as electron donor under λ≥420 nm light irradiation.⁹⁰ Choi's group investigated the effects of anchoring groups (carboxylate (c-RuL₃: C2, C4, C6) vs. phosphonate (p-RuL₃: P2, P4, P6), see Fig. 7) on the photoactivity of Ru-complex dye-sensitized TiO₂ suspensions,^{97,98} and inferred that the adsorption of p-RuL₃ on TiO₂ is strong enough not to be hampered by the presence of EDTA, whereas that of c-RuL₃ is significantly inhibited. As a result, p-RuL₃-sensitized TiO₂ exhibited much higher activity (even an AQY of 28% under λ≥420 nm light irradiation over P2-Pt/TiO₂ was obtained) for the H₂ production than c-RuL₃-sensitized TiO₂, although the visible light absorbing capabilities are comparable among those Ru-complexes with carboxylate and phosphonate as anchoring groups.^{97,98}

Since the above chemical anchoring through carboxylate or phosphonate is not sufficiently stable in an aquatic environment,⁹⁹⁻¹⁰² Choi's group reported an alternative approach to attaching Ru-complex molecules at the TiO₂/H₂O interface as shown in Fig. 8.⁹⁹ TiO₂ particle surfaces are coated with perfluorosulfonate polymer (Nafion, cation-exchange resin), and then Ru(bpy)₃²⁺ as a cationic form are bound within the nafion (Nf) layer through electrostatic attraction. The visible-light-induced H₂ production activity on Ru(bpy)₃²⁺-Nf/TiO₂/Pt is far more efficient than that of Ru(dcbpy)₃-TiO₂/Pt through chemical tight interaction, and exhibits an AQY of 2.60% under λ≥420 nm light irradiation. The roles of the Nafion layer on TiO₂ are proposed to be twofold: providing binding sites for cationic dye and enhancing the local activity of protons in

the surface region.⁹⁹ Kruth and co-workers adopted a new strategy to improve the stability of the Ru-complex (N3) with carboxyl anchoring group on TiO₂ surface, that is, the encapsulation of the N3/TiO₂ assembly in an amino-group-containing polyallylamine layer anchored to TiO₂, which showed a stable visible-light-induced H₂ production activity from a slurry reactor over a period of several days.¹⁰¹

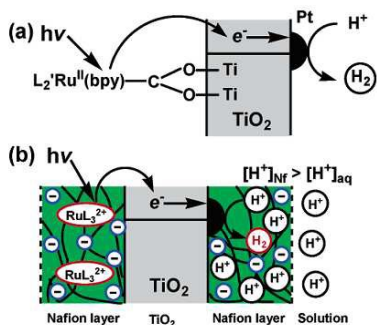


Fig. 8 Two alternative approaches for visible-light-induced H₂ production in (a) Ru(dcbpy)₃-TiO₂ and (b) Ru(bpy)₃²⁺-Nf/TiO₂ systems. Figures reproduced with permission from ref. 99. Copyright 2006, American Chemical Society.

The interaction between Ru-complex and semiconductor can also be covalently binding through coordination of Ru(bpy)₂Cl₂ with pyridine (py) covalently functionalized graphene (G).¹⁰² The obtained Ru(bpy)₂(py)Cl/G/Pt evoked fast photoinduced electron transfer from Ru(bpy)₂(py)Cl moiety to Pt/G sheet, and also demonstrates remarkable enhanced photoactivity and sufficient stability for H₂ production.¹⁰² Furthermore, Matsuoka's group reported Ru-complex incorporated Ti-based metal-organic frameworks (MOFs) by employing Ru(tpy)₂ complex (tpy = bis(4'-(4-carboxyphenyl)-terpyridine) as an organic linker, and the resulted Ti-MOF-Ru(tpy)₂ exhibits photoactivity for H₂ production from sacrificial electron donor solution under visible light irradiation at wavelengths up to 620 nm.¹⁰³ On the contrary, Wang's group demonstrated a visible-light-derived H₂ production system based on Ru(dcbpy)₃ noncovalent functionalized RGO nanocomposite.⁷⁹ After Pt nanoparticles (NPs) were deposited on Ru(dcbpy)₃-RGO sheets, the activity was improved greatly compared with those of Ru(dcbpy)₃-sensitized Pt/RGO nanocomposite. The enhancement of the photocatalytic performance was attributed to the dye molecules contacting directly with RGO, which served not only as an excellent supporting matrix for anchoring the dye molecules but also as a superior electron mediator to adjust electron transfer.⁷⁹

(2) Binuclear Ru-complexes. Amadelli and co-workers have found that simple molecular devices that couple the functions of a sensitizer (surface binding and electron injection) and an antenna (intramolecular energy transfer from high absorbing chromophoric groups) can be attained by suitable choosing molecular components and appropriate synthetic assembly.¹⁰⁴ It means that the use of molecules with "antenna-sensitizer" structure may be a viable strategy to overcome the problems of light harvesting in the dye-sensitized systems. By using binuclear Ru-complex (Ru₂(bpy)₄L₁-PF₆) and mononuclear ones (Ru(bpy)₂(him)₂-NO₃ and N719) (see Fig. 7) as sensitizer of Pt/TiO₂, the present authors revealed that the best photosensitization of Ru₂(bpy)₄L₁-PF₆ is mainly caused by its largest conjugation system, the wider visible responsive region stemmed from the "antenna effect" with multipath electron transfer (MLCT and MMCT)

processes. Simultaneously, it was found that the loosely attached dyes ($\text{Ru}_2(\text{bpy})_4\text{L}_1\text{-PF}_6$ and $\text{Ru}(\text{bpy})_2(\text{him})_2\text{-NO}_3$) without anchoring group possess higher activity for H_2 production than the tightly linked Ru-complex (N719) with carboxyl as anchoring group.^{105,106} Accordingly, a “dynamic equilibrium” hypothesis was proposed, that is, the dynamic equilibrium between the linkage of the ground state dye with TiO_2 and the divorce of the oxidation state dye from the TiO_2 surface plays a crucial role in the photosensitization behavior as shown in Fig. 9.^{105,106} The multipath electron transfer processes in binuclear Ru-complex with “antenna-sensitizer” structure and the loosely attached dye for restraining the charge recombination through “dynamic equilibrium” would be good choice on the dye molecule design. Thereafter, a more efficient binuclear $\text{Ru}_2(\text{bpy})_4(\text{BL})(\text{ClO}_4)_2$ ($\text{BL} = 2,2'-((1\text{E},1'\text{E})-(((\text{E})\text{-diazene-1,2-diyl-bis}(2,1\text{-phenylene))\text{-bis}(azanylylidene))\text{-bis}(methanylylidene)))$, see Fig. 7) is prepared and utilized to sensitize TiO_2 for H_2 production according to the above “antenna-sensitizer” and “dynamic equilibrium” concepts. It was found that the corresponding dye-sensitized TiO_2 suspension without Pt loading shows a high AQY of 16.8% (at 420 nm) and 7.3% (at 475 nm) with a considerable stability though the understanding of the real mechanism on this type of binuclear Ru-complex dyes is still insufficient.^{107,108}

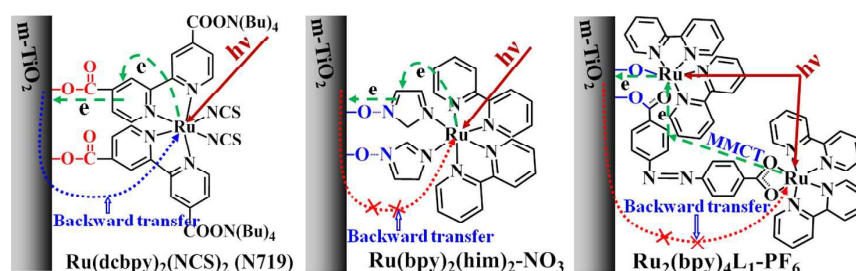


Fig. 9 Photoinduced electron transfer cycle in the three types of dye-sensitized Pt/ TiO_2 nanoparticles. Figure reproduced with permission from ref. 106. Copyright 2008, Elsevier.

On the whole, Ru-complexes possess excellent visible light absorption ability in the region of 400-600 nm, and usually exhibit satisfactory photosensitization. Among those $\text{Ru}(\text{bpy})_3^{2+}$ derivatives, the bpy ligands have been typically functionalized with $-\text{COOH}$ or $-\text{PO}_3\text{H}_2$ group(s) to anchor Ru-complex on semiconductor through chemical linkages, in which dye molecules indicate dominance of the electron injection process in deactivating the excited sensitizer.⁸⁸ Nevertheless, such chemical anchoring is not sufficiently stable in an aquatic environment, and can be prepared only in the acidic pH region.^{99,100} Obviously, photoactivity of Ru-complex dye-sensitized semiconductors is strongly affected by the attachment modes between the dye and semiconductor, and the co-existing species (such as electron donor and co-catalyst) in the suspension systems, which dominate the charge generation, separation, transfer and recombination. Therefore, there are several directions for the further development of Ru-complex dyes: 1) further optimization of the dye attachment modes with semiconductor through suitable structure designing so as to obtain more efficient and stable H_2 production system; 2) beyond the attachment functionality, ligand modification can be used to tune the redox and spectroscopic properties of the sensitizer so as to construct high performance Ru-based dyes; 3) the most important point is taken some strategies, such as using dye co-sensitization, coupling multiple photoactive metal centers based on the “antenna-sensitizer” concept, to extend and increase absorption in the visible region. Finally, the factors influencing the light harvesting, the charge separation/recombination, and the

interaction among dye/semiconductor/electron donor should be further clarified so as to deeply understand the photochemical behavior and sensitization mechanism of Ru-complexes on semiconductors.

Table 1 Summary of Ru-complex-sensitized semiconductors for photocatalytic H₂ production

Catalyst	Reaction condition	H ₂ production activity	AQY/%	Ref.
Ru(bpy) ₃ ²⁺ •C ₁₂ -Pt/TiO ₂ /RuO ₂	λ≥400 nm, 50 μM dye, pH4.50	1.5 mL h ⁻¹	5.0%	38
Ru(bpy) ₃ ²⁺ -Pt/NS-K ₄ Nb ₄ O ₁₇	λ≥420 nm, 50 μM dye, 10 mM EDTA, pH5.50	~4.5 μmol h ⁻¹	10.5% at λ=450 nm	49
Ru[(4,4'-X ₂ -bpy) ₂ (4,4'-(CH ₂ PO ₃ H ₂) ₂ -bpy)]-HCa _{2-x} Sr _x Nb ₃ O ₁₀ , HCa ₂ Nb _{3-y} Ta _y O ₁₀	λ=420 nm, 10 mM EDTA, pH5.50	~60 μmol h ⁻¹ (Ru-CH ₃ -HCa ₂ Nb ₃ O ₁₀)	10% at λ=460 nm	60
Ru(dcbpy) ₃ ²⁺ or SnP-TiO ₂ /Pt	λ≥420 nm, 50 μM dye, 10 mM EDTA	~20 μmol h ⁻¹	--	61
Ru(bpy) ₃ ²⁺ -Pt/TiO ₂ /RuO ₂	λ≥400 nm, MV ²⁺ , 0.2 mM dye, pH 3.00	0.03 mL h ⁻¹	--	64
Ru(bpy) ₂ (4,4'-tridecyl-2,2'-bpy) ²⁺ -RuO ₂ /TiO ₂	λ≥435 nm, 0.10 mM dye, 20 mM EDTA	0.80-1.08 mL h ⁻¹	--	65
Ru(bpy) ₃ ²⁺ -Pt/SnO ₂ /RuO ₂	full spectrum, 37.5 μM dye, EDTA	1.23 mL h ⁻¹	2.4%	66
Ru(bpy) ₃ ²⁺ or Ru(bpym) ₃ ²⁺ -Pt/TiO ₂	λ≥420 nm, 1.0 mM dye, EDTA	80.1 μL h ⁻¹ (Ru(bpym) ₃)	--	67
Ru(bpy) ₃ ²⁺ , EY or CuPc-TiO ₂ /RuO ₂ -MV ²⁺	Sunlight, 6% MeOH	~60 (Ru(bpy) ₃ ²⁺), 70 (CuPc), or 58 (EY) μmol h ⁻¹	--	68
[Ru(bpy) ₃ ²⁺] _{0.03} -Ti _{1.83} O ₄ -MV ²⁺	λ≥400 nm, 10.2% dye, 0.2 mM colloidal Pt, 20 mM EDTA	71.5 μmol h ⁻¹	--	69
Ru(bpy) ₃ ²⁺ /GO	λ=532 nm laser, 20vol% CH ₃ OH	~2 μmol h ⁻¹	--	70
Ru(dcbpy) ₃ ²⁺ -Pt/TiO ₂	λ≥420 nm, 0.1 mM dye, 1 mM EDTA (or TEOA)	1.4 (EDTA), 0.56×10 ⁻⁷ (TEOA) M min ⁻¹	--	71
Ru(dcbpy) ₃ ²⁺ -Pt/K _{4-x} H _x Nb ₆ O ₁₇ •nH ₂ O	λ=450±50 nm, 5×10 ⁻⁷ μmol g ⁻¹ dye, 50 mM KI, pH3.00	~2.5 μmol in 1000 min	Initial 0.3%	72
Ru(dcbpy) ₃ ²⁺ -Pt/ K _{0.80} Ti _{1.71} Li _{0.29} O _{3.97}	λ≥420 nm, water	2.4 μmol h ⁻¹ g ⁻¹	~1.4%	74
Ru(dcbpy) ₃ ²⁺ -(Zeolite/TiO ₂ or Nb ₂ O ₅)-MV ²⁺ /Pt	λ≥420 nm, 50 μmol g ⁻¹ dye, 35wt% Zeolite	--	1.0% at λ=450 nm	75
Ru(dcbpy) ₃ ²⁺ -Pt/meso-TiO ₂	λ≥420 nm, 10 μM dye, 10 mM EDTA	20 μmol h ⁻¹	--	76
Ru(bpy) ₂ (dcbpy)(PF ₆) ₂ -Ti-MCM-48	λ≥400 nm, TEOA, Pt	~80 μmol g ⁻¹ in 6 h	--	77
Ru(dcbpy) ₃ -Al ₂ O ₃ -TiO ₂ /Pt	λ≥420 nm, 8.3 μM dye, 10 mM EDTA, pH3.00	50 μmol h ⁻¹	--	78
Ru(dcbpy) ₃ ²⁺ -RGO/Pt	λ≥400 nm or full spectrum, 5wt% TEOA, pH7.00	15.2 mmol g ⁻¹ in 6 h (full spectrum)	4.89%	79
Ru(dcbpy) ₃ ²⁺ -TiO ₂ /RGO/Pt	λ≥400 nm, 2 mM EDTA, pH3.00	959 μmol g ⁻¹ in 5 h	--	80
[Ru(dcbpy) ₂ (dpq)] ²⁺ -Pt/TiO ₂	full spectrum, 1 mM dye	0.25 mL h ⁻¹	--	81
[RuL(bpy) ₂](PF ₆) ₂ -Pt/TiO ₂	λ≥420 nm, 6.0wt% dye, TEOA	386.7 μmol in 3 h	--	82
N3-Pt/TiO ₂	λ≥410 nm, 0.1 M NaI, acetonitrile/water(5/95)	~9 μmol min ⁻¹	4.5% at λ=517 nm	83
N3(or Z907)-Pt/TiO ₂	λ≥420 nm, 10 mmol TEOA	~100 mL (mmol dye) ⁻¹ in 400 min.	--	84
N719-Pt/TiO ₂	λ≥390 nm, 0.3 M MeOH in TEOA	~4 μmol h ⁻¹	--	85
N719-Pt/TiO ₂	λ≥400 nm, 0.1 μmol dye, 10% TEOA	1.35 μmol h ⁻¹	0.38%	87
[Ru(bpy) ₂ (4-(2,2'-bipyrid-4-yl)-phenylphosphonic acid)](PF ₆) ₂ -K _{4-x} H _x Nb ₆ O ₁₇ /Pt	λ≥400 nm, Γ solution, pH2.00	~2 μmol in 12 h	~3%	88
Ru(bpy) ₂ (4,4'-(PO ₃ H ₂) ₂ -bpy) ²⁺ (RuP ²⁺) or Ru(bpy) ₃ ²⁺ (Ru ³⁺)-(NS-H ₄ Nb ₆ O ₁₇ or R-HCa ₂ Nb ₃ O ₁₀)/Pt	λ≥420 nm, 8.0 μmol g ⁻¹ dye; 10 mM EDTA	~20 μmol h ⁻¹	25% at λ=450 nm	90
Ru(bpy) ₂ (4,4'-(PO ₃ H ₂) ₂ -bpy) ²⁺	λ=450±20 nm, 20 μM RuP, 10	~9 μmol h ⁻¹	--	91

(RuP ²⁺)- HCa ₂ Nb ₃ O ₁₀ /Pt	mM EDTA				
Ru(bpy) ₂ (4,4'-(CH ₂ PO ₃ H ₂ -bpy) ₂) ²⁺ (RuP)-TiO ₂ -CoP(Co ^{III} Cl(dmgh) ₂ (pyridyl-4-hydrophosphonate))	λ _≥ 420 nm, 0.1 M TEOA buffered solution, pH7.00	~6 μmol in 4 h, 42 mol H ₂ h ⁻¹ (CoP)	--		92
Ru(bpy) ₂ (4,4'-(CH ₂ PO ₃ H ₂ -bpy) ₂) ²⁺ (RuP)-(TiO ₂ particles or mesoporous film)-CoP	λ _≥ 420 nm, 0.1 μmol RuP, 0.2 mmol CoP, 0.1 M TEOA buffered solution, pH7.00	3.0 μmol h ⁻¹	--		93
Ru(bpy) ₂ (4,4'-(CH ₂ PO ₃ H ₂ -bpy) ₂) ²⁺ (RuP)-(TiO ₂ or ZrO ₂)-NiP	λ _≥ 420 nm, 0.3 μmol RuP; 0.1 μmol NiP.	16.1 (ZrO ₂) and 1.7 (TiO ₂) μmol in 2 h	10%		94
Ru(bpy) ₂ (4,4'-(CH ₂ PO ₃ H ₂ -bpy) ₂) ²⁺ (RuP)-TiO ₂ -[NiFeSe]-hydrogenase	λ _≥ 420 nm, EDTA/tris buffer with [NiFeSe]-H ₂ ase (10 mL, 5 mM solution), pH7.00	~1.10 μmol h ⁻¹	TOF=20 s ⁻¹		95
Ru(bpy) ₂ (4,4'-(CH ₂ PO ₃ H ₂ -bpy) ₂) ²⁺ (RuP) or N3-TiO ₂ -[NiFeSe]- hydrogenase	λ _≥ 420 nm, TEOA buffer with <i>Db</i> [NiFeSe]-H ₂ ase (20 μL, 1 μM solution), pH7.00	3.56 μmol h ⁻¹	TOF=50 s ⁻¹		96
P ₂ , P ₄ , P ₆ or C ₂ , C ₄ , C ₆ : p-RuL ₃ or c-RuL ₃ -Pt/TiO ₂	λ _≥ 420 nm, 10 mM EDTA, pH3.00	3.5 (P ₂) and 1.14 (C ₂) μmol min ⁻¹	28% (P ₂)		98
Ru(bpy) ₃ ²⁺ -Nf-TiO ₂ /Pt, Ru(dcbpy) ₃ ²⁺ -TiO ₂ /Pt	λ _≥ 420 nm, 4 mM EDTA	80 μmol h ⁻¹ (Ru(bpy) ₃ ²⁺)	2.6% at λ= 420-550 nm		99
Ru(bpy) ₃ ²⁺ -G-Nf-TiO ₂ /Pt	λ _≥ 420 nm, [G]=1 mM, 10 mM EDTA, pH4.60.	~9 μmol h ⁻¹	--		100
N3-TiO ₂ /PAAm	λ _≥ 420 nm, 0.5 μmol [PdCl ₂ (PPh ₃) ₂ , MeCN/NEt ₃	19.9 mL in 110 h	--		101
Ru(bpy) ₂ (py)Cl/G/Pt	λ _≥ 400 nm or full spectrum, 20vol% CH ₃ OH/H ₂ O, pH3.00	39.3 μmol mg ⁻¹ (full spectrum)	--		102
Ti-MOF-Ru(tpy) ₂	λ _≥ 420 nm, 0.01 M TEOA, 0.05 mM H ₂ PtCl ₆	~5 μmol in 3 h	~0.2% at λ= 500 nm		103
Ru ₂ (bpy) ₄ L ₁ -PF ₆ , or Ru(bpy) ₂ (him) ₂ -NO ₃ -Pt/m-TiO ₂	λ _≥ 420 nm, 20vol% CH ₃ OH	1018.7 μmol h ⁻¹ g ⁻¹ (Ru ₂ (bpy) ₄ L ₁ -PF ₆)	--		106
Ru ₂ (bpy) ₄ (BL)(ClO ₄) ₂ or Ru ₂ (dcbpy) ₄ (BL)(ClO ₄) ₂ -P25	λ _≥ 400 nm, 10 vol% TEOA	236.4 μmol h ⁻¹ (Ru ₂ (bpy) ₄ (BL)(ClO ₄) ₂)	16.8% at λ= 420 nm.		108

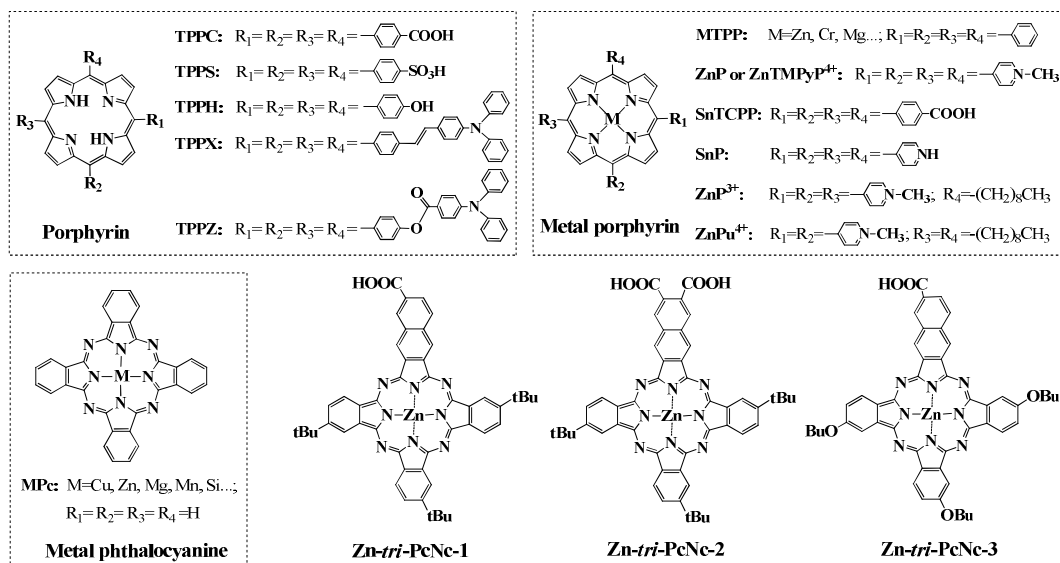


Fig. 10 Basic molecular structures of typical porphyrins and phthalocyanines as well as their analogues used in the dye-sensitized semiconductor suspension systems for photocatalytic H₂ production.

3.3 Other metal complexes

(1) **Metal porphyrins/phthalocyanines and analogues.** Except for the most popular Ru-complex dyes, some

other transition metal complexes, such as metal porphyrins (MPs) and metal phthalocyanines (MPcs), have also been widely utilized as sensitizer to extend the spectral responsive region.^{109,110} Their corresponding molecular structures and symbols are shown in Fig. 10, and Table 2 summarized those reports related to heterogeneous photocatalytic H₂ production systems sensitized with MPs or MPcs sensitizers.^{61,68,85,86,111-133}

Porphyrins possess rigid two-dimensional 18- π -electron aromatic structures with large absorption coefficients in the green to red region (Q-bands) and the blue region (Soret bands), which bear many reaction sites and easy synthesis of highly asymmetric structures. In particular, a zinc porphyrin (ZnP)-based solar cell co-sensitized with organic dye by using a Co-complex electrolyte gives an unprecedented photovoltaic conversion efficiency (12.3%),^{109,110} superior to any Ru-complex dye-sensitized device. This advance stimulates the investigations on the modified porphyrins as sensitizer for DSSCs, but the development of porphyrins as sensitizer in H₂ production especially in heterogenous system is very limited.¹¹¹⁻¹²⁰

In 2006, Ishihara's group reported water splitting for H₂ and O₂ production over Pt/KTa(Zr)O₃ sensitized with various porphyrins and its analogues, such as tetrakis(4-carboxyphenyl)porphine (TPPC), tetraphenylporphine tetrasulfonic acid (TPPS), Co-tetraphenylporphyrin (Co-TPP), Cr-tetraphenylporphyrin (Cr-TPP), chlorophyll a, cyanocobalamin (VB₁₂), Zn-TPP dimer (Zn-TPPD, pentamethylene bis[4-(10,15,20-triphenylporphin-5-yl)benzoate]di-zinc(II)), Co-phthalocyanine (CoPc), and Cr-phthalocyanine (CrPc) (see Fig. 10), and found that VB₁₂ modified Pt/KTa(Zr)O₃ exhibited the best activity with an AQY of 12.2% at 300 nm.¹¹¹ Their further investigations demonstrated that Pt loaded on dye-modified KTa(Zr)O₃ was slightly oxidized to form PtO_x with low catalytic activity for the H₂ oxidation reaction, and the photoluminescence (PL) spectra suggest that excitation energy was transferred between KTa(Zr)O₃, Cr-TPP, and Pt co-catalyst.^{112,113} Furthermore, the results of the wavelength dependency of the photoactivity indicates that the water splitting reaction on the dye-modified KTa(Zr)O₃ proceeds via a two-step excitation of both KTaO₃ and dye similar to photosynthesis in green plants.^{112,113} This is clearly unlike the common dye sensitization process, where the photocatalytic reaction occurs with the injection of photoexcited electrons from the dye into the TiO₂'s CB. Therefore, a Z-type excitation mechanism was proposed, where the photoexcited electrons of Cr-TPP first transfers to Pt (but not to the semiconductor), and those of KTa(Zr)O₃ are transferred to the vacant band in the vacant LUMO level of Cr-TPP, which is physically adsorbed on the KTa(Zr)O₃ surface and works as a photoexcited electron acceptor of KTa(Zr)O₃, and the Pt co-catalyst and KTa(Zr)O₃ are the possible active sites for H₂ and O₂, respectively.^{112,113} The same Z-type mechanism was also used to explain the improved photoactivity of tantalum (oxy)nitride (TaON) modified by various porphyrins, and found that the modification dye and PtO_x co-catalysts are necessary to achieving H₂ production.¹¹⁴ Moreover, it was confirmed that Zn-TPPD remained after the photoreaction under visible light irradiation for 6 h, indicating the porphyrins improved the photoactivity without decomposition.¹¹¹⁻¹¹⁴

On the contrary, many other researches on H₂ production over porphyrin-sensitized semiconductors still are typical dye sensitization mechanism, and the photoactivity of porphyrin can be mainly attributed to the Q-band but not to the Soret band of which absorption intensity is much higher.^{61,68,85,86,115-120} For example, Inoue's group observed that visible-light-driven H₂ production coupled with the photochemical oxygenation of cyclohexene with water in an acetonitrile aqueous suspension of Pt/TiO₂ NPs sensitized by Sn(IV)-porphyrin (SnTCPP) bearing carboxyl as anchoring group (Fig. 10).¹¹⁵ In which, it still is typical dye

sensitization mechanism.¹¹⁵ Similarly, Durrant's group reported a zinc-substituted cytochrome c (ZnCyt-c) sensitized Pt/loaded mesoporous TiO₂ electrodes, and observed an efficient electron injection from the triplet state of ZnCyt-c into TiO₂, which results in a long-lived charge-separated state.¹¹⁶ Moreover, EDTA as sacrificial electron donor in the electrolyte leads to an enhanced H₂ production activity with a QY of ~10%.¹¹⁶

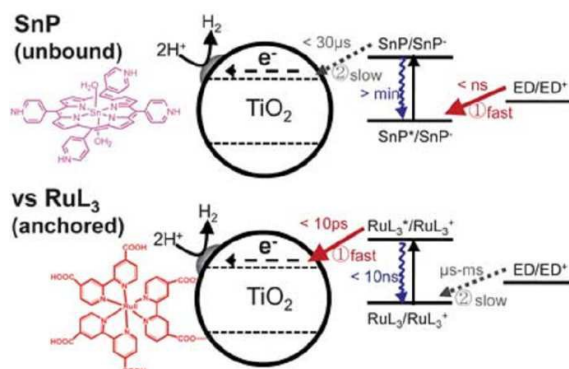


Fig. 11 Schematic illustration of the electron transfer dynamics occurring on (a) SnP and (b) Ru(dcbpy)₃ sensitized TiO₂ particle. Figure reproduced with permission from Ref. 61. Copyright 2010 The Royal Society of Chemistry.

As mentioned above, a strong chemical binding between the semiconductor surface and the Ru-complex molecules usually maximize the electronic coupling between the excited dye molecular orbital and the semiconductor CB, and thus those Ru-complexes are fixed on the semiconductor surface through anchoring groups (e.g. carboxylate, and phosphonate).^{67,71-99,105-108} However, such chemical anchoring bond can be made only in a specific pH range and not inherently stable in an aquatic environment.^{61,71,78,98,99} Choi's group reported a water-soluble tin-porphyrin [Sn^{IV}(OH₂)₂TPy^HP]⁶⁺ (SnP, TPyP = 5,10,15,20-tetrakis(4-pyridyl) porphyrinato)] sensitized Pt/TiO₂ for H₂ production with an AQY of 35% at 550 nm,⁶¹ which even exhibits much better activity than that of anchored Ru(dcbpy)₂²⁺ though the SnP cannot adsorb on TiO₂ as shown in Fig. 11.⁶¹ It was found that the H₂ production is mediated through the formation of the π -radical anion (SnP⁻) that subsequently transfers electron to TiO₂ through transient absorption spectroscopy, which makes the adsorption of SnP on TiO₂ not required and the H₂ production is active over a wide pH range.⁶¹ This is clearly contrasted with the common Ru-complex-sensitized TiO₂ where the dye adsorption is essentially required and the H₂ production is limited to the acidic condition where the dye adsorption on TiO₂ is allowed.⁶¹ Moreover, Ishihara's group investigated the effects of adsorption states (physical adsorption and covalent attachment) of porphyrins on the photoactivity of PtO_x/TaON.¹¹⁴ In their porphyrins used, TPPC and hemin form covalent attachments with the TaON surface through their carboxyl groups, and the other dyes attached by physical adsorption. It was found that the porphyrins attached with physical adsorption showed more positive effects on the photoactivity of TaON because these dyes adsorbed onto the TaON surface via the porphyrin ring may act as the electron acceptor of TaON (Z-type mechanism as mentioned above). The distance between the porphyrin ring and the TaON surface was shorter than that for TPPC or hemin with covalent attachments. This is an advantage for electron transfer between porphyrins and TaON, and thus the photoactivity of TaON was much improved by modification with physically adsorbed dyes.¹¹⁴

In addition to the attachment modes and adsorption degrees between the dye and semiconductor, different semiconductors, dyes and the co-existing sacrificial electron donor species are also important factors influencing the photosensitization.^{85,86} Wada's group investigated the effects of co-existing electron donor species (MeOH and TEOA) on the H₂ production activity of dye (N719, TPPC or TPPS) sensitized Pt-loaded metal oxide nanoparticles (TiO₂, SnO₂, and ZnO) suspension under $\lambda > 390$ nm light irradiation, and found that the combination of oxide semiconductors, dyes and electron donor species dominates the major variation of the electron injection and the following charge recombination kinetics, which is significantly influenced by the adsorption-desorption nature of dyes and electron donor species.^{85,86} The observed H₂ production activity by varying dyes, semiconductors, and electron donors is clearly originated by the surface chemical nature of semiconductors with dyes and co-existing species but not to the CB or CB level shift of semiconductors by changing the pH of surrounding solution, which typically utilized to discuss the results of H₂ production.⁸⁶ Moreover, the co-existing species (MeOH and TEOA) shows an opposite effect for TiO₂ and SnO₂ in terms of H₂ production due to the completely different electron transport mechanism.^{85,86} This investigation revealed that the combinational effect among semiconductors, dyes and co-existing species in surrounding medium is quite important for the dye-sensitized semiconductors in order to achieve high photoactivity.

Also, Zhilina's group found that Pt/TiO₂ sensitized by water-insoluble ZnP derivatives shows H₂ production activity comparable with that by water-soluble ZnP complex,¹¹⁸ and the H₂ production activity of ZnP-sensitized Pt/TiO₂ has a maximum at pH4-5 when using EDTA, ascorbic acid (AA) and oxalic acid (OA) as electron donor, as does the adsorption of these donors on TiO₂; whereas the photoactivity increases sharply in alkaline solutions when using TEOA as electron donor.¹¹⁹ Moreover, TONs for ZnPs varied from 50 for water-soluble ZnP up to 150-185 for water-insoluble ones, and thus they thought that it is expedient to prepare photocatalysts for water splitting on the basis of water insoluble MPs.^{118,119} Similarly, Kaneke's group investigated the effects of electron donor (TEOA, AA, phenol, acetone, methanol, FeCl₂ and hydroquinone (HQ)) on H₂ production activity of Pt/TiO₂ sensitized with various porphyrins (TPPC, TPPS, tetrakis(4-pyridylphenyl)porphine (TPPPy)) and Ru(bpy)₃²⁺.⁶⁷ Among those, only EDTA and TEOA are effective to produce H₂, while reversible donors (such as Fe²⁺, HQ, AA, and phenol) are not effective.⁶⁷ The dependence of H₂ evolved in TEOA solution on pH is different from that in an EDTA solution, which is ascribed to the slower oxidation of TEOA in an acidic solution as compared with that in an alkaline solution.⁵⁹

Metal phthalocyanines (MPcs), which are structurally related to porphyrins but are even more conjugated macrocycles, can absorb in the vis/near-IR region with Soret band at 300-400 nm and a Q-band centered around 650-800 nm. The latter with extinction coefficients over $\sim 10^5$ M⁻¹ cm⁻¹ allows an efficient photon harvesting in red/near-IR region, but the development of MPcs as sensitizers in heterogeneous photocatalytic H₂ production is rare.^{68,121-125} In 2008, Hamed's group compared the photosensitization for H₂ production of three types of dye (CuPc, Ru(bpy)₃²⁺, and Eosin Y (EY)) on the TiO₂/RuO₂ containing MV²⁺ as electron relay under solar or UV radiation, and found that the ranking of dyes in terms of the degree of enhancement of H₂ production activity is as follows: CuPc > Ru(bpy)₃²⁺ > EY, indicating the potential of MPcs as sensitizer in the dye-sensitized semiconductors.⁶⁸ Ishihara's group reported that the redox potential of MPcs could affect the photoactivity of dye-modified KTa(Zr)O₃, and CrPc with a redox potential of -0.8 V (vs. SCE) is the most effective one for improving water splitting activity among those MPcs tested.¹²¹ In 2010, Domen's group

reported the composite of MgPc and mesoporous g-C₃N₄ (mpg-C₃N₄) shows a stable photocatalytic H₂ production activity from TEOA solution even under irradiation at $\lambda > 600$ nm though the AQY is very low (0.07%) at 660 nm light irradiation.¹²² More recently, Yang's group reported axially covalently functionalized graphene (G) or RGO with MnPc or SiPc, which exhibits an AQY of 0.06% at 670 nm light irradiation.^{123,124} In comparison to graphene, the MnPc/G nanohybrid shows a substantially improved H₂ production activity due to the facilitated intermolecular electron transfer and the suppressed charges recombination, demonstrating that MPcs covalently functionalized graphene is a novel photocatalyst for H₂ production.^{123,124} Wang's group reported overall water splitting for H₂ and O₂ production over BiOCl/CuPc in rhodamine B (RhB) methanol aqueous solution based on dye co-sensitization, in which the photosensitized RhB molecules supplied photogenerated holes which took part in the O₂ evolution reaction, and the H₂ production activity is improved by loading CuPc.¹²⁵ The considerable enhancement of photoactivity is due to the quick transfer of photogenerated electrons from dye to BiOCl and the enhanced charge separation efficiency due to oxygen vacancies on BiOCl surface acting as active electron traps.¹²⁵

Generally, simple MPcs often exhibit low H₂ production activity and quantum yield caused by the lack of electron transfer direction of excited state and easy aggregation due to their flat nature and large π -system, which usually result in rapid deactivation of the excited dye.¹⁰⁹ Recently, the present authors synthesized a series of ZnPc derivatives (ZnPcNcs, see Fig. 10) for efficient red/near-IR-light-induced H₂ production.¹²⁶⁻¹²⁹ By comparing the photoactivity over different dye-sensitized semiconductors (TiO₂ or g-C₃N₄), it was found that the symmetry, direction of electron transfer, position and number of electron-pulling/pushing groups of ZnPcNcs significantly affect the photosensitization effect.¹²⁶⁻¹²⁹ More importantly, restraining the aggregation of Zn-*tri*-PcNc-1 on Pt/g-C₃N₄ through co-adsorption of chenodeoxycholic acid (CDCA) can further improve the H₂ production activity with AQY enhanced from 1.13% to 1.85% at 700 nm light irradiation, which should be the record value in the red/near-IR light region to the best of our knowledge.¹²⁶

(2) Other transition-metal complex dyes. Except for the above MPs and MPcs, some other transition metal complexes are also used in heterogenous photocatalytic H₂ production systems.¹³⁰⁻¹³³ In 1988, Bulatov's group reported a Pt(alizarine)₂-sensitized TiO₂ for H₂ production under visible light irradiation.¹³⁰ Eisenberg's group reported two kinds of Pt-complex, Pt(dcbpy)(bdt) (bdt = 1,2-benzenedithiolate) and Pt(dcbpy)(met) (met = *cis*-1,2-dicarbomethoxyethylene-1,2-dithiolate), sensitized Pt/TiO₂ for visible-light-induced H₂ production,¹³¹ and found that a major limitation to the effectiveness of these chromophores is their instability upon oxidation based on the H₂ production activity over different Pt-complex-Pt/TiO₂ and electrochemical data.¹³² Also, Wang and co-workers reported a new nickel-thiourea-triethylamine complex (Ni-Tu-TETN) adsorbed on g-C₃N₄ for photocatalytic H₂ production.¹³³

As a whole, the depth and quantity on the investigations of MPs, MPcs and other transition metal complexes for heterogenous photocatalytic H₂ production are very limited compared with those Ru-complex dyes, and the high cost of Pt-complexes (often exhibits limited visible light absorption ability),¹³⁰⁻¹³² or electron relay seems less prospect in the future as compared to MPs and MPcs. Therefore, the present authors think the development of low cost, high efficiency and wide spectral responsive MPs/MPcs (and their analogues) should be the future directions for the heterogenous photocatalytic H₂ production systems, which

may include: 1) exploiting more efficient asymmetric MPs/MPcs through structure designing; 2) deeply investigating the interaction of MPs/MPcs with semiconductors and the electron transfer mechanism among them; 3) co-sensitization of MPs/MPcs with other types of dyes having complementary spectral absorption ability because of their rather narrow light responsive region; 4) co-catalyst of these types of dye-sensitized semiconductors is still precious Pt, and some low-cost noble-metal-free materials can be considered.

Table 2 Summary of the other metal-complex-sensitized semiconductor for photocatalytic H₂ production

Catalyst	Reaction condition	H ₂ production activity	AQY /%	Ref.
TPPC or TPPS-TiO ₂ /Pt	$\lambda \geq 390$ nm, MeOH in TEOA (0.3 M)	~8 μmol in 3 h	--	86
TPPS, TPPC, ZnTPP, CoPc, CrPc, CoTPP, CrTPP, Chlorophyll A or VB ₁₂ -Pt/K _{0.95} Ta _{0.92} Zr _{0.08} O ₃	full spectrum, 30 mL water, pH11.00	575.0 (H ₂) and 280.4 (O ₂) $\mu\text{mol h}^{-1}\text{g}^{-1}$ (VB ₁₂)	12.2% at $\lambda=300$ nm	111
Cr-TPP/PtO _x /K _{0.95} Ta _{0.92} Zr _{0.08} O ₃	full arc; $\lambda \geq 385$ nm or $\lambda \leq 385$ nm, 1.2 μmol dye	513 (H ₂) and 257 (O ₂) $\mu\text{mol h}^{-1}\text{g}^{-1}$ (full arc)	ECE=0.013%	112
Cr-TPP/PtO _x /K _{0.95} Ta _{0.92} Zr _{0.08} O ₃	$\lambda \leq 385$ nm, K _{0.95} Ta _{0.92} Zr _{0.08} O ₃ , 1.2 μmol dye	51.4 (H ₂) and 23.2 (O ₂) $\mu\text{mol h}^{-1}\text{g}^{-1}$	--	113
PtO _x /Zn-TPPD/TaON	$\lambda \geq 420$ nm, 0.5% dye, 0.24 M Na ₂ S	95.6 $\mu\text{mol h}^{-1}\text{g}^{-1}$	TON=173.6 (dye) ⁻¹	114
SnTCPP/Pt/TiO ₂	$\lambda \geq 480$ nm, 0.28 mmol SnTCPP, 10vol% CH ₃ CN	~12 μL in 1500 min	--	115
ZnCyt-c-Pt/TiO ₂ (ZnCyt-c: Zinc-substituted cytochrome c)	$\lambda \geq 475$ nm, NaPi buffer solution, 10 mM EDTA	~0.7 μmol in 40 min	10 \pm 5% per one photon	116
TPPH-RGO/Pt with CTAB	full spectrum, 2 mg CTAB, RGO:TPPH(2:1), 10vol% TEA	~12 mmol g ⁻¹ in 4 h	3.6%	117
ZnP/Pt/TiO ₂ (ZnP: Zinc porphyrin derivatives)	$\lambda \geq 520$ nm, 50 mM EDTA	~6 $\mu\text{mol h}^{-1}$	0.2%	118
ZnP/Pt/TiO ₂	$\lambda \geq 520$ nm, 50 mM EDTA	--	TON=182 (9 h)	119
Porphyrin-based MOF/ MV ²⁺ /Pt colloidal	$\lambda \geq 420$ nm, 15 mM EDTA	~1000 $\mu\text{mol g}^{-1}$ in 8 h	<0.01%	120
MgPc-mpg-C ₃ N ₄ /Pt	$\lambda \geq 420$ nm or $\lambda \geq 640$ nm, 10vol% TEOA	~4.5 $\mu\text{mol h}^{-1}$ ($\lambda \geq 640$ nm)	0.07% ($\lambda=660$ nm)	122
SiPc/N-usRGO/Pt	$\lambda \geq 400$ nm or UV-vis, 10% TEOA	4.5 $\mu\text{mol mg}^{-1}$ in 6 h (UV-vis)	0.56% ($\lambda=420$ nm)	123
MnPc/G/Pt	$\lambda \geq 400$ nm or UV-vis, 10% TEOA, 2 mg PVP	8.5 $\mu\text{mol mg}^{-1}$ in 10 h (UV-vis)	0.06% at $\lambda=670$ nm	124
CuPc/BiOCl	full spectrum, water-MeOH (or-RhB)	~4 $\mu\text{mol h}^{-1}$ (MeOH); ~90 (O ₂) and 80 (H ₂) $\mu\text{mol h}^{-1}$ (MeOH-RhB)	--	125
Zn-tri-PcNc-1-g-C ₃ N ₄ /Pt, co-adsorbed CDCA	$\lambda \geq 500$ nm, 5 $\mu\text{mol g}^{-1}$ dye, 50 mM AA	125.2 $\mu\text{mol h}^{-1}$	1.85% at $\lambda=700$ nm	126
ZnPcNcs-Pt/g-C ₃ N ₄	$\lambda \geq 500$ nm, 5 $\mu\text{mol g}^{-1}$ dye, 50 mM AA	263 $\mu\text{mol h}^{-1}$	0.97%	127
Zn-tri-PcNc-2-g-C ₃ N ₄ /Pt, Zn-tetrad-Nc-3-g-C ₃ N ₄ /Pt	$\lambda \geq 500$ nm, 5 $\mu\text{mol g}^{-1}$ dye, 50 mM AA	132 (Zn-tri-PcNc-2), 26.1 (Zn-tetrad-Nc) $\mu\text{mol h}^{-1}$	1.13% ($\lambda=685$ nm)	128
Zn-tri-PcNc-1-TiO ₂ /Pt, Zn-tetrad-Nc-3-TiO ₂ /Pt	$\lambda \geq 420$ nm, 5 $\mu\text{mol g}^{-1}$ dye, 10 mM EDTA	115.2 $\mu\text{mol h}^{-1}$ (Zn-tri-PcNc-1)	0.2% at $\lambda=700$ nm	129
Pt(alizarine) ₂ /TiO ₂	$\lambda=500$ nm, EDTA	--	0.5%	130
Pt(dcbpy)(met) or Pt(dcbpy)(bdt)-Pt/TiO ₂	$\lambda \geq 410$ nm, 12.6 mM TEOA	--	TON= 84 (95 h)	131
[Pt(tpy)(C \equiv C-C ₆ H ₅)]PF ₆ ⁻ /Pt/TiO ₂	$\lambda \geq 410$ nm, 12.6 mM TEOA	--	TON= ~100 (10 h)	132
Ni-Tu-TETN-C ₃ N ₄	Sunlight, 0.05 mmol Ni ²⁺ , 3 mmol Tu, TEOA, lactic acid	12 mmol in 8 h	0.2% at $\lambda=420$ nm	133

3.4 Metal-free organic dyes

Since many metal complex dyes, especially Ru- and Pt-complexes, are quite expensive, metal-free organic dyes, exhibiting low-cost, variety, tunable structure and light absorption region, have been arousing tremendous interest for a long time. Especially, xanthene dyes, cation organic dyes, D- π -A organic dyes and analogues, have been utilized as efficient dyes to sensitize semiconductors for visible-light-derived H₂ production.^{32,50,62,63,64-66,68,70,87,113,125,134-198} Their corresponding molecular structures and symbols are listed Fig. 12, and Table 3 summarized typical reports related to their photocatalytic H₂ production systems.

(I) **Xanthenes and cation organic dyes.** Xanthene-based dyes, such as eosin Y (EY), rhodamine B (RhB), rhodamine 6G (Rh6G), erythrosine (Er), erythrosin B (ErB), erythrosin yellowish (ErY), fluorescein (FL), eosin bluish (EB), rose bengal (RB), uranine (UR), and phloxin (Ph), are the most used metal-free organic dyes in the field of dye-sensitized semiconductors.^{50,62-66,68,113,125,134-179} Typically, xanthenes-based dyes can absorb the solar light in the region of 400-600 nm with maximal absorption peaks at ~490-560 nm, similar to that of common Ru-complex dyes, and thus is taken as alternative of the expensive Ru-complexes. As the most popular representative, EY has almost the same long history as that of Ru-complexes used in dye-sensitized semiconductor systems.^{50,62,69,113,134,136-159,162-170,173,174,178,179}

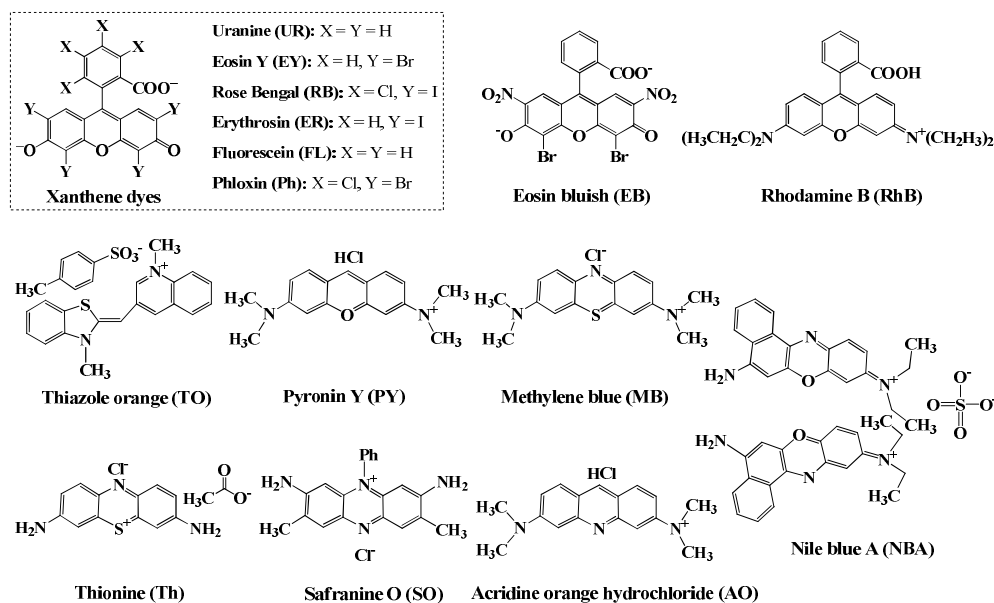


Fig. 12 Typical molecular structures of some xanthenes and cation organic dyes used in the dye-sensitized semiconductor suspension systems for photocatalytic H₂ production.

Early in 1981, Grätzel's group carried out an overall water splitting system over Pt/TiO₂/RuO₂ with addition of RhB, and found that RhB showed better sensitization effect than Ru(bpy)₃²⁺ for H₂ production.⁶⁴ In 1984, they found that adsorption of EY onto TiO₂ surface is a prerequisite for successful photosensitization, and the electron injection into TiO₂ takes place from the excited single state (S₁) of the adsorbed EY, while the back-electron transfer occurs via a rapid intraparticle reaction between EO⁺...e_{cb}⁻ pairs associated with the same TiO₂ host aggregate.¹³⁴ Moreover, it was found that the light-induced charge separation can be sustained in the semiconductor for at least several microseconds, which is long enough to trap the injected electron by

the deposited co-catalyst.¹³⁴ Shimidzu's group, however, proposed a different mechanism in 1985, that is, a reductive electron-transfer mechanism through the excited triplet state (T_1) of xanthenes.¹³⁵ They found that heavy-halogenated xanthenes (e.g., RB, ER, and EB) have high QYs for H_2 production but tend to photodehalogenate, while nonhalogenated xanthenes (e.g., UR and RhB) have high durability against any photodeterioration but have moderate photoactivities when they are used as sensitizers of Pt-loaded semiconductors, in which the excited T_1 state of the dye is a precursor of the reduced dye by TEOA, and the activity is determined mainly by the QY of the dye's real excited T_1 state.¹³⁵ Therefore, they used external heavy-atom (i.e. I) additives and durable nonhalogenated dyes (e.g., UR and RhB) to fabricate dye-sensitized systems, which showed a pronounced advantages of high QY and high durability for H_2 production.¹³⁵

Lu's group has conducted extensive and in-depth investigations on xanthene dyes, especially EY, sensitized various semiconductors for H_2 production since 2006.¹³⁶⁻¹⁵⁷ For example, they reported various systems based on Pt-loaded TiO_2 or its doped products,¹³⁶⁻¹⁴¹ zeolites,^{142,143} silica gel,¹⁴⁴ MWCNT,^{145,146} RGO or G,¹⁴⁷⁻¹⁵² g- C_3N_4 ,^{153,154} organic-inorganic hybrid material,¹⁵⁵ and even some polyoxometalates.^{156,157} Among those, some highly efficient H_2 production systems, such as EY-Pt/Ti-MCM-41 (with a AQY of 12.01%),¹⁴² EY-Pt/silica gel (with a AQY of 10.4%),¹⁴⁴ and EY-Pt/mpg- C_3N_4 (with a AQY of 24.0%),¹⁵³ were obtained under $\lambda \geq 420$ nm light irradiation. In addition, a high AQY of 19.1% under $\lambda \geq 420$ nm light irradiation over a multilayer EY-sensitized Pt/ TiO_2 via Fe^{3+} coupling was attained, demonstrating a general way to develop efficient visible-light-responsive photocatalyst by using metal ions linking between organic dye molecules.¹³⁶ More significantly, the constructed EY/RB co-sensitized Pt-loaded graphene (ER-G/Pt) exhibits a high AQY up to 37.3% at two-beam monochromic light (520 and 550 nm) irradiation.¹⁴⁸

Ishihara's group reported some water-soluble xanthene dyes (e.g., Rh6G, RB, FL, and EY) sensitized $PtO_x/KTa(Zr)O_3$ for overall water splitting, and found that the H_2 production activity depends strongly on the dye's redox potential, and a dye with a redox potential of -0.8 V (vs. Ag/AgCl) would give a high activity.¹¹³ Among those xanthene dyes tested, FL and EY showed low photosensitization on the H_2 production, while Rh6G and RB showed comparatively high positive effects.¹¹³ Moreover, Abe's group construct a stable dye-sensitized system in water by a chemical fixation of xanthenes on Pt/ TiO_2 particles via silane-coupling agent, and found that the obtained EY-Pt/ TiO_2 exhibited steady H_2 production from TEOA solution under visible light with TON of >10000 and QY of ~10% at 520 nm.¹⁵⁸ The H_2 production reproduced even after the exchange of TEOA solution, while the H_2 production from the mixture of EY and Pt/ TiO_2 ceased in 10 h, indicating the dye-fixed system possessing several advantages such as stability and less influence of pH.¹⁵⁸

Except for the above xanthene dyes, some cationic organic dyes (see Fig. 12), such as thiazole orange (TO), pyronin Y (PY), methylene blue (MB), thionin acetate (Th), safranin O (SO), Nile blue A (NBA), and acridine orange hydrochloride (AO), were also exhibited photosensitized H_2 production activity.^{70,180-182} Garcia's group reported that cationic dyes (e.g., MB, AO, PY, and $[Ru(bipy)_3]^{2+}$) showed positive effects on the visible-light-driven H_2 production activity of graphene oxide (GO), while a neutral dye (e.g., CuPc) had low modification effects.⁷⁰ Those positive dyes (i.e., MB) can intercalate inside the intergallery space of a few layers of G, and the H_2 production activity of the formed MB@GO was improved by 1.5 times compared with MB/GO.⁷⁰ Yamashita's group constructed a H_2 production system (TO-SCA[4]/Pt- TiO_2) by using 4-sulfocalix [4]arene (SCA[4]), bearing both phenolic hydroxyl groups and sulfonate moieties, as a linker between Pt/ TiO_2

and a cationic dye (TO), which provides key properties for formation of surface complexes as well as ion exchange capacity.¹⁸⁰ The obtained TO-SCA[4]/Pt-TiO₂ exhibited photoactivity for H₂ production even under irradiation at $\lambda > 550$ nm, and an AQY of 10.4% was obtained at 460 nm light irradiation.¹⁸⁰ It demonstrates that SCA[n] acting as linker has potential for combining other types of cationic dyes for efficient visible light harvesting without complicated procedures.

(2) D- π -A organic dyes and analogues. Recently, synthetic D- π -A organic dyes exhibited good photovoltaic conversion efficiencies in DSSCs applications,¹⁸³ and some of them were also utilized in dye-sensitized H₂ production systems due to its convenient modulation of the intramolecular charge-transfer nature and the absorption property.^{32,50,83,87,184-198} For this type of dyes, coumarin, merocyanine, triphenylamine, phenothiazine, carbazole and their derivatives are the most popular electron donor moiety. Their corresponding molecular structures and symbols are depicted in Fig. 13, and Table 3 summarizes the recent development on their heterogeneous H₂ production systems.

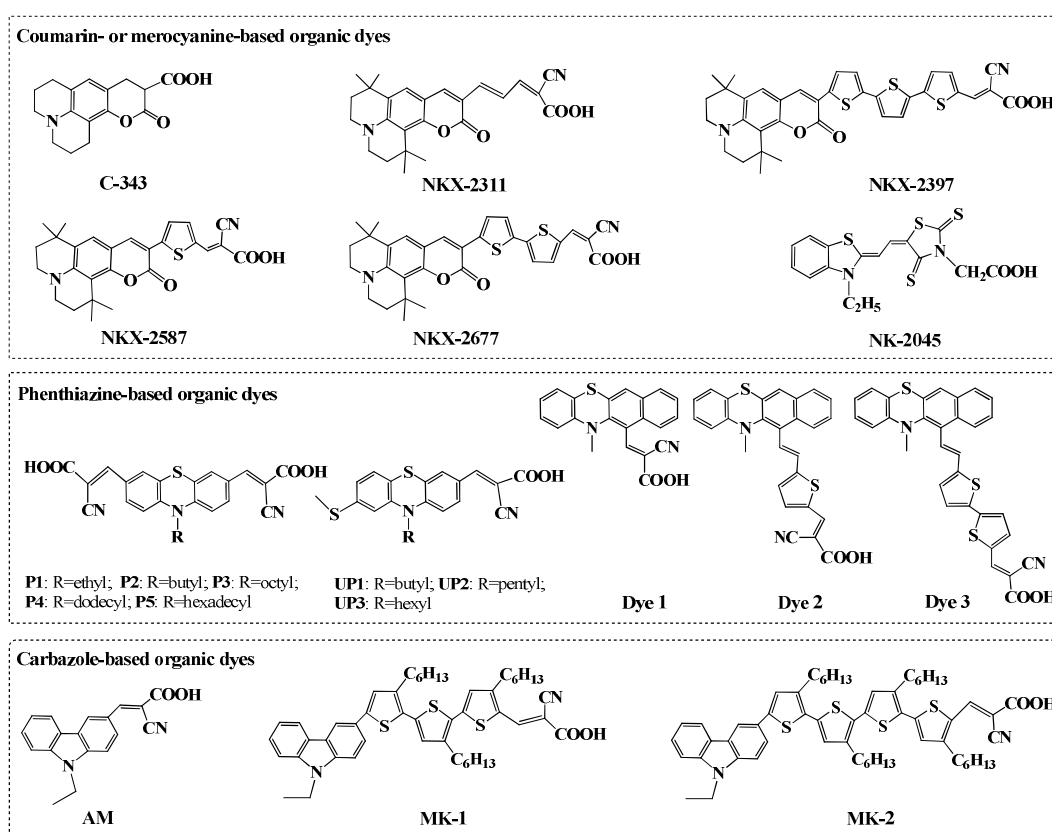


Fig. 13 Typical molecular structures and symbols of typical D- π -A organic dyes used in the dye-sensitized semiconductor suspension systems for photocatalytic H₂ production.

Abe's group intensively investigated the photocatalytic behavior and mechanism of coumarin (C-343, NKX-2311, 2587, 2677, 2697), carbazole (MK-1, MK-2), and merocyanine (NK-2045) dyes (see Fig. 13) sensitized semiconductors.^{32,83,184-187} For example, a Z-type overall water splitting system containing a coumarin-sensitized H₄Nb₆O₁₇ for H₂ evolution and IrO₂-Pt/WO₃ for O₂ evolution in the presence of I₃⁻/I⁻ redox mediator was fabricated as shown in Fig. 14.^{32,184} It was found that the oxidized states of coumarin dyes

having an oligo-thiophene unit are stable in water to achieve sustained overall water splitting though the QY of H_2 evolution is still low ($\leq 0.1\%$ at 500 nm, $\sim 0.05\%$ at 480 nm even for the best dye NKX-2677).^{32,184} They pointed out two reasons for the low efficiency, one is the low efficiency in electron transfer from the dye molecules outside to the Pt co-catalysts inside through the micrometer sized $H_4Nb_6O_{17}$ particles; the other is the intrinsically low rate of electron injection from I^- to dyes in aqueous media.^{32,184} Also, the effect of water amount in water-acetonitrile solution containing I^- as electron donor over coumarin (C-343) or merocyanine (NK-2045) sensitized Pt/TiO₂ systems was investigated.^{83,185-187} It was found that addition of acetonitrile, a good solvent for I^- and dye, significantly improve the H_2 production activity, which decreases with enhancing water amount in the mixed solution due to the decrease in energy gap between the redox potential of I_3^-/I^- and the HOMO of the dye.^{83,185-187} These results demonstrate that the influence of solvent on the dye's energy potentials must be considered in constructing an efficient dye-sensitized system for use in aqueous solutions.

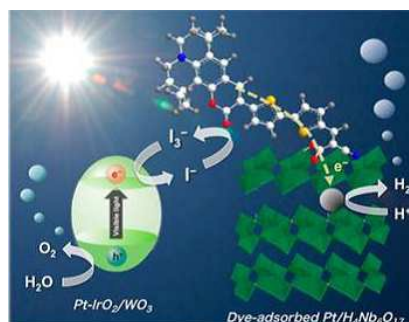


Fig. 14 Photocatalytic water splitting using a mixture of coumarin-dye-adsorbed Pt/ $H_4Nb_6O_{17}$ (50 mg) and IrO_2 -Pt/ WO_3 (100 mg) suspended in a 5 mM of KI aqueous solution under visible light ($\lambda \geq 400$ nm). Figure reproduced with permission from ref. 32. Copyright 2009, The Royal Society of Chemistry.

Kang's group investigated the significance of hydrophilic characters of triphenylamine-based dyes (with thiophene and 2-cyanoacrylic acid as π -bridge and electron accepting moieties, respectively) in dye-sensitized system, and found that the visible-light-induced H_2 production activity and optimum amounts of the dyes grafted to Pt/TiO₂ are affected substantially by the hydrophilic and steric effects.^{188,189} Park's group investigated the effect of number of anchoring groups on the applicability of triphenylamine-based dyes (D1, D2, D3: with different numbers ($n=1, 2,$ and 3) of carboxylate groups, respectively) sensitized Pt/TiO₂ for H_2 production.¹⁹⁰ It was found that the number of anchoring groups seems to be significantly important because of its effects on the binding states of dyes to TiO₂ as well as on other physicochemical properties such as extinction coefficient and HOMO-LUMO position, and use of dyes with multi-anchoring groups is more desirable than those with a single anchoring group.¹⁹⁰ In addition, Yang and Zheng's group used triphenylamine (TPA) as electron donor to covalently functionalize Pt-loaded graphene (G) to fabricate Pt/G-TPA nanocomposite, and found the TPA moiety attached on graphene may harvest irradiation light and transfer photoinduced electrons to graphene though the QY for H_2 production is not high enough.¹⁹²

Son's group reported phenothiazine-based dyes with two anchoring groups (P1-P5: long alkyl chains modified phenothiazine and two 2-cyanoacrylic acid as donor and accept moieties respectively without π -bridge) sensitized Pt/TiO₂ for H_2 production, and all of them exhibit much higher activity than that of N719 and EY.¹⁹³ Watanabe and Ishihara's group investigated the spacer effects in benzo[*b*]phenothiazine-based dyes

(containing several thiophene and 2-cyanoacrylic acid as π -bridge and accept moieties, respectively) for H_2 production over dye-sensitized TiO_2 in TEOA solution, and found that the H_2 production activity and stability can be improved when numerous π -conjugated bridges are inserted as spacers between the donor and the anchor moiety,¹⁹⁴ and Dye 3 bearing the longest spacer exhibits the best H_2 production activity with a TON of 4460 after 16 h and a quantum yield of 1.65% at 420 nm.¹⁹⁴ More recently, Pal's group reported a series of thiopenothiazine-based dyes (UP1, UP2 and UP3) for H_2 production show pronounced light harvesting capability at a slightly wide visible region (400–650 nm).⁵⁰ The resulting thiopenothiazine@ TiO_2 /Pt exhibits high H_2 production activity at neutral conditions, and the UP3-sensitized Pt/ TiO_2 (UP3@PT) shows H_2 production up to 1048 mmol (TON 1397) with an excellent AQY of ~50% under $\lambda \geq 400$ nm light irradiation, much higher than the other photocatalysts such as UP1@PT, UP2@PT, and pure TiO_2 . The enhanced activity in dye@ TiO_2 composite is ascribed to the addition of methine unit in the dye, which reduces the charge recombination and increases the light harvesting.⁵⁰

More recently, the present authors reported an indole-based dye (LI-4: with pyrrole and 2-cyanoacrylic acid as π -bridge and accept moieties, respectively, and a carbazolyl group linked to the pyrrole ring through a C-N bond to suppress the possible dye aggregation) sensitized g- C_3N_4 for H_2 production with an AQY of 11.7%, 5.0%, and 2.2% under 420, 475, and 550 nm light irradiation, respectively.¹⁹⁵ Pal's group reported a new highly efficient photocatalyst containing carbazole-based dye (AM, or MK-2) and nafion coated Pt/ TiO_2 (NPT), and found that the D1@NPT sensitized by the simple and cost effective AM shows an AQY of 19.16% for H_2 evolution under $\lambda \geq 400$ nm light irradiation with TEOA as sacrificial agent.⁸⁷ Their results showed that the spacer group with an extended π -spacer linker to the carbazole-based dye increases the light-harvesting ability and photoactivity of the NPT at neutral pH, and thus a high AQY of 26.64% for H_2 evolution under $\lambda \geq 400$ nm light irradiation was obtained from carbazole-based dye (MK-2) sensitized NPT.⁸⁷ The improved activity is due to the combined effects of several factors such as the synergistic effect of nafion- TiO_2 , strong visible light absorption, and low charge recombination.⁸⁷ The same group synthesized a pyridine pyrazole functionalized naphthylbisimide (NBI) core-based dye (NDIPYPZ) as sensitizer of TiO_2 /G (graphene), and found that the ability of the molecule to accept electron by the naphthyl core or to give away electron via donor pyridine pyrazole.¹⁹⁶ The obtained NDIPYPZ/ $sTiO_2$ -rGO exhibits high H_2 production activity of 10 mmol $g^{-1} h^{-1}$ with TON of 4790 from water-methanol system without any noble metal loading.¹⁹⁶

In addition, some n-type organic semiconductors, such as perylene diimide (PDI) and its derivatives, are also used as dyes of semiconductors for visible-light-responsive H_2 production.^{197,198} For example, Wang's group used molecular aggregates of perylene tetracarboxylic diimide (PTCDI, a kind of air-stable n-type organic semiconductor), which is designed based on two key criteria (one is the electron donor-acceptor feature of PTCDI resulting from the presence of electron-rich 4-dimethylaminobenzyl moiety, and the other is bisolvent-induced π - π stacking morphology with the assistance of dodecyl modification), as a sensitizer to combine with Pt/ TiO_2 nanoparticles via solution processing.¹⁹⁸ Although the photoactivity of the fabricated PTCDI/Pt/ TiO_2 is unsatisfied, PDI-based dye-sensitized semiconductors hold potential for practical application due to their excellent light harvesting, good photochemical and thermal stability, and flexible structural design as mentioned by the authors.¹⁹⁸ More recently, Ghosh and Devi's group used a conjugated azo compound, 4-((2-hydroxynaphthalen-1-yl)diazenyl)benzoic acid (4ABBN) as organic linker to assist

electron conduction and transfer of ZnO to develop a ZnO-azo composites with combined features of ZnO and 4ABBN.¹⁹⁹ In which 4ABBN acts as dye to facilitate visible light absorption, and causing an enhanced visible-light-responsive H₂ production activity without co-catalysts.¹⁹⁹

Generally, the advantage of metal-free organic dyes is the ease of tuning their photophysical properties through the structural modification. For instance, the absorption spectra of organic dyes can be tuned by careful consideration of the HOMO-LUMO levels via changing the length of the conjugated system and the electron-donation ability of the donor moiety. The above research results indicate that organic dyes are a very promising choice with a desired synergy to efficiently harness solar light for H₂ production. Undoubtedly, deeper insight the effect of dye structures on the photoexcited electron transfer and photocatalytic mechanism is very important for the development of metal-free organic dye-sensitized H₂ production systems.

Table 3 Summary of metal-free organic dye-sensitized semiconductor systems for photocatalytic H₂ production

Catalyst	Reaction condition	H ₂ production activity	AQY /%	Ref.
EB, RB, RhB, or ER-Pt/ZnO	$\lambda \geq 420$ nm, 0.4 mM dye, 0.2 M TEA	1.35 $\mu\text{mol min}^{-1}$ with I ⁻ (RB)	0.98%	135
EY-Pt/TiO ₂ through Fe ³⁺	$\lambda \geq 420$ nm, 0.79 M TEOA, pH7.00	275 $\mu\text{mol h}^{-1}$	19.1%	136
EY-Pt/Na ₂ Ti ₂ O ₄ (OH) ₂	$\lambda \geq 420$ nm, 15vol% TEA	75.45 $\mu\text{mol h}^{-1}$	14.97%	137
EY-Pt/N-TiO ₂	$\lambda \geq 420$ nm, 0.79M TEOA	160 μmol in 2h.	--	138
EY-(S/TiO ₂ or P/TiO ₂)/Pt, S (P) is treated by sulfuric (phosphoric) acid	$\lambda \geq 420$ nm, 95 mM TEOA, pH7.00	50.6 (S/TiO ₂) and 55.8 (P/TiO ₂) $\mu\text{mol h}^{-1}$	8.9%(S/TiO ₂) 9.8%(P/TiO ₂)	139
EY-TiO ₂ /CuO	$\lambda \geq 420$ nm 15vol% TEA	10.56 $\mu\text{mol h}^{-1}$	5.1%	141
EY-Pt/Ti-MCM-41	$\lambda \geq 420$ nm, 15vol% TEA	0.921 mL h ⁻¹	12.0%	142
EY-Pt/MWCNT	$\lambda \geq 420$ nm, TEA	3.4 mmol h ⁻¹ g ⁻¹	12.1% at $\lambda = 420$ nm	145
EY-CuO/Cr ₂ O ₃ -MWCNTs	$\lambda \geq 420$ nm, 15% TEOA	67.2 μmol in 3 h	5.43% at $\lambda = 450$ nm	146
EY-Pt/RGO	$\lambda \geq 420$ nm, EY/RGO(10/3), 15% TEOA	720.3 μmol in 96 h ($\lambda = 520$ nm)	9.3% at $\lambda = 520$ nm	147
EY/RB co-sensitized G/Pt (ER-G/P)	$\lambda = 520+550$ nm, 15% TEOA, EY, RB and H ₂ PtCl ₆	--	37.3% (ER)	148
EY/RB co-sensitized (ER)-G/Pt; ER-TiO ₂ /Pt; ER- GO/Pt	$\lambda \geq 420$ nm, 15% TEOA containing EY, RB and H ₂ PtCl ₆	36.7 $\mu\text{mol h}^{-1}$ (ER)	9.4%	148
RB-(G, GO, MWCNT)/(Pt, Pd, Rh, Ru, Au, Ag, and Ir)	$\lambda \geq 420$ nm, catalyst suspension containing electron donor	~16 $\mu\text{mol h}^{-1}$ (Ru)	18.5% at $\lambda = 550$ nm	149
EY-G/(Co or CoS _x)	$\lambda \geq 420$ nm, 1 mM EY, 10% TEOA	~ 700 μmol in 3 h	8.71% at $\lambda = 520$ nm	150
EY-CoSn _x O _y /G	$\lambda \geq 420$ nm, 1 mM EY, 10% TEOA	976.4 μmol in 3 h	20.1% at $\lambda = 430$ nm	151
EY-RGO/MoS ₂ (layered); EY-MoS ₂ (particles)	$\lambda \geq 420$ nm, 15% TEOA	88.5 $\mu\text{mol h}^{-1}$ (layered)	24.2% at $\lambda = 460$ nm	152
EY-mpg-C ₃ N ₄ /Pt	$\lambda \geq 420$ nm, 15% TEOA, H ₂ PtCl ₆	115.5 $\mu\text{mol h}^{-1}$	19.4% at $\lambda = 550$ nm	152
EY-Pt/POM α -[AlSiW ₁₁ (H ₂ O) ₃₉] ⁵⁻	$\lambda \geq 420$ nm, TEOA-H ₂ PtCl ₆	~300 μmol in 5h	28% at $\lambda = 520$ nm	156
EY-fixed Pt/TiO ₂	$\lambda \geq 460$ nm, TEOA	~7 mmol in 21 h	10% at $\lambda = 520$ nm	158
ErB-Pt@TiO ₂	$\lambda = 500+400$ nm, 15wt % TEOA	~16 μmol in 2 h	--	160
RhB-Co/TiO ₂	$\lambda \geq 400$ nm, water	227.3 $\mu\text{mol h}^{-1}$ g ⁻¹	--	161
EY-Ni(OH) ₂ /TiO ₂	$\lambda \geq 420$ nm, 1.0wt% Ni(OH) ₂ , 5%	15.76 $\mu\text{mol h}^{-1}$	--	162

	TEOA			
EY-Pt/mesoporous TiO ₂	$\lambda \geq 400$ nm, DEOA	~ 2.5 mL h ⁻¹	--	164
ErB-Pt/g-C ₃ N ₄ nanosheets	$\lambda \geq 550$ nm, 5% TEOA, 0.2 g ErB	162.5 $\mu\text{mol h}^{-1}$	33.4% at $\lambda = 460$ nm	171
ErB-MoS _x -g-C ₃ N ₄	$\lambda \geq 420$ nm, 39 μM (NH ₄) ₂ MoS ₄ , 0.79 M TEOA, pH7.00	120 μmol in 5 h	8.3% at $\lambda = 545$ nm	172
EY-RGO or EY-Pt/RGO	$\lambda \geq 420$ nm, $w_{\text{EY}}:w_{\text{RGO}}:w_{\text{Pt}}$ (1:1:0.1), 15% TEOA	0.4 mmol h ⁻¹ g ⁻¹	--	173
RhB-Pt/Uio-66(Zr) (MOF)	$\lambda \geq 420$ nm, 10% TEOA, pH7.00	116 $\mu\text{mol h}^{-1}\text{g}^{-1}$	--	175
EB-Uio-66 (MOF)	$\lambda \geq 420$ nm, 30 mg ErB, 0.5 wt% Pt	4.6 $\mu\text{mol h}^{-1}$	0.25% at $\lambda = 420$ nm	176
ErB-MIL-101 (MOF)-Ni/NiO _x	$\lambda \geq 420$ nm, 30 mg ErB	125 $\mu\text{mol h}^{-1}$	--	177
EY-GN (rGO/Ni)	$\lambda \geq 420$ nm, 0.2 mM EY, 77 mM TEA	94.3 $\mu\text{mol h}^{-1}$	30.3% at $\lambda = 470$ nm	178
EY-TiO ₂ -CoL(co-cat.) Co(phen) ₂ L(PF ₆) ₃	$\lambda \geq 420$ nm, 4 μmol EY, 5% TEOA	90 μmol in 6 h	TON=90/Co L2	179
TO-SCA[4]/Pt-TiO ₂	$\lambda \geq 450$ nm, 0.2 M TEOA	~ 200 $\mu\text{mol h}^{-1}$	10.4% at $\lambda = 460$ nm	180
Cation dyes (Th, NBA, MB, SO), and EY, RhB-TiO ₂	Visible light, 5% TEOA	2000 μmol in 20 h (EY-Pt/TiO ₂)	--	181
Coumarin -Pt/H ₄ Nb ₆ O ₁₇ and IrO ₂ -Pt/WO ₃	$\lambda \geq 400$ nm, 5 mM KI	~ 25 (H ₂) and ~ 10 (O ₂) μmol in 8 h (NKX2677)	$\leq 0.1\%$ at $\lambda = 500$ nm	184
Merocyanine (NK-2045-Pt(in)/H ₄ Nb ₆ O ₁₇)	$\lambda \geq 410$ nm, 10 mmol NaI, acetonitrile/water (95/5)	> 70 μmol in 2 h	--	185
Merocyanine (NK-2045- Pt/TiO ₂), coumarin (C-343- Pt/TiO ₂)	$\lambda \geq 410$ nm, 10 mmol NaI, 95vol% acetonitrile	~ 3.5 $\mu\text{mol min}^{-1}\text{(M)}$; ~ 2.6 $\mu\text{mol /min}^{-1}\text{(C)}$	1.8% ($\lambda = 517$ nm)	186
Merocyanine (NK-2045- Pt/TiO ₂)	$\lambda \geq 440$ nm, 10 mmol NaI, 99vol% acetonitrile	~ 16 $\mu\text{mol h}^{-1}$	2% at $\lambda = 517$ nm	187
Triphenylamine-based dye (D-H, DMOM, DEO1,2, 3)-Pt/TiO ₂	$\lambda \geq 420$ nm, 0.3 μmol dye, 10 mM EDTA, pH3.00	~ 120 μmol in 5 h for DEO2	--	188
Triphenylamine-based dyes (HD, PD, MOD, MO4D) -Pt/TiO ₂	$\lambda \geq 420$ nm, 5 mM EDTA, pH3.00	--	0.27% at $\lambda = 436$ nm (MOD)	189
Triphenylamine-based dye (D1, D2, D3)-Pt/TiO ₂	$\lambda \geq 420$ nm, 10 mM TEOA or EDTA	~ 40 mol in 90 min (TEOA)	--	190
Triphenylamine-based dye DEO1-TiO ₂ + TiO ₂ mediator + Pt/TiO ₂	$\lambda \geq 420$ nm, 10 mM EDTA, pH4.00	~ 9 μmol in 8 h	--	191
4-(diphenylamino)benzaldehyde (TPA-CHO)-G/Pt	UV-vis, 1 M KI	~ 14 μmol in 6 h	0.45% mol/E	192
Phenothiazine-based dyes (P1-P5)-Pt/TiO ₂	$\lambda \geq 420$ nm, 0.495 μmol dye, 10% TEOA, pH7.00	250 μmol in 5h for P5	TON=1026	193
LI-4 and Zn-tri-PcNc-1 co-sensitized g-C ₃ N ₄	$\lambda \geq 420$ nm, 5 $\mu\text{mol g}^{-1}$ dye, 50 mM AA, CDCA	371.4 $\mu\text{mol h}^{-1}$	1.75% at $\lambda = 700$ nm	195
Naphthylbisimide based sensitizer (NDIPYPZ)-TiO ₂ /RGO	full spectrum, 10% CH ₃ OH	10 mmol h ⁻¹ g ⁻¹	TON=4790/6h	196
Pt/TiO ₂ /PDI nanowires	$\lambda \geq 420$ nm, 10% TEOA	100 $\mu\text{mol g}^{-1}$ in 24 h	--	197
Perylene tetracarboxylic diimide (PTCDI)/Pt/TiO ₂	$\lambda \geq 420$ nm, 10% TEOA	0.075 $\mu\text{mol h}^{-1}$	0.05% at $\lambda = 550$ nm	198
ZnO-4ABBN	Visible, MeOH	102 mmol in 4 h	--	199
Surface complex Binaphthol bn(OH) ₂ -Pt/TiO ₂	$\lambda \geq 430$ nm, 10% TEOA	~ 7 $\mu\text{mol h}^{-1}$	0.02% at $\lambda = 450$ nm	202
Surface complex C ₆₀ (OH) _x -Pt/TiO ₂	$\lambda \geq 420$ nm, 10 mM EDTA	~ 19 μmol in 5 h	TON=80/15 h	204
Surface complex EDTA-Pt/TiO ₂	$\lambda \geq 420$ nm, EDTA	~ 0.9 μmol in 3h	--	205
Surface complex-bisphenol A (BPA) or 4-chlorophenol (4-CP) + F-TiO ₂ /Pt	$\lambda \geq 300$ nm, 0.5 g L ⁻¹ catalyst	100 (4-CP) and 88 (BPA) μmol in 35 h	3.34 % (BPA)	206
Surface complex-Phenolic resin (PR)-Pt/TiO ₂	$\lambda \geq 420$ nm, 50 mM Na ₂ S, pH12.50	~ 700 $\mu\text{mol g}^{-1}$ in 4 h	TON=4.3/3 h	207

P3HT-g-C ₃ N ₄	$\lambda \geq 400$ nm, 3wt% P3HT, Na ₂ S-Na ₂ SO ₃	560 $\mu\text{mol h}^{-1}$	2.9% at $\lambda = 420$ nm	208
P3HT-Pt-g-C ₃ N ₄ -Au	$\lambda \geq 420$ nm, 10% TEOA	320 $\mu\text{mol h}^{-1}$	--	209
P3HT-Pt/g-C ₃ N ₄	$\lambda \geq 500$ nm, saturated AA solution	3045 $\mu\text{mol h}^{-1}$	77.4% ($\lambda = 720$ nm)	210
PANI-CdS	$\lambda \geq 420$ nm, Na ₂ S-Na ₂ SO ₃	59.8 $\mu\text{mol h}^{-1}$	--	211
PPy/g-C ₃ N ₄	$\lambda \geq 400$ nm, H ₂ O	385 μmol in 25 h	--	212
g-PAN/g-C ₃ N ₄	$\lambda \geq 400$ nm, 10% TEOA	37 $\mu\text{mol h}^{-1}$	--	213

3.5 New strategies for wide visible-light-responsive H₂ production systems

(1) **Surface ligand-to-metal charge transfer complexes.** In contrast to the common dye sensitization, another type of sensitization mechanism based on the surface ligand-to-metal charge transfer (LMCT) complex of adsorbates on TiO₂ nanoparticles was also proposed in photocatalysis. In 2014, Choi's group pointed out the difference of the surface LMCT process and the dye sensitization mechanism for photocatalytic application as shown in Fig. 15.²⁰⁰ In the case of surface LMCT sensitization, the electron is photoexcited directly from the ground state adsorbate (without involving the excited state of the adsorbate) to TiO₂'s CB. The oxidized adsorbate (with the hole left) could be further degraded into smaller molecules. Otherwise, it would be regenerated by the recombination with the photoexcited electron (back electron transfer) or by reacting with suitable electron donors. Therefore, unlike the common dye sensitization mechanism where the sensitizer itself should absorb the visible light, a variety of organic or inorganic compounds (that do not absorb visible light) with suitable HOMO levels can be potential LMCT sensitizers.

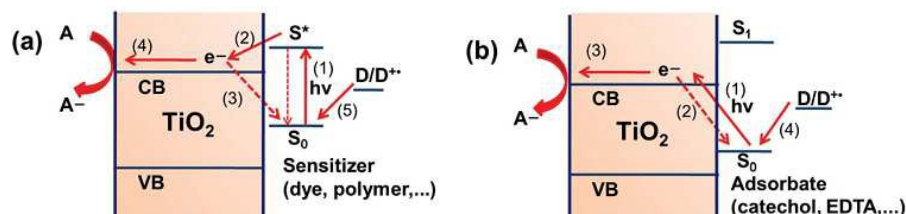


Fig. 15 The schematic illustration of two similar types of visible light sensitization of TiO₂. (a) Dye sensitization; (b) LMCT sensitization. Figure reproduced with permission from ref. 200. Copyright 2014, The Royal Society of Chemistry.

Early in 1983, Grätzel's group found that 8-hydroxy-orthoquinoline (HOQ) can be used to modify TiO₂ to form a bright yellow orange-colored powders with visible-light-induced H₂ production activity though neither TiO₂ nor HOQ absorbs visible light.⁶⁵ Rajh and co-workers investigated the improving optical and charge separation properties of Vitamin C (VC) modified TiO₂ through electron paramagnetic resonance (EPR), and found that charge pairs in this system are instantaneously separated into two phases: the holes on the donating organic modifier and the electrons in TiO₂'s CB.²⁰¹ Ohtani's group reported a intramolecular LMCT with binaphthol (bn(OH)₂) modified TiO₂/Pt (formation of a deep yellow-colored surface complex) for H₂ production even with irradiation of $\lambda > 540$ nm and a AQY of 0.2% was obtained at 450 nm.²⁰² Gómez's group investigated the LMCT complex formed on adsorption of catechol on anatase NPs using *in situ* photoelectrochemical and spectroscopic techniques, and evidenced that the electron transfer from the adsorbate to the anatase by the development of a negative photopotential of an anatase film electrode in

contact with a catechol solution upon 514.5 or 632.8 nm laser illumination.²⁰³

Choi's group reported LMCT formed between water-soluble fullerol ($C_{60}(OH)_x$) or common electron donors (such as EDTA) and Pt/TiO₂ for visible-light-responsive H₂ production,^{204,205} and found the H₂ production accompanied by the simultaneous degradation of organic pollutants (such as 4-CP and BPA) in water using surface-modified TiO₂ under solar irradiation.²⁰⁶ Also, phenolic resin (PR with polyhydroxy to reaction with TiO₂) was used as an economical dye of TiO₂ to achieve a stable and visible-light-responsive activity through LMCT mechanism.²⁰⁷ Recently, Kim's group reported a near-IR-absorbing squaraine dye (VJ-S) sensitized core/shell nanocomposite r-NGOT/Pt (where TiO₂ is the core and reduced nanosized graphene oxide (r-NGO) is the shell) for H₂ production,⁶³ the main absorption band of VJ-S is not responsible for the sensitized H₂ production, and thus thought that its sensitization mechanism is different from that of the conventional dye-sensitized system. Namely, an electron in the ground state (HOMO) of the squaraine dye can be directly transferred to TiO₂ without involving the excited LUMO state by absorbing visible light as shown in Fig. 16. The presence of r-NGO between VJ-S and the TiO₂ surface facilitates the LMCT-type electron transfer through a strong π - π interaction.⁶³

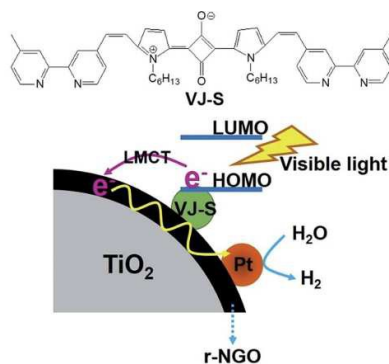


Fig. 16 Chemical structure of VJ-S and schematic diagram of surface LMCT mechanism in VJ-S/r-NGOT/Pt. Figure reproduced with permission from ref. 63. Copyright 2015, The Royal Society of Chemistry.

Unlike the common dye sensitization where the dye itself should efficiently absorb visible light, surface LMCT complexes of adsorbates formed on semiconductor surface can introduce new visible light absorbance bands though the adsorbate itself does not absorb visible light, and sunlight on them can induce a visible-light-responsive H₂ production activity through surface LMCT process. Since the popular dye sensitization always requires efficient Ru-complexes or organic dyes that often exist high cost, unstable, poisonous, and other problems such as environmental pollution in the synthesis process with more or less, this surface LMCT process has a great deal of flexibility in its design and application, such as a wide variety of organic compounds, extremely low cost, and eco-friendly. Although the corresponding investigations on LMCT induced H₂ production are limited, and even its general activity, stability and light responsive region in environmental application are also unsatisfactory, LMCT sensitization should be deeply investigated to make it a more general method of solar energy utilization in H₂ production and environmental remediation.

(2) Dye co-sensitization for broad spectral response. A useful strategy to extend the spectral responsive region for H₂ production should be the combination of two or more dyes with complementary absorption spectra to co-sensitize semiconductors. In 2012, Lu's group constructed a dye co-sensitized graphene/Pt

(ER-G/Pt) by combination of EY and RB, which exhibited a high AQY up to 37.3% at two-beam monochromatic light (520 and 550 nm) irradiation.¹⁴⁸ Although the ER-G/Pt can work better than either single dye-sensitized G/Pt under $\lambda \geq 420$ nm light irradiation, it is still lack of utilization of the whole visible light region of solar light due to the limited spectral responsive region ($\lambda \leq 600$ nm) of both EY and RB. Very recently, the present authors reported a co-sensitized $g\text{-C}_3\text{N}_4$, where D- π -A organic dye (LI-4) and ZnPc derivative (Zn-*tri*-PcNc-1) are adopted as dyes due to their complementary absorption ability, for efficient H_2 production under the vis/near-IR light region (400-800 nm as shown in Fig. 17) with high AQY of 16.3%, 7.7%, and 1.75% under 420, 500, and 700 nm monochromatic light, respectively.¹⁸⁵ Where the adsorbed LI-4 and Zn-*tri*-PcNc-1 can be excited by corresponding spectral responsive region under the vis/near-IR light, and then the photogenerated electrons are injected into $g\text{-C}_3\text{N}_4$ for H_2 production at Pt sites and the oxidation state of dyes can be regenerated by accepting electrons from electron donors for recycling. This work gives a clear advance toward panchromatic responsive photocatalytic application by combining two different dyes with complementary absorption spectra on one kind of semiconductor.¹⁹⁵

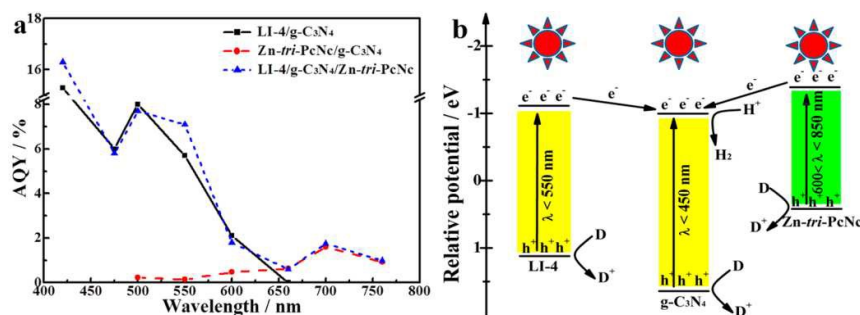


Fig. 17 (a) Wavelength-dependent AQY curves of various dye-sensitized $g\text{-C}_3\text{N}_4$ under different monochromatic light irradiation; (b) proposed co-sensitization mechanism of $g\text{-C}_3\text{N}_4$ for photocatalytic H_2 production. Figures reproduced with permission from ref. 195. Copyright 2015, American Chemical Society.

(3) Some conducting polymer: a possible broad spectral responsive dye. Recently, some conducting polymers such as poly(3-hexylthiophene) (P3HT), polyaniline (PANI), and polypyrrole (PPy), were used to improve the H_2 production activity of semiconductors.²⁰⁸⁻²¹² In 2011, Yan and Huang introduced a P3HT-Pt/ $g\text{-C}_3\text{N}_4$ composite for H_2 production from $\text{Na}_2\text{S}\text{-Na}_2\text{SO}_3$ solution, and found that the absorption intensity of $g\text{-C}_3\text{N}_4$ -P3HT increases remarkably with enhancing P3HT amount accompanied by absorption edge redshift of ~ 200 nm (to 656 nm) compared with $g\text{-C}_3\text{N}_4$ alone.²⁰⁸ The H_2 production activity increases by up to 300 times when 3wt% P3HT is added, corresponding to quantum yield of 2.9% at 420 nm. The efficient charge transfer between $g\text{-C}_3\text{N}_4$ and P3HT is seemingly responsible for the enhanced activity.²⁰⁸ Recently, the same group constructed a tightly coupled heterostructure of $g\text{-C}_3\text{N}_4/\text{Au}/\text{P3HT}/\text{Pt}$ by a self-assembling method, the corresponding visible-light-responsive H_2 production activity at an optimal P3HT content of 0.5wt% was $320 \mu\text{mol h}^{-1}$ in TEOA solution.²⁰⁹ In which, P3HT was thought as an “electric wire” which transfers the electrons to the far end (to separate the electron-hole pairs) where Pt use them for H_2 production, and the combination of electrons on the Au surface with the holes from the HOMO of P3HT is favourable for preventing the charge recombination in the body of $g\text{-C}_3\text{N}_4$ and P3HT. Therefore, Pt could obtain more electrons for H_2 production, and $g\text{-C}_3\text{N}_4$ can retain more holes for the oxidation of TEOA as shown in Fig. 18.²⁰⁹

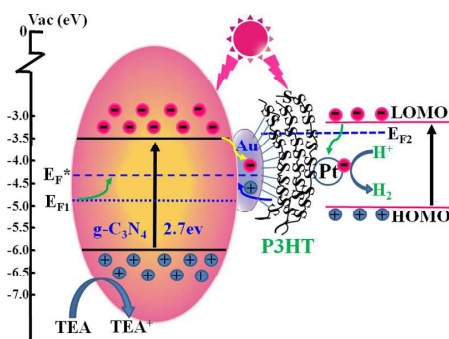


Fig. 18 Schematic of the photocatalytic mechanism of $g\text{-C}_3\text{N}_4/\text{Au}/\text{P3HT}/\text{Pt}$ heterostructure. Figure reproduced with permission from ref. 209. Copyright 2015, The Royal Society of Chemistry.

Similarly, the present authors fabricated a robust surface heterojunction (SHJ) photocatalyst (P3HT-Pt/ $g\text{-C}_3\text{N}_4$) through optimizing the composition and photoreaction conditions (especially the effect of oxidation half reaction by using different sacrificial agents), and found the AQY of P3HT-Pt/ $g\text{-C}_3\text{N}_4$ containing 3wt% P3HT at 420 nm can be enhanced to 77.4% by using an optimal AA concentration.²¹⁰ In addition, the P3HT-Pt/ $g\text{-C}_3\text{N}_4$ can produce H_2 with impressive AQY of 59.4%, 20.2%, 3.2% and 0.68% at 500, 600, 700 and 800 nm monochromatic light irradiation, respectively. That is, the P3HT can response rather wide solar light region (up to 800 nm), which almost cannot be reached by other types of dyes. The extremely high photoactivity is caused by the wide visible light absorption, efficient charge transfer at the interface of P3HT/ $g\text{-C}_3\text{N}_4$, and suitable oxidation half-reaction caused by the added AA as sacrificial agent as shown in Fig. 19.²¹⁰ This not only demonstrates a new direction for the solar fuel conversion over the large family of polymer-based semiconductors, but also emphasizes the importance of oxidation half-reaction caused by the sacrificial agent, which significantly affects the photoactivity for H_2 production.

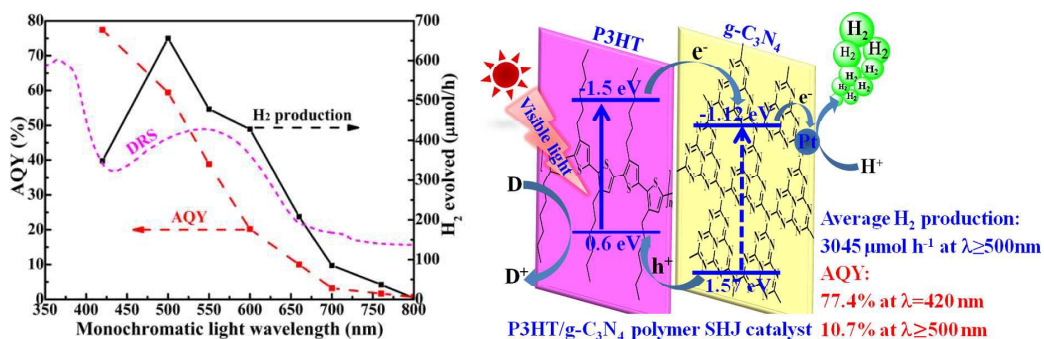


Fig. 19 Wavelength-dependent photoactivity and AQY curve (left) and the proposed mechanism (right) of 3 wt% P3HT/ $g\text{-C}_3\text{N}_4$ SHJ catalyst in 250 mM AA solution. Figures reproduced with permission from ref. 210. Copyright 2015, American Chemical Society.

Except for P3HT, PANI and PPy were also combined with semiconductors to visible-light-induced H_2 production.²¹¹⁻²¹³ By use PANI as a template, Guo's group fabricated a series of PANI-CdS composites, where electrons transferring from PANI to CdS can increase the amount of photoelectrons, and thus the PANI-CdS composite with optimal molar ratio has a H_2 production activity of 59.82 $\mu\text{mol h}^{-1}$, which is 7.7 times as high as that of CdS.²¹¹ Chen's group reported that an enhanced photoactivity of $g\text{-C}_3\text{N}_4$ for H_2 evolution from pure

water is achieved by loading dispersed PPy nanoparticles at a very low weight ratio.²¹² The surface junction formed by the dispersed PPy nanoparticles on g-C₃N₄ and the hole oxidized p-doped PPy facilitate the photogenerated charge separation, and causing the H₂ production activity increases up to 50 times for g-C₃N₄ with 1.5wt% PPy on g-C₃N₄ in a pure water system, excluding the need for sacrificial agents.²¹² Different the above sensitization mechanism, Chen and Hao's group used graphitized polyacrylonitrile (g-PAN) nanosheets as electron acceptor and transfer channel from g-C₃N₄ as shown in Fig. 20, and 5wt% g-PAN/g-C₃N₄ has optimal H₂ production activity of 37 $\mu\text{mol h}^{-1}$, exceeding 3.8 times over the pristine g-C₃N₄.²¹³

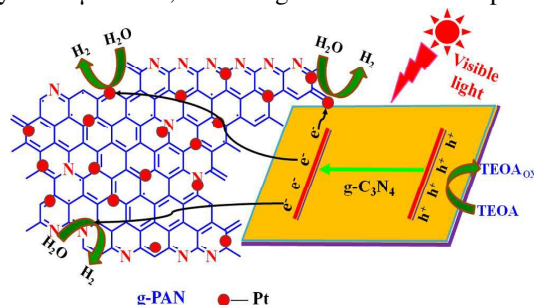


Fig. 20 Schematic illustration for the enhanced photogenerated charge carriers separation and transfer in the g-PAN/g-C₃N₄ composites for under visible light irradiation ($\lambda > 400$ nm). Figures reproduced with permission from ref. 213, Copyright 2014, American Chemical Society.

Generally, those conducting polymers used can absorb visible light, and the co-existing components (polymers and g-C₃N₄) can give a co-excited mechanism by the combination of irradiations with different wavelengths as shown in Fig. 19. It is similar to the heterojunction for efficient separation of the photogenerated carriers, but different from Z-type system as shown in Fig. 4b. As we know, the light absorbing materials in polymer bulk heterojunction solar cells are usually p-type polymer semiconductors, which act as electron donors and can respond at wider spectral region compared with the sensitizers used in DSSCs. For example, P3HT with a bandgap of 1.9-2.1 eV can absorb a broad visible light region (400-700). Moreover, those polymers have some additional advantages such as higher charge carrier mobility, dissolubility, processability and long-term stability, which are beneficial for greatly enhanced H₂ production activity when they are combined with inorganic semiconducting nanoparticles. Different from the above investigations on conducting polymer modification of visible-light-responsive g-C₃N₄, in which the corresponding photoactivity and AQY for H₂ production under $\lambda > 600$ nm light irradiation are not given, the present authors showed that the P3HT-Pt/g-C₃N₄ system can produce H₂ with impressive AQY in a much broader spectral region (400-800 nm) as shown in Fig. 19,²¹⁰ which almost cannot be reached by other types of dyes up till now. Therefore, the extremely high photoactivity is caused by the wide spectral absorption and efficient charge transfer at the interface of P3HT/g-C₃N₄. It would pave a new way to fabricate more efficient and cost-effective photocatalysts for promoting the development of solar-to-hydrogen conversion.

(4) Plasmonic metal/semiconductor heterostructures. Localized surface plasmon resonance (LSPR) effect is made up of collective oscillations of free electrons in metal (for example, Au, Ag and Cu) NPs driven by the electromagnetic field of incident light and because of which metal NPs absorb visible and IR light in particular regions.²¹⁴⁻²¹⁶ Recently, LSPR of metal NPs/semiconductors nanostructured materials has been

successfully applied to photocatalytic and/or PEC water splitting for H₂ production under visible light irradiation.^{13,18,214-223} In this type of photocatalysts, the nanostructured plasmonic metal NPs are often combined with a semiconductor (e.g., Fe₂O₃, TiO₂, CdS), and the photocatalytic reactions are initiated as a result of excitation of electrons in plasmonic metals by LSPR under visible light absorption, during which LSPR promotes the generation of e⁻-h⁺ pairs in semiconductor.²¹⁴ Usually, the enhanced H₂ production activity can be ascribed to three main mechanisms: 1) the near-field enhancement of the localized plasmons, 2) the increase of the scattering effect, and 3) the excitation e⁻-h⁺ pairs in the semiconductor due to the plasmonic energy transfer from the metal NPs to the semiconductor.²¹⁴⁻²¹⁶

Generally, suitable plasmonic metal type and nanostructure design benefit a higher H₂ production activity of the metal NPs/semiconductor photocatalysts.^{18,217-223} Barreca and Fornasiero's group prepared ε-Fe₂O₃ nanorod arrays on Si(100) substrates via chemical vapor deposition (CVD) followed by Ag or Au deposition with a radio frequency (RF) plasmochemical reactor and annealing in air at 400°C, and found that the obtained Ag/ε-Fe₂O₃ and Au/ε-Fe₂O₃ nanocomposites yielded a high dispersion of metal NPs into the oxide matrix, with a spatial distribution and chemical state dependent on the nature of the metal itself.¹⁸ That is, Au NPs mostly concentrate on the top of columnar ε-Fe₂O₃ arrays, while Ag-containing aggregates are evenly distributed through out the entire Fe₂O₃ thickness as shown in Fig. 21, which then causing different light harvesting and H₂ production efficiency (Fig. 21).¹⁸ The incorporation of Au NPs into ε-Fe₂O₃ enabled to obtain a significant H₂ production under visible light, while no appreciable visible-light-responsive activity was observed due to the partial Ag surface oxidation to Ag₂O, which precludes the contribution from LSPR process.¹⁸ Also, Tanaka et al. and co-workers showed that the preparation methods of Au/TiO₂ greatly influence the H₂ production activity under visible light, and the SPR of Au NPs exhibited stronger photoabsorption at ~550 nm.²¹⁷ These authors also suggested that the co-existence of large (>10 nm) and small (< 5 nm) Au NPs in Au/TiO₂ prepared by multistep photodeposition method contributed to stronger SPR photoabsorption and enhanced H₂ production activity under visible light.²¹⁸ Moreover, a Janus morphology of Au/TiO₂ generates extremely strong localization of the plasmonic near-field close to the Au/TiO₂ interface, leading to the enhancement of photoabsorption and the carrier generation, and thus causing a higher H₂ production activity.²¹⁹ Torimoto and co-workers prepared a novel CdS@SiO₂//Au@SiO₂ hybrid photocatalyst, in which Au NPs and CdS NPs separated by an insulating SiO₂ layer, and found that the Au NP core acts as light harvesting unit and the local electric field around Au NP cores is enhanced *via* LSPR, while the SiO₂ layer works as an insulator layer to prevent the direct electron transfer from CdS to Au NPs.²²⁰

The introduction of LSPR into photocatalysis can efficiently improve the H₂ production activity under visible light irradiation, and offered a new opportunity to solve the problem of the limited efficiency of photocatalysts.²²¹⁻²²³ However, the electron-transfer pathway is not fully understood though some efforts have been made to illustrate the working mechanism of plasmonic metal NPs/semiconductors nanostructured photocatalysts.²²¹⁻²²³ In addition, metal NP size, shape and other parameters are sensitive to the LSPR absorption, which may affect the electron-transfer efficiency and the final photocatalytic performance. For further comprehend the picture of this area and make comparisons possible, readers are encouraged to consult the recent informative reviews.²¹⁴⁻²¹⁶

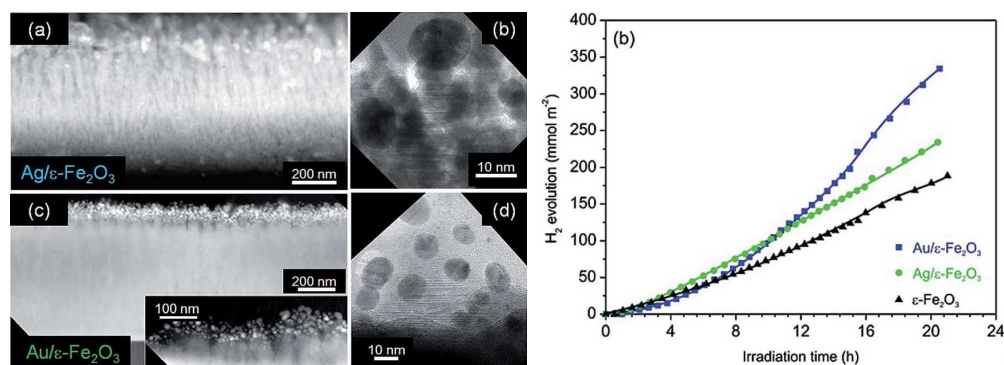


Fig. 21 Cross-sectional STEM-high angle annular dark field (HAADF) images of (a) Ag/ε-Fe₂O₃ and (c) Au/ε-Fe₂O₃ (the high-Z NPs appear brighter than the matrix), TEM images of the sample surface with (b) Ag and (d) Au NPs (left). The integrated H₂ production on ε-Fe₂O₃, Ag/ε-Fe₂O₃, and Au/ε-Fe₂O₃ under solar illumination (right). Figures reproduced with permission from ref. 18. Copyright 2014, The Royal Society of Chemistry.

On the whole, various light-absorbing materials, such as surface LMCT complexes,^{63,65,201-207} conducting polymers,²⁰⁸⁻²¹³ plasmonic metal NPs,^{13,18,214-223} and even inorganic heteropoly blue anions,²²⁴⁻²²⁶ give some new directions for extending the spectral absorption region and/or enhancing the photoactivity for H₂ production. However, the corresponding investigations on photochemical behavior and photocatalytic mechanism are rather insufficient compared with Ru-complexes and xanthene dyes, and thus the following research directions could be identified: 1) the mechanism and stability of surface LMCT complexes should be further investigated so as to exploit more low-cost and efficient H₂ production systems; 2) intensive investigation on the interaction and charge carriers transfer mechanism between conducting polymers and semiconductors is vital for attaining wider spectral responsive region and higher solar light utilization efficiency; 3) although a 1+1≈2 dye co-sensitization system for H₂ production was fabricated as shown in Fig. 22,¹⁹⁵ constructing 1+1>2 co-sensitization system through designing and choosing dyes with more suitable complementary absorption spectra and synergistic effect should be attracting in the practical application.

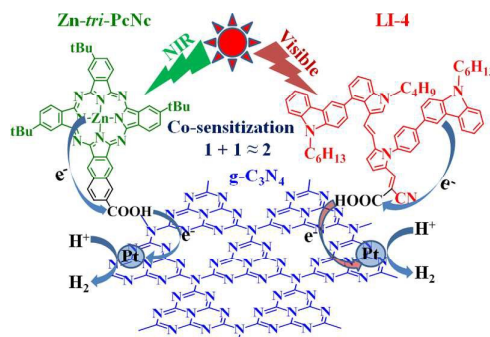


Fig. 22 Visible/near-IR-light-induced H₂ production over g-C₃N₄ co-sensitized by organic dye and zinc phthalocyanine derivative. Figure reproduced with permission from ref. 195. Copyright 2015, American Chemical Society.

4. An overview of the components of dye-sensitized H₂ production system

Except for the light-absorbing dye, the semiconductor as electron relay and reaction matrix, co-catalyst as active sites, and sacrificial electron donor for dye regeneration also significantly affect the photoactivity because those dominate the photogenerated charge generation, separation, transfer and recombination in a dye-sensitized semiconductor system. Therefore, the photosensitization between one dye and different semiconductors and/or electron donors may be very different, or even vice versa. Ray's group reported that H₂ production activity was affected by several factors such as Pt loading, solution pH, EY/TiO₂ mass ratio, TEOA concentration, and even light intensity, and found that the oxidation of TEOA and formaldehyde formation are correlated with H₂ production in both solar and visible lights.¹⁵⁹ However, their reaction mechanisms were different, and formaldehyde is oxidized by h⁺/HO• to produce H₂ under solar light.¹⁵⁹ These investigations would be helpful in developing proper design for solar H₂ production systems. Some overviews on the effects of those components in dye-sensitized H₂ production systems are given as follows.

4.1 Semiconductors

In dye-sensitized systems, it is no longer necessary that the bandgap of semiconductor straddles the potentials of water reduction and oxidation as shown in Fig. 1 since the dye would act the role of light harvesting. This gives the dye-sensitized systems a great deal of flexibility in its component design and application. Nevertheless, semiconductor is still an important matrix for supporting dye adsorption for light harvesting, co-catalyst adsorption for H₂ and/or O₂ production, dye regeneration, and electron relay/transfer, and thus its CB level should be lower than the LUMO level of dye and higher than the potential of water reduction as shown in Fig. 6. Therefore, semiconductors usually require high specific surface area and stability, good electron transfer property and dye affinity, energy level matching with dye, as well as low cost and toxicity, *etc.* Furthermore, in some dye-sensitized systems with two-step (Z-type) excitation¹¹¹⁻¹¹³ and semiconductor/dye²¹⁰⁻²¹² mechanisms, the semiconductors can also absorb photons in addition to the visible absorbing of dye.

Except for the most popular TiO₂ and its doped products, some other metal-containing semiconductors, such as SnO₂,^{66,86} ZnO,^{136,199} niobates,^{32,49,50,72,73,88-91,184,185} titanates,^{68,74,137,163,165} tantalate,^{111-113,182} TaON,¹¹⁴ BiOCl,¹²⁵ polyoxometalates,¹⁵⁶ CdS,^{211,215} inorganic nickel species,¹⁶⁹ and even some magnesium aluminum silicate minerals,^{155,170} are widely used as electron relay in the dye-sensitized H₂ production systems. Moreover, a series of porous materials such as zeolites and its oxide-loaded products,^{75,143} mesoporous metal oxides and its semiconductor loaded materials,^{74,77,142,143,165-168} and even metal-organic frameworks (MOFs),^{103,120,175-177,227,228} are also utilized as electron carrier in dye-sensitized photocatalytic H₂ production. Interestingly, different from those dye adsorption in porous materials, some photoactive dyes such as Ru(tpy)₂, TCPP, and [Ir(ppy)₂(bpy)]⁺-derived dicarboxylate ligands were incorporated into MOFs as parts of linkers for efficient H₂ production under visible light.^{103,120,227}

With the development of carbon nanostructured materials and analogues, some metal-free semiconductors were also employed as a visible-light-driven photocatalyst for H₂ production. Compared to typical metal-containing visible-light-active semiconductors, the photoactivity of metal-free semiconductors is limited due to the strong photogenerated charge recombination. Therefore, metal-free semiconductors such as MWCNT,^{145,146,148,149,174} GO/RGO,^{70,79,102,117,123,124,147-152,173,178,192} and g-C₃N₄,^{122,126-128,133,153,154,171,172,195,208-213} were adopted in dye-sensitized systems for H₂ production. Those results demonstrate the feasibility of using

G/GO/RGO and g-C₃N₄ as an efficient reaction matrix and/or electron relay mediator, which holds tremendous potential for practical applications.

4.2 Co-catalysts

As we know, co-catalysts on semiconductor can extract photogenerated carriers, host active sites for catalytic H₂ and/or O₂ production, reduce the overpotential loss for gas evolution, and thus improve the activity and stability of photocatalysts by suppressing the charge recombination and/or photocorrosion. Currently, majority of the developed photocatalytic systems use noble-metal-based co-catalysts, such as Pt, Ru, Rh, Pd, Au, Ag, or their alloys, to achieve high H₂ production activity. Among which, Pt is the most effective co-catalyst due to its largest work function and lowest overpotential for H₂ evolution. Nevertheless, large-scale usages of these noble metals as co-catalysts are questionable due to the high cost and scarcity in nature. Therefore, the development of noble-metal-free co-catalysts with high catalytic efficiency is substantially desirable for the practical applications. Since there are some informative reviews on the co-catalysts (including noble-metal-free co-catalysts) for the H₂ production in photocatalysis and photoelectrocatalysis,²²⁹⁻²³² herein the limited examples of co-catalysts used in dye-sensitized semiconductors for H₂ production are focused on.

In a dye-sensitized system, the recombination process between the semiconductor's CB electrons coming from excited state dye and the oxidation state dye is usually competitive with the H₂ production process, and co-catalysts on semiconductor surface can promote both the photogenerated carrier separation and H₂ evolution as active sites. Also, co-catalysts usually enhance the dye adsorption capacity on the semiconductor. For example, Lu's group reported that the number of adsorbed EY on M/TiO₂ (M=Pt, Ru and Rh) increased with enhancing noble metal loading significantly.¹⁴⁰ It indicates that co-catalysts can promote both the dye adsorption (adsorption effect) and the charge separation of CB-e⁻ and VB-h⁺ pairs (charge separation effect), which then lead to an enhanced H₂ production activity. For a long time, most works based on dye-sensitized semiconductors take Pt as the only co-catalyst for H₂ production as can be seen from Table 1-3, and researches on using noble-metal-free co-catalysts are still relatively rare though dye-sensitized H₂ production has been investigated for more than 30 years. Recent researches indicated a number of noble-metal-free co-catalysts including inorganic Ni-based species,^{62,162,163,169,177,178} Cu-based species,^{141,146} Co-based species,^{150,151,161} molybdenum sulfide,^{152,172} [NiFeSe]-hydrogenase,^{95,96} and molecular Co/Ni co-catalyst,^{58,92-92,179,233} are promising as substitutes for Pt co-catalyst in dye-sensitized semiconductor systems.

Nickel, as one of earth-abundant elements, its metal and inorganic species as co-catalysts have been received growing attentions owing to its electrochemical stability and low cost.^{62,162,163,177,178} In 2014, Du's group reported Ni(OH)₂ can act as an efficient co-catalyst for H₂ production over EY-sensitized TiO₂ in TEOA solution, and 1.0% Ni(OH)₂/TiO₂ showed an optimal H₂ production activity of ~15.76 μmol h⁻¹, which is ~90 times higher than pure TiO₂ under the same condition.¹⁶² After 5 h of irradiation, the composite with Ni(OH)₂ shows much higher activity than TiO₂ with other first-row transition metal-based oxide/hydroxides as co-catalyst.¹⁶² More recently, Li's group investigated the effects of titanate nanotube (TNT) modified with different nickel precursors on the EY-sensitized H₂ production activity, and found that more Ni²⁺ intercalate into the TNT's interlayer when NiCl₂ is used as a precursor.¹⁶³ During the calcination process, the titanate transforms into anatase TiO₂, and Ni²⁺ ions are reduced and doped partly in TiO₂, which then promotes the

formation of oxygen defects and increases the conductivity of TNT. The formed Ni particles can be oxidized in air to form core/shell structure (Ni@NiO), and the enhanced photoactivity of EY-sensitized Ni-modified TNT can be attributed to the higher conductivity and more effective formation of Ni@NiO structure.¹⁶³ Yuan and Xue's group also reported that Ni/NiO_x particles on ErB-sensitized MOFs (MIL-101) can boost H₂ production from TEOA solution under visible light, and the highest H₂ production activity of 125 μmol h⁻¹ was achieved from the system containing 5wt% Ni-loaded ErB-sensitized MIL-101.¹⁷⁷ The enhancement on H₂ production is attributed to the efficient charge transfer from photoexcited dye to the Ni co-catalyst via MIL-101. Moreover, the Ni/NiO_x co-catalysts show excellent stability for long-term photoreaction.¹⁷⁷

Li's group prepared graphene decorated with Ni nanoparticles via one-pot reduction using graphene oxide (GO) as a precursor, and found that the as-prepared composite (GN) exhibits a great synergetic effect of RGO and Ni for H₂ production, and the highest AQY for dye-sensitized H₂ production at 470 nm reaches 30.3% under the optimal conditions.¹⁷⁸ Similarly, a NiS_x co-catalyst decorated graphene nanohybrid (NiS_x/G) was also prepared by Lu's group, in which Ni²⁺ was first adsorbed onto graphene and subsequently reacted with S²⁻ to yield NiS_x/G.⁶² It was found that the NiS_x/G exhibited H₂ production activity is 2-fold higher than that of pristine NiS_x under visible light, and the highest AQY of 32.5% is reached at 430 nm when EY is used as sensitizer. In this system, graphene not only provides a large area and two-dimensional substrate for the confined growth of NiS_x but also greatly enhances the transfer of photoelectrons from excited EY to the NiS_x, and thus causing the great enhancement of H₂ production.⁶² More interestingly, Xu's group reported that a series of Ni-based inorganic nanoparticles, such as metallic Ni, NiO, NiS, and NiSe, are capable of producing H₂ from TEOA solution when sensitized by xanthene dyes (ErB, ErY, RB, EY and FL).¹⁶⁹ Among those, the best H₂ production activity comes from the using of ErY as dye and NiS synthesized in ethyleneglycol as the catalyst, and the highest quantum yield is ~15% at 520 nm.¹⁶⁹ This system needs no conventional oxide semiconductor just by introducing the heterogeneous Ni-based nanoparticles into molecular systems as catalysts for H₂ production, in which photons are captured by dye for activation of the electrons, which then adopted by NiS catalyst with suitable Ni 3d and S 3p hybrid orbital, and Ni with a reduced valence state facilitates the H₂ production.¹⁶⁹ The high activity of NiS is contributed by its high electrochemical activity, metallic nature, unsaturated Ni environment and suitable Fermi energy level.¹⁶⁹

Similarly, Lu's group reported that CuO as co-catalyst incorporated TiO₂ (CuO/TiO₂) is of benefit to the EY adsorption, charge separation, electron transfer, and the water reduction sites.¹⁴¹ The electrons excited from the EY molecules which are strongly adsorbed both on TiO₂ and CuO inject into the CBs of both TiO₂ and CuO, the electrons in TiO₂'s CB subsequently transfers to CuO's CB, which results in a build-up of excess electrons in CuO's CB. Consequently, the accumulation of excess electrons in CuO causes a negative shift in the Fermi level, and thus the enhancement of H₂ production activity (with an AQY of 5.1%) and a good stability was obtained over the EY-sensitized 1.0wt% CuO/TiO₂ in DEA-water mixture under λ≥420 nm light irradiation.¹⁴¹ The same group fabricated a ternary composite photocatalyst (CuO/Cr₂O₃-MWCNTs-EY) through a simple impregnation-pyrolysis process, in which MWCNTs act as catalyst and carrier, CuO and Cr₂O₃ as co-catalyst and/or charge transferring sites.¹⁴⁶ The visible-light-driven H₂ production activity over CuO/Cr₂O₃-MWCNTs-EY is higher than that of CuO or Cr₂O₃ loaded MWCNTs-EY, demonstrating that simultaneous loading of CuO and Cr₂O₃ is vital to achieve the high activity.¹⁴⁶

In 2012, Yang's group prepared Co-doped TiO₂ (Co/TiO₂) by a Co(NO₃)₃ solution impregnation followed by calcination at 450°C, and used its RhB-sensitized product (RhB-Co/TiO₂) to construct an overall water splitting system for nearly stoichiometric H₂ and O₂ productions of ~227.3 and ~98.9 μmol h⁻¹ g⁻¹, respectively.¹⁶¹ It was found that the synergic effect between the RhB and Co is crucial to the water splitting reaction under visible light, and the presence of Co²⁺ on TiO₂ surface can facilitate electron transfer to the TiO₂ CB and the downshift of VB, and thus resulting in the high accumulated H₂ and O₂ production.¹⁶¹ In 2014, Lu's group fabricated a CoS_x/G and Co/G nanohybrids by one-step photoreduction and in-situ chemical deposition methods.¹⁵⁰ After sensitized by EY, CoS_x/G and Co/G nanohybrids exhibited improved H₂ production activities because graphene promotes the photogenerated electrons transfer from excited dye to the active sites such as Co or CoS_x.¹⁵⁰ Similarly, an amorphous CoSn_xO_y composite decorated graphene nanohybrid (CoSn_xO_y/G) sensitized by EY also exhibits an AQY of 20.1% at 430 nm light irradiation.¹⁵¹

In 2012, Lu's group reported a limited-layered MoS₂ co-catalyst/graphene nanohybrid, and found that the electrical coupling and synergistic effect between MoS₂ and RGO sheets greatly facilitate the electron transfer from excited dye (EY) to the active edge sites of MoS₂, where prolonged lifetime of photogenerated electrons and the improved charge separation efficiency are accomplished, and thus enhance significantly the H₂ production activity.¹⁵² EY-RGO with an limited-layered MoS₂ shows efficient H₂ production activity from TEOA solution with an AQY of 24% at 460 nm.¹⁵² Li's group prepared ErB-sensitized MoS_x loaded g-C₃N₄ (ErB-MoS_x-g-C₃N₄), and found that MoS_x as co-catalyst can promote the electron transfer among excited ErB, g-C₃N₄ and MoS_x, and then causing higher activity and stability for H₂ production than both ErB-g-C₃N₄ and ErB-MoS_x under λ≥420 nm light irradiation.¹⁷²

Hydrogenases (H₂ases), which are Fe- or Fe/Ni-containing microbial enzymes, can catalyze the reversible and selective interconversion of H₂ and 2H⁺/2e⁻.^{95,96} Armstrong's group reported a H₂ production system consisting of a [NiFeSe]-H₂ases adsorbed directly on a Ru-complex-sensitized TiO₂ nanoparticle.^{95,96} This integrated sacrificial hybrid system can produce H₂ at room temperature from neutral water and in the absence of soluble redox-mediators though its activity is lower than the maximum that hydrogenases can acquire. Although H₂ases have only limited scope for applications on an industrial scale because of the fragility of the enzyme,⁹² enlightened by the active sites in natural H₂ases to promote H₂ generation, the complexes of earth-abundant metals, such as Co, and Ni, have been used as the alternative co-catalysts in dye-sensitized semiconductors for catalyze water reduction as shown in Fig. 23.^{92-94,179-233}

Reisner's group reported a series of molecular Co/Ni co-catalysts applications in dye-sensitized systems.^{58,92-94,233} Among which, the molecular Co co-catalysts ((Et₃NH) [CoP₁] and (Et₃NH)[CoP₂], see Fig. 23) with phosphonate groups to provide a linkage to RuP-sensitized TiO₂.^{92,93} The obtained composites show visible-light-responsive H₂ activity from neutral water at room temperature using TEOA as electron donor. However, the photodegradation of the obtained composites occurs at the ligand framework of CoP₁, which can be readily repaired by addition of fresh ligand, and thus causing in TON above 300 mol H₂ (mol CoP)⁻¹ in water. This studies support that a molecular Co species, rather than metallic Co or Co-oxide precipitate, are responsible for H₂ production on TiO₂, and the electron transfer from the TiO₂ to CoP co-catalysts occurs quantitatively on a 10 ms time-scale, which is about a hundred times faster than charge-recombination with the oxidized RuP.⁹³ Moreover, the same group prepared a molecular Ni co-catalyst (NiP) with aDuBois-type

$[\text{Ni}(\text{P}_2^{\text{R}'}\text{N}_2^{\text{R}''})_2]^{2+}$ core containing an outer coordination sphere with phosphonate groups (see Fig. 23).⁹⁴ In their phosphonated RuP-sensitized NiP-loaded TiO_2 system, the electron transfer occurs via a “through particle” mechanism, where RuP* is oxidatively quenched upon injection of an electron into TiO_2 , which can subsequently be harvested by NiP, a visible-light-responsive H_2 production activity reached a maximum with 0.1 μmol NiP loading, whereby an overall TON_{NiP} of $278 \pm 19 \text{ h}^{-1}$ (after 30 h) is obtained.⁹⁴

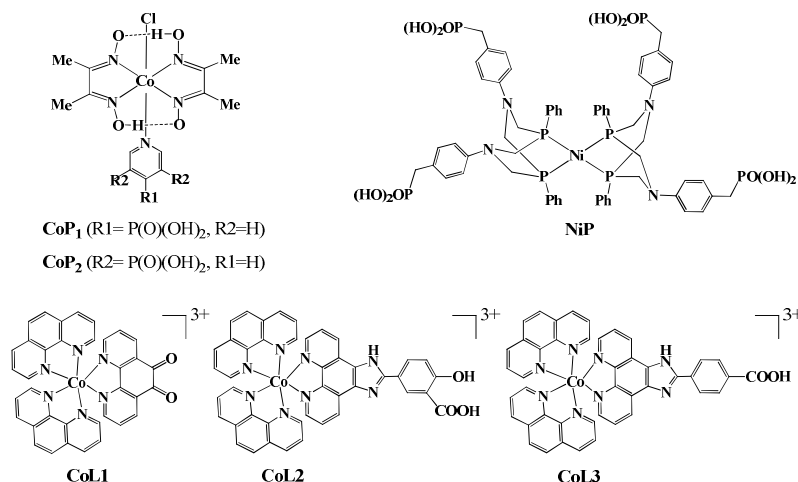


Fig. 23 Molecular structures and symbols of some molecular Co/Ni co-catalysts of dye-sensitized semiconductor systems for H_2 production.

Similarly, a molecular Ni co-catalyst was used in CQDs-sensitized system, and found that CQDs can absorb UV and visible light and directly transfer photoexcited electrons to solution based molecular electron acceptors and catalysts, and a maximum activity with respect to CQD of $398 \mu\text{mol H}_2 (\text{gCQD})^{-1} \text{ h}^{-1}$ and a TOF_{Ni} of 41 h^{-1} optimized for NiP are achieved under full solar spectrum irradiation.⁵⁸ By using transient absorption spectroscopy, they observed that the first reduction of the co-catalyst from Co^{III} to Co^{II} can proceed efficiently even without hole scavenger at sufficiently high co-catalyst coverage.²³³ In contrast, the second reduction from Co^{II} to Co^{I} , which is required for H_2 production, appears to be at least 10^5 slower, suggesting it requires efficient hole scavenging and almost complete reduction of all the adsorbed CoP to Co^{II} . Ru-complex sensitization enables visible light photoactivity though it is partly offset by slower and less efficient hole scavenging.²³³ More recently, Yin and Fan's group used three Co-complexes (CoL1–CoL3, Fig. 23) as co-catalysts of EY-sensitized TiO_2 in TEOA solution, and 2wt% CoL2/ TiO_2 exhibits a TON of 90 (based on CoL2) for H_2 production under visible light.¹⁷⁹ In addition, the EY-sensitized CoL2/ TiO_2 displays much higher H_2 production activity and stability compared with the homogeneous system though the H_2 production activity is deteriorated due to the desorption of CoL2 from TiO_2 surface and photolysis of the EY sensitizer.¹⁷⁹

Generally, the above limited applications of molecular Co/Ni co-catalysts in dye-sensitized systems demonstrate its feasibility for visible-light-responsive H_2 production though there still some problems such as instability (both photoinstability and decomposition during catalytic turnover), relatively low H_2 production activity (as compared with those metal or metal oxides loaded systems), and desorption from semiconductors (lead to obvious loss of H_2 production activity).^{58,92-94,179} Nevertheless, the above investigations pave a way for fabricating noble-metal-free heterogeneous dye-sensitized H_2 production systems based on transition metal

complexes though there is necessity for active and stable molecular catalysts for use in such systems.

4.3 Sacrificial reagents

In a dye-sensitized system, sacrificial electron donors also play a vital role since the dye regeneration and electron injection to semiconductor are assisted by the electron donor. The most commonly used electron donors are TEOA and EDTA for H₂ production, and the reversible shuttle such as IO₃⁻/I⁻ (I⁻), Fe²⁺ are used for the water splitting for H₂ and O₂ productions as shown in Table 1-3. Unlike the dye molecules and semiconductors, which are significantly affected by the relative energy level positions and their interaction, the effects of electron donors are more complicated. For example, the electron donor solution would influence pH of the reaction, dye adsorption, and even the redox potential of dye as well as the band structures of semiconductors, and then the charge transfer and injection. All those would further affect the final photoactivity for H₂ production.^{67,71,83,85,86,119,126,195,210}

Malinka and co-workers reported that the effect of electron donors on the H₂ production activity of ZnP-sensitized Pt/TiO₂ suspensions follows the order EDTA > OA > AA, as does the adsorption of these donors on TiO₂, which is determined by the pH of the suspension.¹¹⁹ Moreover, the photoactivity has a maximum at pH 4-5 for EDTA, AA and OA solutions, whereas it increases sharply in alkaline solutions when using TEOA as electron donor because the oxidation of TEOA in an alkaline solution is faster than that in an acidic solution.¹¹⁹ Kaneko's group reported the effects of electron donors (EDTA, TEOA, AA, phenol, acetone, methanol, FeCl₂, hydroquinone(HQ)) on the photoactivity of some porphine dyes and Ru-complex sensitized Pt/TiO₂ nanoparticles, and found that those reversible donors, such as Fe²⁺, HQ, AA, and phenol, are not effective, and only EDTA and TEOA are effective to produce H₂.⁶⁷ Similarly, the dependence of H₂ evolved in a TEOA solution on pH was different from that in an EDTA solution.⁶⁷ Furlong and co-workers found that the adsorption of Ru(dcbpy)₃²⁺ molecules on TiO₂ occurs when the pH of the dispersion is below the isoelectric point (IEP) of TiO₂ (pH 6.10) and increases as the pH is decreased to 4.00.⁷¹ Moreover, addition of EDTA reduces the dye adsorption at low pH 4.00, and the same phenomenon is observed with TEOA at pH 10.00.⁷¹ In addition, Ray's group found that concentration of TEOA also played a major role during H₂ production over EY-sensitized Pt/TiO₂, which varied as a function of TEOA concentration and followed Langmuir-type isotherm.¹⁵⁹ All above results suggest that H₂ production activity of dye-sensitized systems can be optimized with respect to the types and concentration of electron donor as well as pH of surrounding solution, which further determine the surface concentrations of electron donor and dye on the semiconductor.^{67,71,119,159}

Also, co-existing electron donor species would influence the electron transfer/injection processes of a dye-sensitized system. Abe's group found that the H₂ production activity of N3-Pt/TiO₂ in a water-acetonitrile solution containing iodide as an electron donor decreased with enhancing the water proportion in the solution, which is due to the decreasing electron transfer efficiency from I⁻ to dye because of the decrease in the energy gap between the redox potential of I³⁻/I⁻ and HOMO of dyes.⁸³ Maitani and Wada's group found that the combination of dye and co-existing species dominates the charge recombination, which then resulting in significant differences in the H₂ production activities over dye (N719, TPPC and TPPS) sensitized Pt/TiO₂ (or SnO₂ and ZnO) systems.^{85,86} Interestingly, the co-existing species (MeOH and TEOA) exhibit the opposite effect for TiO₂ and SnO₂ in terms of H₂ production, which are attributed to the completely different electron

transport mechanism. It demonstrates that the combinational effect among semiconductors, dyes, and co-existing species in surrounding medium is quite important for the dye-sensitized systems.^{85,86}

Although many investigations showed that the electron donor species can significantly affect the overall activity of the dye-sensitized systems through varying the oxidation half reaction,^{67,71,85,86,119,159} the relative explanations are far insufficient compared to that of dyes, semiconductors and co-catalysts. Recently, the present authors found that the H₂ production activities of dye-sensitized systems can be significantly affected by the types of electron donor (such as EDTA, TEOA, AA, and Na₂S-Na₂SO₃).^{126,195,210} Especially, the AQY of P3HT-Pt/g-C₃N₄ is improved from 4.2% to 77.4% at 420 nm when the electron donor is change from Na₂S-Na₂SO₃ to AA.²¹⁰ Although the regeneration ability of the oxidized dye in AA solution is the most unfavorable among those electron donors tested due to the minimal potential difference between redox potential of AA and HOMO of dyes in terms of the relative energy levels, all photocatalysts used exhibit the highest H₂ production activities with AA as electron donor. This result strongly suggests that the dye-sensitized system is sensitive not only to the relative energy levels but also to the electron transfer kinetics that are related to the interaction among dye molecules, semiconductor, and electron donors.

As mentioned above, many electron donors can form surface LMCT on semiconductors, and the LMCT excitation could also contribute to the visible-light-driven photoactivity.²⁰⁴⁻²⁰⁶ Theoretically, by choosing an suitable organic pollutants (with functional groups) as ligand and electron donor to form surface LMCT complexes on the semiconductors, H₂ production accompanying with the oxidative degradation of those pollutants could be attained through the surface LMCT excitation mechanism. Moreover, solar light can be fully utilized since those semiconductors can also be excited by the UV light in addition to the visible-light-driven surface LMCT excitation. Therefore, one can make the H₂ production process self-sustained accompanied by the simultaneous degradation of organic pollutants in water, which would be attracting in developing general method of solar energy utilization in H₂ production and environmental remediation.

4.4 Effects of nanostructures of dye-sensitized system on the electron transfer mechanism

Up till now, efficiency and stability issues limit greatly the applications of dye-sensitized H₂ production systems. On one hand, the rapid back electron transfer is the dominant kinetic pathway, and thus is the primary reason for the low efficiency of dye-sensitized systems.^{31,49,78,90,97,98} To transcend the charge recombination problem, co-catalyst especially Pt NPs are usually deposited to promote the activity by competitively scavenging the injected electrons from the excited dye into the metal phase (Schottky barrier electron trapping).⁷⁸ Whereas its prerequisite is that the dye excited electrons must be transferred to semiconductors before the dye molecules can relax back to the ground state.³¹ If the oxidized dye is not rapidly reduced by the sacrificial (or reversible) electron donors, the electrons injected into semiconductor can transfer back to the oxidized dye, regenerating the dye. On the other hand, dye instability is also a significant problem limiting the long-term H₂ production activity and stability of a dye-sensitized semiconductor, which include the dye desorption, oxidization and/or decomposition during the photocatalytic processes. For example, Ru-complexes are unstable in the 3+ oxidation state and susceptible to nucleophilic attack by water and buffer anions on a time scale of tens of seconds;³¹ and a major limitation to the effectiveness of some Pt-complexes (Pt(dcbpy)(met) and Pt(dcbpy)(bdt)) on Pt/TiO₂ is their instability upon oxidation.^{131,132}

Therefore, fast electron transfer between the sacrificial (and/or reversible) electron donor and the oxidized dye is critical to both the activity and stability of the H₂ production systems.³¹

Chemical attachment of the dye to the high surface area semiconductor is an important and subtle issue.^{31,49,90,97,98} Carboxylate and phosphonate are the most frequently used anchoring groups in DSSCs, and provide strong electronic coupling for ultra-fast electron injection from the dye excited state. However, dye-sensitized semiconductors for H₂ production necessarily operate in aqueous solution, making hydrolysis of those ester bonds a significant problem.^{31,49,90} Choi's group investigated the effects of surface anchoring groups (carboxylate (c-RuL₃) vs. phosphonate (p-RuL₃) on the photoactivity of dye-sensitized TiO₂,^{97,98} and inferred that the adsorption of p-RuL₃ on TiO₂ is strong enough not to be hampered by the presence of EDTA, whereas that of c-RuL₃ is significantly inhibited. As a result, p-RuL₃-sensitized TiO₂ exhibits much higher activity than c-RuL₃-sensitized TiO₂ though the visible light absorbing capabilities are comparable among those complexes with carboxylate and phosphonate groups.^{97,98} However, the photodesorption of phosphonate-bound dyes in water is accelerated in the presence of oxygen, and the electron injection efficiency of dye molecules decreases with increasing number of phosphonate groups though multiple ligands with phosphonic functionalities can hinder the dye desorption.^{97,98} The above results suggest that further work on optimizing dye attachment and electron injection efficiency is needed.^{31,97,98}

To overcome the instability of the dye-sensitized photocatalyst via ester-like linkage in water, Arakawa's group reported a strong chemical fixation of dye on TiO₂ particles by utilizing dehydration of carboxyl group of xanthenes with amino group of silane-coupling agent fixed on TiO₂ surface, and the resulted EY-fixed Pt/TiO₂ exhibits high efficiency and steady H₂ production from TEOA solution under long-term irradiation.¹⁵⁸ Kruth and co-workers encapsulated N3/TiO₂ assembly in an amino-group-containing polyallylamine layer anchored to TiO₂, the obtained photocatalyst shows a stable H₂ production activity over a period of several days under visible light irradiation.¹⁰¹ In addition, the interaction between Ru-complex and semiconductor can also be covalently binding through coordination of Ru(bpy)₂Cl₂ with pyridine (py) covalently functionalized graphene (G), and the obtained Ru(bpy)₂(py)Cl/G/Pt evokes fast electron transfer from Ru(bpy)₂(py)Cl moiety to Pt/G sheet with enhanced photoactivity and sufficient stability for H₂ production from water.¹⁰²

Except for the above chemical interaction through anchoring group or covalently linkage, Choi's group reported an alternative approach to attaching Ru-complex at the TiO₂/H₂O interface as shown in Fig. 8.⁹⁹ Where Ru(bpy)₃²⁺ cations are bounded within the nafion (Nf) layer coated on TiO₂ particle surfaces through electrostatic attraction, and its H₂ production activity is far more efficient than that of Ru(dcbpy)₃-Pt/TiO₂ through chemical tight attachment.⁹⁹ Furthermore, the same effect was also observed by introducing guanidinium cations into nafion-coated Ru(bpy)₃²⁺-Pt/TiO₂ system.¹⁰⁰ In which, Guanidinium cations located near the TiO₂ surface can repel the oxidized dye molecules to retard the recombination with CB electrons, which is confirmed by time-resolved diffuse reflectance spectroscopic and luminescence measurements. The dual roles of Guanidinium cations in the nafion layer increase the photoelectron density in TiO₂ CB and subsequently enhance the H₂ production activity.¹⁰⁰ Similarly, Lu's group reported a stable H₂ production system by introducing a lacunary Keggin-type polyoxometalate (SiW₁₁) layer on Pt/TiO₂, in which SiW₁₁ as an excellent electron relay greatly facilitates the electron transfer from the reduced dye species (EY•⁻) to TiO₂ and suppresses the decomposition of EY•⁻, and thus causing enhancement of the photoactivity and stability of

SiW11/TiO₂.¹⁵⁷ Also, Choi's group found that the H₂ production activity can be markedly enhanced by introducing a thin Al₂O₃ overlayer (~1 nm thick) on Ru(dcbpy)₃²⁺-Pt/TiO₂ with EDTA as electron donor.⁷⁸ According to the time-resolved diffuse reflectance (TDR) spectroscopy, the yield of the electron injection from the excited dye to TiO₂ is little affected by the Al₂O₃ thin layer, but it can retard the charge recombination between the CB electrons and the oxidized dye molecules.⁷⁸

The above results indicate that those additional layers such as nafion, Al₂O₃, and even polyoxometalate, on semiconductor surfaces play an important role in retarding the charge recombination,^{78,99,100,157} and highlight the physical isolation in space between the semiconductor surface and the oxidized dye molecules is a general way to develop more efficient and stable dye-sensitized photocatalyst. Nevertheless, those physical isolations should not affect the necessary electron injection and regeneration of dye, which are very important for the long-term activity and stability for H₂ production. Based on the above considerations and the present authors' relative results such as the loosely attached dyes (Ru₂(bpy)₄L₁-PF₆ and Ru(bpy)₂(him)₂-NO₃) without anchoring group linked with TiO₂ possess higher H₂ production activity than the ester-linked Ru-complex (N719) with carboxyl groups,¹⁰⁵⁻¹⁰⁸ a "dynamic equilibrium" hypothesis was proposed, that is, the dynamic equilibrium between the linkage of the ground state dye with TiO₂ and the divorce of the oxidization state dye from TiO₂ surface plays a crucial role in the photochemical behavior of dye-sensitized system as shown in Fig. 9.^{105,106} This conjecture is further validated by a more efficient binuclear Ru₂(bpy)₄(BL)(ClO₄)₂ designed on the "dynamic equilibrium" concept, its loose attachment on TiO₂ surface does not affect the excited dye's electron injection but can effectively restrain the electron transfer backward through the oxidized dye divorcing from TiO₂ surface, and corresponding dye-sensitized TiO₂ without Pt-loading shows a high AQY of 16.8% (at 420 nm) and 7.3% (at 475 nm) with a considerable stability.^{107,108}

Except for the attachment functionality, a rational architecture including the morphology and nano-organization of dye-sensitized semiconductor system is also crucial for ultimate performances for H₂ production since it would influence the dynamics of electron/hole recombination (including bulk recombination and surface recombination) processes. For example, Fang and co-workers prepared Pt@TiO₂ core-shell nanostructures (Fig. 24) through a one-step hydrothermal method. Upon ErB sensitization, the Pt@TiO₂ core-shell photocatalysts exhibit high visible-light activity for H₂ production, and a synergic effect that allows for a greatly enhanced activity for H₂ production was observed when the ErB and TiO₂ are co-excited through the combination of two irradiation beams at different wavelengths.¹⁶⁰ The enhancement is attributed to the rational spatial distribution of three components (ErB, TiO₂, Pt) on their nano-organization, and the vectored transport of photogenerated electrons from ErB to Pt particles via the TiO₂ particle bridge. The presented core-shell structures and the observed synergic effect would provide a new direction for improving the efficiency of composite photocatalysts by using selective excitation wavelengths.¹⁶⁰

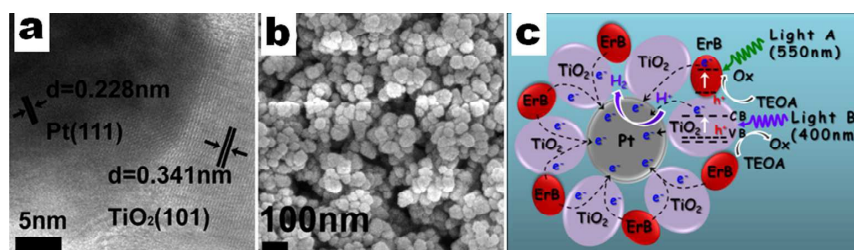


Fig. 24 HRTEM (a) and SEM (b) images of the Pt@TiO₂ core-shell nanostructures, and the schematic illustration (c) of its ErB-sensitized product's photocatalytic H₂ production mechanism under irradiation of light A (550 nm) and/or light B (400 nm). Figures reproduced with permission from ref. 160. Copyright 2014, Beilstein-Institut.

Lu's group prepared mesoporous g-C₃N₄ (mpg-C₃N₄) with high surface area and abundant nanopores in the range of 20–40 nm by a novel directly pyrolyzing urea without templates as shown in Fig. 25a.¹⁵³ The resultant mpg-C₃N₄ could serve as a promising host matrix to the assembled EY molecules and Pt co-catalyst to promote the activity via improving light harvesting and enhancing mass transfer, and the TEM image (Fig. 25b) of EY-sensitized mpg-C₃N₄/Pt indicated that Pt NPs with small particle size of ~3-5 nm can be uniformly decorated throughout on mpg-C₃N₄.¹⁵³ The specifically structural properties of mpg-C₃N₄/Pt are favorable to assembly dye molecules and enhance mass transferring, and thus causing a highly efficient and stable photocatalyst for H₂ production with an AQY of 19.4% at λ=550 nm light irradiation (Fig. 25c), which is among the highest reported for the photosensitization H₂ production systems in the visible light range, especially at longer wavelengths.¹⁵³

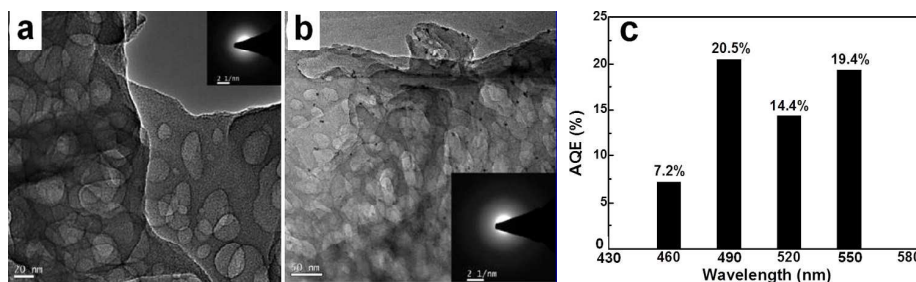


Fig. 25 TEM images of mpg-C₃N₄ (a) and EY-mpg-C₃N₄/Pt (b), and AQEs (c) of H₂ production over EY-mpg-C₃N₄/Pt (1 wt%) photocatalyst under different wavelengths of monochromic light irradiation. Figures reproduced with permission from ref. 153. Copyright 2012, American Chemical Society.

Similarly, Barreca and Fornasiero's group prepared high purity Pt/ α -Fe₂O₃ nanosystems by means of a hybrid synthetic route, consisting of PE-CVD of Fe₂O₃ deposits on FTO followed by sputtering of Pt and eventual annealing in air, and evidenced that the material compositional, structural and morphological features, with particular regard to the Pt oxidation state and α -Fe₂O₃ nano-organization, can be finely tailored as a function of the adopted processing conditions, which then strongly affect the nanosystem's efficiency for PEC water splitting.¹² For example, the as-prepared Pt/Fe₂O₃ with a sputtering time of 50 min (sample Pt(50)) were formed by Fe₂O₃ dendritic nanostructures grown perpendicularly to the substrate, whose surface appeared uniformly decorated by Pt NPs of 4 ± 1 nm (Fig. 26a). After annealing, the sample Pt(50)+A still has a morphology similar to the pristine one (Fig. 26b vs. a) but with a modest size increase of Pt NPs (7 ± 2 nm). When annealing was performed prior to sputtering, the obtained sample (A+Pt(50)) showed a remarkable morphological evolution with more rounded features and a higher porosity than the corresponding as-prepared one (Fig. 26c vs. a), and a similar topology was observed also for sample A+Pt(50)+A (Fig. 26d), for which annealing was carried out even after Pt deposition. Correspondingly, a statistical analysis of FESEM data

evidenced a slight increase of Pt NP dimensions from 6 ± 2 to 8 ± 2 nm.¹² Their results indicated that simple variations of the thermal treatment procedure allowed a fine control of Fe₂O₃ nano-organization and Pt redox chemistry, and thus there is a clear interplay between charge recombination kinetics and PEC efficiency. It demonstrated that the engineering of nanosystems should be an efficient pathway for improving the solar-to-hydrogen conversion efficiency.

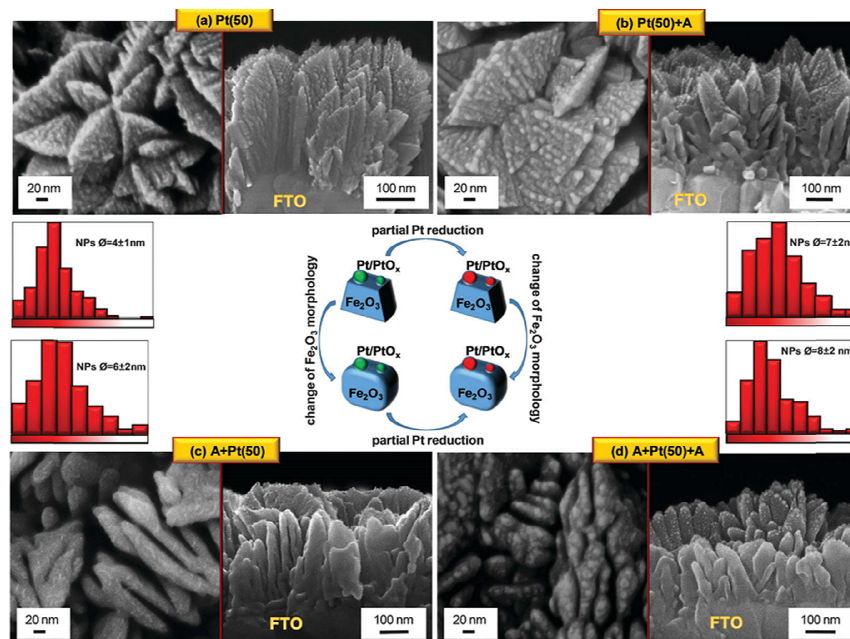


Fig. 26 Plane-view (left) and cross-sectional (right) FESEM images of the as-prepared and annealed Pt/Fe₂O₃ obtained with a sputtering time of 50 min. In each case, the histogram of Pt particle size distribution is also reported. The sketch at the center of the figure displays the main morphological and chemical differences between the four samples. Figures reproduced with permission from ref. 12. Copyright 2015, the Owner Societies.

Generally, the development of means to efficiently couple various components of a dye-sensitized system is crucial for the achievement of high efficient and stable H₂ production, and thus careful understanding of the whole system in terms of not only the performance of individual units but the interactions between them and their operational harmony is needed to maximize the solar-to-hydrogen conversion efficiency. In addition, optimal interfacial charge carrier transfer characteristics, matching energy level among various components, and rational nanosystem architecture, are some of the areas that need to be considered in the field of dye-sensitized semiconductor H₂ production.

5. Conclusions and outlook

Dye-sensitized systems liberate the semiconductors from the thermodynamic limitations for water splitting, but many challenges still remain in improving solar-to-hydrogen conversion efficiency, such as further extending the spectral responsive regions, suppressing the backward reactions, and matching H₂ production activity with dye regeneration under operating conditions. From our perspective, the following future research directions for dye-sensitized semiconductors could be identified.

1) Most importantly, new dyes and/or strategies should be developed to extend the photoabsorption region for efficient, low-cost, stable and even panchromatic light responsive solar-to-hydrogen conversion. Many current dyes only possess its own characteristic absorption bands with absorption edges shorter than 600 nm, and thus novel dyes that can utilize longer-wavelength photons with enhanced H₂ production activity at any given wavelength are highly desired. Some emerging strategies include dye co-sensitization by using dyes with complementary absorption spectra, heterostructure fabricated with conducting polymers and inorganic semiconductor, and surface LMCT excitation on semiconductors by choosing suitable organic pollutants as ligand. Although these strategies are potential for extending the photoabsorption into the visible and even near-IR regions, some fatal problems should be faced. For example, the co-sensitized dyes active under irradiation of $\lambda \geq 600$ nm are very scarce, the corresponding activity, stability and spectral responsive region of surface LMCT complexes are unsatisfactory, and thus the development of dyes with enhanced photoactivity under the visible and red/near-IR rays will become an important objective in the long term.

2) Stability is another critical problem in dye-sensitized system since it necessarily operates in aqueous solution, in which dye desorption, oxidization and/or decomposition are inevitable during the photocatalytic processes. Among those reported linkage modes for electron injection from the dye excited state, the fixation of dye molecules on semiconductors by introducing a linker stronger than common chemical or physical adsorption can significantly improved the stability. Beyond the dye fixation modes, the physical isolation in space between the semiconductor and the oxidized dyes and suitable dye designing based on “dynamic equilibrium” concept should be promising strategies, which can more effectively retard the charge recombination, and thus causing a long-term high photoactivity and stability for H₂ production. Moreover, surface modifications are essential in facilitating the charge separation and the surface reaction kinetics, which also improve the durability of photocatalytic systems for H₂ production.

3) Next is the development of means to efficiently couple various components of dye-sensitized system for achieving energy level matching and optimal photoreaction conditions. For example, electron donors are closely related to the oxidation half reaction and the dye regeneration for sustainable H₂ production, the nano-organization control of the photocatalyst/co-catalyst and the interactions among dye/semiconductor/co-catalyst are also significantly affect the photoactivity because those dominate the charge generation, separation, transfer and recombination in a dye-sensitized system. Careful understanding of the whole system in terms of not only the performance of individual units but the interactions between them and their operational harmony is needed to maximize the solar-to-fuel conversion efficiency.

4) Finally, better understanding of the photocatalytic mechanisms of dye-sensitized systems, including light harvesting, charge transfer characteristics across the interface of dye/semiconductor/co-catalyst/electron donor, and the elementary reactions on H₂ production and electron donor oxidation, is vital for the improvement of the solar-to-hydrogen conversion efficiency. As shown in this Review, the nanostructural control can not only activate the semiconductor for water splitting but also facilitate charge separation and improve the stability of the material under photoexcitation. Only with a comprehensive understanding of all of these processes, low-cost, high efficient and wide vis/near-IR light responsive dye-sensitized semiconductor systems may be developed, which is the prerequisite to establish a sustainable society based on solar hydrogen energy.

Abbreviations

AA	Ascorbic acid
4ABBN	4-2-hydroxynaphthalen-1-yl diazenylbenzoic acid
ALD	Atomic layer deposition
AO	Acridine orange hydrochloride
AQY	Apparent quantum yield
bdt	1,2-benzenedithiolate
bpy	2,2'-bipyridine
bnOH	binaphthol
BPA	bisphenol A
bpym	trisbipirimidin
CB	Conduction band
CDCA	Chenodeoxycholic acid
CoP	Co ^{III} Cl(dmgh) ₂ (pyridyl-4-hydrophosphonate)
CoPc	Co-phthalocyanine
Co-TPP	Co-tetraphenylporphyrin
4-CP	4-chlorophenol
CQDs	Carbon quantum dots
CrPc	Cr-phthalocyanine
Cr-TPP	Cr-tetraphenylporphyrin
CVD	chemical vapor deposition
dcbpy	4,4'-dicarboxy-2,2'-bipyridine
dpq	2,3-bis-(2'-pyridyl)-quinoxaline
DSSCs	Dye-sensitized solar cells
EB	Eosin bluish
ECE	Solar energy conversion efficiency
EDTA	Ethylenediaminetetraacetic acid
EPR	Electron paramagnetic resonance
Er	Erythrosine
ErB	Erythrosin B
ErY	Erythrosin yellowish
EY	Eosin Y
FL	Fluorescein
G	Graphene
g-PAN	Graphitized polyacrylonitrile
hfa	1,1,1,5,5,5-hexafluoro-2,4-pentanedionate
HOMO	Highest occupied molecular orbital
HOQ	8-hydroxy-orthoquinoline
HQ	Hydroquinone
IEP	Isoelectric point
LMCT	Ligand-to-metal charge transfer
LUMO	Lowest unoccupied molecular orbital
LSPR	Localized surface plasmon resonance
MB	Methylene blue
met	<i>cis</i> -1,2- dicarbomethoxyethylene-1,2-dithiolate

MLCT	Metal-to-ligand charge transfer
MOFs	Metal-organic frameworks
MPs	Metal porphyrins
MPcs	Metal phthalocyanines
MV	Methyl viologen
N3	<i>cis</i> -Ru(dcbpy) ₂ (NCS) ₂
N719	(n-Bu ₄ N) ₂ - <i>cis</i> -Ru(dcbpy) ₂ (SCN) ₂
NBA	Nile blue A
NBI	Naphthylbisimide
NDIPYPZ	Naphthylbisimide NBI core-based dye
Nf	Nafion
NHE	Normal hydrogen electrode
NPs	Nanoparticles
OA	Oxalic acid
PANI	Polyaniline
Pcs	Phthalocyanines
PDI	Perylene diimide
PEC	Photoelectrochemical
PE-CVD	Plasma enhanced-chemical vapor deposition
Ph	Phloxin
P3HT	Poly 3-hexylthiophene
PL	Photoluminescence
PPAAm	Polymerised polyallylamine
PPy	Polypyrrole
PR	Phenolic resin
PTCDI	Perylene tetracarboxylic diimide
PVP	Polyvinylpyrrolidone
PY	Pyronin Y
QY	Quantum yield
R	Electron relay
RB	Rose bengal
RF	Radio frequency
RGO	Graphene oxide
RhB	Rhodamine B
Rh6G	Rhodamine 6G
RuP ²⁺	Ru(bpy) ₂ (4,4'-(PO ₃ H ₂) ₂ -bpy) ²⁺
S	Sensitizer
SBR	Surface back reaction
SCE	Saturated calomel electrode
SHJ	Surface heterojunction
SnTCPP	Sn(IV)-porphyrin
SO	Safranine O
TDR	Time-resolved diffuse reflectance spectroscopy
TEOA	Triethanolamine
Th	Thionin acetate

TMEDA	N, N, N', N'-tetramethylethylenediamine
TNT	Titanate nanotube
TO	Thiazole orange
TON	Turnover number
TPA	Triphenylamine
TPPC	tetrakis(4-carboxyphenyl)porphine
TPPS	tetraphenyl- porphine tetrasulfonic acid
TPPPy	tetrakis(4-pyridylphenyl)porphine
TPyP	5,10,15,20-tetrakis(4-pyridyl) porphyrinato
UR	Uranine
VB	Valence band
VB ₁₂	Cyanocobalamin
VC	Vitamin C
Z907	<i>cis</i> -Ru(dcbpy)(4,4'-(dinonyl)bpy)(SCN) ₂
ZnCyt-c	Zinc-substituted cytochrome c
ZnP	Zinc porphyrin derivatives
Zn-TPPD	pentamethylene bis[4-(10,15,20- triphenyl- porphin-5-yl)benzoate]di-zinc(II)

Acknowledgments

The present work was financially supported by the Natural Science Foundation of China (21573166, 21271146, 21271144, 21171134, 20973128, and 20871096), Funds for Creative Research Groups of Hubei Province (2014CFA007), Program for New Century Excellent Talents in University of China (NCET-07-0637) and Fundamental Research Funds for the Central Universities (2042014kf0228), China.

References

- 1 T. Hisatomi, J. Kubota and K. Domen, *Chem. Soc. Rev.*, 2014, **43**, 7520-7535.
- 2 A. Fujishima and K. Honda, *Nature*, 1972, **238**, 37-38.
- 3 Y. Ma, X. L. Wang, Y. S. Jia, X. B. Chen, H. X. Han and C. Li, *Chem. Rev.*, 2014, **114**, 9987-10043.
- 4 J. Mao, K. Li and T. Y. Peng, *Catal. Sci. Technol.*, 2013, **3**, 2481-2498.
- 5 D. Kim, K. K. Sakimoto, D. Hong and P. D. Yang, *Angew. Chem. Int. Ed.*, 2015, **54**, 3259-3266.
- 6 A. J. Bard and M. A. Fox, *Acc. Chem. Res.*, 1995, **28**, 141-145.
- 7 A. Kudo and Y. Miseki, *Chem. Soc. Rev.*, 2009, **38**, 253-278.
- 8 H. L. Wang, L. S. Zhang, Z. G. Chen, J. Q. Hu, S. J. Li, Z. H. Wang, J. S. Liu and X. C. Wang, 2014, **43**, 5234-5244.
- 9 X. B. Chen, S. H. Shen, L. J. Guo and S. S. Mao, *Chem. Rev.*, 2010, **110**, 6503-6570.
- 10 C. Du, X. Yang, M. T. Mayer, H. Hoyt, J. Xie, G. McMahon, G. Bischooping and D. Wang, *Angew. Chem. Int. Ed.*, 2013, **52**, 12692-12695.
- 11 D. Barreca, G. Carraro, A. Gasparotto, C. Maccato, M. E. A. Warwick, K. Kaunisto, C. Sada, S. Turner, Y. Gönüllü, T.-P. Ruoko, L. Borgese, E. Bontempi, G. V. Tendeloo, H. Lemmetyinen and S. Mathur, *Adv. Mater. Interfaces*, 2015, **2**, 1500313.
- 12 M. E. A. Warwick, D. Barreca, E. Bontempi, G. Carraro, A. Gasparotto, C. Maccato, K. Kaunisto, T.-P. Ruoko, H. Lemmetyinen, C. Sada, Y. Gönüllü and S. Mathur, *Phys. Chem. Chem. Phys.*, 2015, **17**, 12899-12907.

- 13 D. Barreca, G. Carraro, V. Gombac, A. Gasparotto, C. Maccato, P. Fornasiero and E. Tondello, *Adv. Funct. Mater.*, 2011, **21**, 2611-2623.
- 14 M. Cargnello, A. Gasparotto, V. Gombac, T. Montini, D. Barreca and P. Fornasiero, *Eur. J. Inorg. Chem.*, 2011, **28**, 4309-4323.
- 15 C. Maccato, D. Barreca, G. Carraro, A. Gasparotto, V. Gombac and P. Fornasiero, *Surf. Coat. Tech.*, 2013, **230**, 219-227.
- 16 G. Carraro, C. Maccato, A. Gasparotto, T. Montini, S. Turner, O. I. Lebedev, V. Gombac, G. Adami, G. V. Tendeloo, D. Barreca and P. Fornasiero, *Adv. Funct. Mater.*, 2014, **24**, 372-378.
- 17 D. Barreca, P. Fornasiero, A. Gasparotto, V. Gombac, C. Maccato, A. Pozza and E. Tondello, *Chem. Vap. Deposition*, 2010, **16**, 296-300.
- 18 G. Carraro, A. Gasparotto, C. Maccato, V. Gombac, F. Rossi, T. Montini, D. Peeters, E. Bontempi, C. Sada, D. Barreca and P. Fornasiero, *RSC Adv.*, 2014, **4**, 32174-32179.
- 19 P. Zhang, J. J. Zhang and J. L. Gong, *Chem. Soc. Rev.*, 2014, **43**, 4395-4422.
- 20 R. Asahi, T. Morikawa, H. Irie and T. Ohwaki, *Chem. Rev.*, 2014, **114**, 9824-9852.
- 21 Q. J. Xiang, J. G. Yu and M. Jaroniec, *Chem. Soc. Rev.*, 2012, **41**, 782-796.
- 22 S. W. Cao, J. X. Low, J. G. Yu and M. Jaroniec, *Adv. Mater.*, 2015, **27**, 2150-2176.
- 23 M. Q. Yang, N. Zhang, M. Pagliaro, and Y. J. Xu, *Chem. Soc. Rev.*, 2014, **43**, 8240-8254.
- 24 T. Y. Peng, D. N. Ke, J. G. Xiao, L. Wang, J. Hu and L. Zan, *J. Solid State Chem.*, 2012, **194**, 250-256.
- 25 D. N. Ke, T. Y. Peng, L. Ma, P. Cai and K. Dai, *Inorg. Chem.*, 2009, **48**, 4685-4691.
- 26 F. Zuo, L. Wang, T. Wu, Z. Y. Zhang, D. Borchardt and P. Y. Feng, *J. Am. Chem. Soc.*, 2010, **132**, 11856-11857.
- 27 K. Li, B. Chai, T. Y. Peng, J. Mao and L. Zan, *ACS Catal.*, 2013, **3**, 170-177.
- 28 J. H. Yang, H. J. Yan, X. L. Wang, F. Y. Wen, Z. J. Wang, D. Y. Fan, J. Y. Shi and C. Li, *J. Catal.*, 2012, **290**, 151-157.
- 29 Y. Bai, I. Mora-Seró, F. De Angelis, J. Bisquert and P. Wang, *Chem. Rev.*, 2014, **114**, 10095-10130.
- 30 K. Fan, R. J. Li, J. N. Chen, W. Y. Shi and T. Y. Peng, *Sci. Adv. Mater.*, 2013, **5**, 1596-1626.
- 31 J. R. Swierk and T. E. Mallouk, *Chem. Soc. Rev.*, 2013, **42**, 2357-2387.
- 32 R. Abe, K. Shinmei, N. Koumura, K. Hara and B. Ohtani, *J. Am. Chem. Soc.*, 2013, **135**, 16872-16884.
- 33 M. Grätzel, *Acc. Chem. Res.*, 1981, **14**, 376-384.
- 34 J. Kiwi and M. Grätzel, *J. Am. Chem. Soc.*, 1979, **101**, 7214-7217.
- 35 J. Kiwi and M. Grätzel, *Nature*, 1979, **281**, 657-658.
- 36 K. Kalyanasundaram and M. Grätzel, *Angew. Chem. Int. Ed.*, 1979, **18**, 701-702.
- 37 J. Kiwi, E. Borgarello, E. Pelizzetti, M. Visca and M. Grätzel, *Angew. Chem. Int. Ed.*, 1980, **19**, 646-648.
- 38 E. Borgarello, J. Kiwi, E. Pelizzetti, M. Visca and M. Grätzel, *Nature*, 1981, **289**, 158-160.
- 39 M. Kapilashrami, Y. Zhang, Y.-S. Liu, A. Hagfeldt and J. Guo, *Chem. Rev.*, 2014, **114**, 9662-9707.
- 40 W. Wang, M. O. Tade and Z. P. Shao, *Chem. Soc. Rev.*, 2015, **44**, 5371-5408
- 41 Y. Q. Qu and X. F. Duan, *Chem. Soc. Rev.*, 2013, **42**, 2568-2580.
- 42 A. Kubacka, M. Fernandez-Garcia and G. Colon, *Chem. Rev.*, 2012, **112**, 1555-1614.
- 43 K. F. Wu, H. M. Zhu and T. Q. Lian, *Acc. Chem. Res.*, 2015, **48**, 851-859.
- 44 M. D. Kärkäs, O. Verho, E. V. Johnston and B. Åkermark, *Chem. Rev.*, 2014, **114**, 7006-7043.
- 45 L. Z. Wu, B. Chen, Z. J. Li and C. H. Tung, *Acc. Chem. Res.*, 2014, **47**, 2177-2185.
- 46 Z. J. Han and R. Eisenberg, *Acc. Chem. Res.*, 2014, **47**, 2537-2544.
- 47 F. E. Osterloh, *Chem. Soc. Rev.*, 2013, **42**, 2294-2320.
- 48 X. H. Lu, S. L. Xie, H. Yang, Y. X. Tong and H. B. Ji, *Chem. Soc. Rev.*, 2014, **43**, 7581-7593.
- 49 K. Maeda, M. Eguchi, W. J. Youngblood and T. E. Mallouk, *Chem. Mater.*, 2008, **20**, 6770-6778.

- 50 A. Tiwari, I. Mondal and U. Pal, *RSC Adv.*, 2015, **5**, 31415-31421.
- 51 I. Mora-seró, S. Giménez, F. Fabregat-santiago, R. Gómez, Q. Shen, T. Toyoda and J. Bisquert, *Acc. Chem. Res.*, 2009, **42**, 1848-1857.
- 52 E. H. Sargent, *Nat. Photon.*, 2012, **6**, 133-135.
- 53 N. Yaacobi-Gross, N. Garphunkin, O. Solomeshch, A. Vaneski, A. S. Susha, A. L. Rogach and N. Tessler, *ACS Nano*, 2012, **6**, 3128-3133.
- 54 T. P. A. Ruberu, Y. M. Dong, A. Das and R. Eisenberg, *ACS Catal.*, 2015, **5**, 2255-2259.
- 55 G. M. Wang, X. Y. Yang, F. Q. Qian, J. Z. Zhang and Y. Li, *Nano Lett.*, 2010, **10**, 1088-1092.
- 56 S. Y. Lim, W. Shen and Z. Q. Gao, *Chem. Soc. Rev.*, 2015, **44**, 362-381.
- 57 J. Liu, Y. Liu, N. Y. Liu, Y. Z. Han, X. Zhang, H. Huang, Y. Lifshitz, S.-T. Lee, J. Zhong and Z. H. Kang, *Science*, 2015, **347**, 970-974.
- 58 B. C. M. Martindale, G. A. M. Hutton, C. A. Caputo and E. Reisner, *J. Am. Chem. Soc.*, 2015, **137**, 6018-6025.
- 59 X. Zhang, F. Wang, H. Huang, H. T. Li, X. Han, Y. Liu and Z. H. Kang, *Nanoscale*, 2013, **5**, 2274-2278.
- 60 K. Maeda, G. Sahara, M. Eguchi and O. Ishitani, *ACS Catal.*, 2015, **5**, 1700-1707.
- 61 W. Kim, T. Tachikawa, T. Majima, C. H. Li, H. J. Kim and W. Choi, *Energ. Environ. Sci.*, 2010, **3**, 1789-1795.
- 62 C. Kong, S. X. Min and G. X. Lu, *ACS Catal.*, 2014, **4**, 2763-2769.
- 63 K. L. V. Joseph, J. Lim, A. Anthonysamy, H. i. Kim, W. Choi and J. K. Kim, *J. Mater. Chem. A*, 2015, **3**, 232-239.
- 64 D. Duonghong, E. Borgarello and M. Grätzel, *J. Am. Chem. Soc.*, 1981, **103**, 4685-4690.
- 65 V. H. Houdling and M. Grätzel, *J. Am. Chem. Soc.*, 1983, **105**, 5695-5696.
- 66 K. Gurunathan, P. Maruthamuthu and M. Sastri, *Int. J. Hydrogen Energ.*, 1997, **22**, 57-62.
- 67 K. Hirano, E. Suzuki, A. Ishikawa, T. Moroi, H. Shiroishi and M. Kaneko, *J. Photoch. Photobio. A*, 2000, **136**, 157-161.
- 68 A. A. Nada, H. A. Hamed, M. H. Barakat, N. R. Mohamed and T. N. Veziroglu, *Int. J. Hydrogen Energ.*, 2008, **33**, 3264-3269.
- 69 F. Sastre, Y. Bouizi, V. Fornés and H. Garcia, *J. Colloid Interf. Sci.*, 2010, **346**, 172-177.
- 70 M. Latorre-Sanchez, C. Lavorato, M. Puche, V. Fornes, R. Molinari and H. Garcia, *Chem. Eur. J.*, 2012, **18**, 16774-16783.
- 71 D. N. Furlong, D. Wells and W. H. F. Sasse, *J. Phys. Chem.*, 1986, **90**, 1107-1115.
- 72 Y. I. Kim, S. Salim, M. J. Huq and T. E. Mallouk, *J. Am. Chem. Soc.*, 1991, **113**, 9561-9563.
- 73 Y. I. Kim, S. J. Atherton, E. S. Brigham and T. E. Mallouk, *J. Phys. Chem.*, 1993, **97**, 11802-11810.
- 74 M. Matsuoka, Y. Ide and M. Ogawa, *Phys. Chem. Chem. Phys.*, 2014, **16**, 3520-3522.
- 75 Y. I. Kim, S. W. Keller, J. S. Krueger, E. H. Yonemoto, G. B. Saupe and T. E. Mallouk, *J. Phys. Chem. B*, 1997, **101**, 2491-2500.
- 76 N. Lakshminarasimhan, E. Bae and W. Choi, *J. Phys. Chem. C*, 2007, **111**, 15244-15250.
- 77 S. Rasalingam, R. Peng, C. M. Wu, K. Mariappan and R. T. Koodali, *Catal. Commun.*, 2015, **65**, 14-19.
- 78 W. Kim, T. Tachikawa, T. Majima and W. Choi, *J. Phys. Chem. C*, 2009, **113**, 10603-10609.
- 79 M. S. Zhu, Y. P. Dong, B. Xiao, Y. K. Du, P. Yang and X. M. Wang, *J. Mater. Chem.*, 2012, **22**, 23773-23779.
- 80 Y. J. Chen, Z. G. Mou, S. L. Yin, H. Huang, P. Yang, X. M. Wang and Y. K. Du, *Mater. Lett.*, 2013, **107**, 31-34.
- 81 K. B. Dhanalakshmi, S. Latha, S. Anandan and P. Maruthamuthu, *Int. J. Hydrogen Energ.*, 2001, **26**, 669-674.

- 82 H. Q. Zheng, H. Yong, T. Ou-Yang, Y. T. Fan and H. W. Hou, *Int. J. Hydrogen Energ.*, 2013, **38**, 12938-12945.
- 83 R. Abe, K. Sayama and H. Sugihara, *J. Sol. Energ –T. Asme*, 2005, **127**, 413-416.
- 84 J. Li, Y. E. L. S. Lian and W. H. Ma, *Int. J. Hydrogen Energ.*, 2013, **38**, 10746-10753.
- 85 M. M. Maitani, C. H. Zhan, D. Mochizuki, E. Suzuki and Y. Wada, *Appl. Catal. B: Environ.*, 2013, **140-141**, 406-411.
- 86 M. M. Maitani, C. H. Zhan, D. Mochizuki, E. Suzuki and Y. Wada, *Appl. Catal. B: Environ.*, 2014, **147**, 770-778.
- 87 A. Kumari, I. Mondal and U. Pal, *New J. Chem.*, 2015, **39**, 713-720.
- 88 K. Vinodgopal, X. Hua, R. L. Dahlgren, A. Lappin, L. Patterson and P. V. Kamat, *J. Phys. Chem.*, 1995, **99**, 10883-10889.
- 89 G. B. Saupe, T. E. Mallouk, W. Kim and R. H. Schmehl, *J. Phys. Chem. B*, 1997, **101**, 2508-2513.
- 90 K. Maeda, M. Eguchi, S. H. A. Lee, W. J. Youngblood, H. Hata and T. E. Mallouk, *J. Phys. Chem. C*, 2009, **113**, 7962-7969.
- 91 K. Maeda, M. Eguchi, W. J. Youngblood and T. E. Mallouk, *Chem. Mater.*, 2009, **21**, 3611-3617.
- 92 F. Lakadamyali and E. Reisner, *Chem. Commun.*, 2011, **47**, 1695-1697.
- 93 F. Lakadamyali, A. Reynal, M. Kato, J. R. Durrant and E. Reisner, *Chem. Eur. J.*, 2012, **18**, 15464-15475.
- 94 M. A. Gross, A. Reynal, J. R. Durrant and E. Reisner, *J. Am. Chem. Soc.*, 2014, **136**, 356-366.
- 95 E. Reisner, J. C. Fontecilla-Camps and F. A. Armstrong, *Chem. Commun.*, 2009, 550-552.
- 96 E. Reisner, D. Powell, C. Cavazza, J. Fontecilla-Camps and F. Armstrong, *J. Am. Chem. Soc.*, 2009, **131**, 18457-18466.
- 97 E. Bae, W. Choi, J. Park, H. S. Shin, S. B. Kim and J. S. Lee, *J. Phys. Chem. B*, 2004, **108**, 14093-14101.
- 98 E. Bae and W. Choi, *J. Phys. Chem. B*, 2006, **110**, 14792-14799.
- 99 H. Park and W. Choi, *Langmuir*, 2006, **22**, 2906-2911.
- 100 J. Park, J. Yi, T. Tachikawa, T. Majima and W. Choi, *J. Phys. Chem. Lett.*, 2010, **1**, 1351-1355.
- 101 A. Kruth, S. Hansen, T. Beweries, V. Brüser and K. D. Weltmann, *ChemSusChem*, 2013, **6**, 152-159.
- 102 B. Xiao, X. M. Wang, H. Huang, M. S. Zhu, P. Yang, Y. Wang and Y. K. Du, *J. Phys. Chem. C*, 2013, **117**, 21303-21311.
- 103 T. Toyao, M. Saito, S. Dohshi, K. Mochizuki, M. Iwata, H. Higashimura, Y. Horiuchi and M. Matsuoka, *Chem. Commun.*, 2014, **50**, 6779-6781.
- 104 R. Amadelli, R. Argazzi, C. Bignozzi and F. Scandola, *J. Am. Chem. Soc.*, 1990, **112**, 7099-7103.
- 105 T. Y. Peng, K. Dai, H. B. Yi, D. N. Ke, P. Cai and L. Zan, *Chem. Phys. Lett.*, 2008, **460**, 216-219.
- 106 T. Y. Peng, D. N. Ke, P. Cai, K. Dai, L. Ma and L. Zan, *J. Power Sources*, 2008, **180**, 498-505.
- 107 U. Veikko, X. H. Zhang, T. Y. Peng, P. Cai and G. Z. Cheng, *Spectrochim. Acta A*, 2013, **105**, 539-544.
- 108 X. H. Zhang, U. Veikko, J. Mao, P. Cai and T. Y. Peng, *Chem. Eur. J.*, 2012, **18**, 12103-12111.
- 109 L. Martin-Gomis, F. Fernandez-Lazaro and A. Sastre-Santos, *J. Mater. Chem. A*, 2014, **2**, 15672-15682.
- 110 M. Urbani, M. Grätzel, M. K. Nazeeruddin and T. Torres, *Chem. Rev.*, 2014, **114**, 12330-12396.
- 111 H. Hagiwara, N. Ono, T. Inoue, H. Matsumoto and T. Ishihara, *Angew. Chem. Int. Edit.*, 2006, **45**, 1420-1422.
- 112 H. Hagiwara, T. Inoue, K. Kaneko and T. Ishihara, *Chem. Eur. J.*, 2009, **15**, 12862-12870.
- 113 H. Hagiwara, M. Nagatomo, S. Ida and T. Ishihara, *Energy Procedia*, 2012, **22**, 53-60.
- 114 H. Hagiwara, M. Nagatomo, C. Seto, S. Ida and T. Ishihara, *Catalysts*, 2013, **3**, 614-624.
- 115 K. Kurimoto, T. Yamazaki, Y. Suzuri, Y. Nabetani, S. Onuki, S. Takagi, T. Shimada, H. Tachibana and H. Inoue, *Photoch. Photobio. Sci.*, 2014, **13**, 154-156.

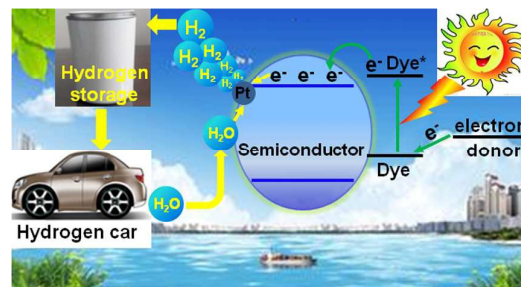
- 116 Y. Astuti, E. Palomares, S. A. Haque and J. R. Durrant, *J. Am. Chem. Soc.*, 2005, **127**, 15120-15126.
- 117 M. S. Zhu, Z. Li, B. Xiao, Y. T. Lu, Y. K. Du, P. Yang and X. M. Wang, *ACS Appl. Mater. Inter.*, 2013, **5**, 1732-1740.
- 118 E. Malinka, A. Khutornoi, S. Vodzinskii, Z. Zhilina and G. Kamalov, *React. Kinet. Catal. Lett.*, 1988, **36**, 407-410.
- 119 E. A. Malinka, G. L. Kamalov, S. V. Vodzinskii, V. I. Melnik and Z. I. Zhilina, *J. Photoch. Photobio. A*, 1995, **90**, 153-158.
- 120 A. Fateeva, P. A. Chater, C. P. Ireland, A. A. Tahir, Y. Z. Khimiyak, P. V. Wiper, J. R. Darwent and M. J. Rosseinsky, *Angew. Chem. Int. Ed.*, 2012, **51**, 7440-7444.
- 121 H. Hagiwara, N. Ono and T. Ishihara, *Chem. Lett.*, 2010, **39**, 178-179.
- 122 K. Takanebe, K. Kamata, X. C. Wang, M. Antonietti, J. Kubota and K. Domen, *Phys. Chem. Chem. Phys.*, 2010, **12**, 13020-13025.
- 123 J. Huang, Y. J. Wu, D. D. Wang, Y. F. Ma, Z. K. Yue, Y. T. Lu, M. X. Zhang, Z. J. Zhang and P. Yang, *ACS Appl. Mater. Inter.*, 2015, **7**, 3732-3741.
- 124 D. D. Wang, J. Huang, X. Li, P. Yang, Y. K. Du, C. M. Goh and C. Lu, *J. Mater. Chem. A*, 2015, **3**, 4195-4202.
- 125 L. Zhang, W. Z. Wang, S. M. Sun, Y. Y. Sun, E. Gao and J. Xu, *Appl. Catal. B: Environ.*, 2013, **132-133**, 315-320.
- 126 X. H. Zhang, L. J. Yu, C. S. Zhuang, T. Y. Peng, R. J. Li and X. G. Li, *ACS Catal.*, 2014, **4**, 162-170.
- 127 X. H. Zhang, L. J. Yu, R. J. Li, T. Y. Peng and X. G. Li, *Catal. Sci. Technol.*, 2014, **4**(9), 3251-3260.
- 128 L. J. Yu, X. H. Zhang, C. S. Zhuang, L. Lin, R. J. Li and T. Y. Peng, *Phys. Chem. Chem. Phys.*, 2014, **16**, 4106-4114.
- 129 X. H. Zhang, L. J. Yu, C. S. Zhuang, T. Y. Peng, R. J. Li and X. G. Li, *RSC Adv.*, 2013, **3**, 14363-14370.
- 130 V. S. Zakharenko, A. V. Bulatov and V. N. Parmon, *React. Kinet. Catal. Lett.*, 1988, **36**, 295-300.
- 131 J. Zhang, P. W. Du, J. Schneider, P. Jarosz and R. Eisenberg, *J. Am. Chem. Soc.*, 2007, **129**, 7726-7727.
- 132 P. Jarosz, P. Du, J. Schneider, S. H. Lee, D. McCamant and R. Eisenberg, *Inorg. Chem.*, 2009, **48**, 9653-9663.
- 133 D. H. Wang, Y. W. Zhang and W. Chen, *Chem. Commun.*, 2014, **50**, 1754-1756.
- 134 J. Moser and M. Grätzel, *J. Am. Chem. Soc.*, 1984, **106**, 6557-6564.
- 135 T. Shimidzu, T. Iyoda and Y. Koide, *J. Am. Chem. Soc.*, 1985, **107**, 35-41.
- 136 Y. X. Li, M. M. Guo, S. Q. Peng, G. X. Lu and S. B. Li, *Int. J. Hydrogen Energ.*, 2009, **34**, 5629-5636.
- 137 Q. Y. Li and G. X. Lu, *J. Mol. Catal. A: Chem.*, 2007, **266**, 75-79.
- 138 Y. X. Li, C. F. Xie, S. Q. Peng, G. X. Lu and S. B. Li, *J. Mol. Catal. A: Chem.*, 2008, **282**, 117-123.
- 139 X. Liu, Y. X. Li, S. Q. Peng, G. X. Lu and S. B. Li, *Photoch. Photobio. Sci.*, 2013, **12**, 1903-1910.
- 140 Z. L. Jin, X. J. Zhang, G. X. Lu and S. B. Li, *J. Mol. Catal. A: Chem.*, 2006, **259**, 275-280.
- 141 Z. L. Jin, X. J. Zhang, Y. X. Li, S. B. Li and G. X. Lu, *Catal. Commun.*, 2007, **8**, 1267-1273.
- 142 Q. Y. Li, Z. L. Jin, Z. G. Peng, Y. X. Li, S. B. Li and G. X. Lu, *J. Phys. Chem. C*, 2007, **111**, 8237-8241.
- 143 X. J. Zhang, Z. L. Jin, Y. X. Li, S. B. Li and G. X. Lu, *Appl. Surf. Sci.*, 2008, **254**, 4452-4456.
- 144 X. J. Zhang, Z. L. Jin, Y. X. Li, S. B. Li and G. X. Lu, *J. Power Sources*, 2007, **166**, 74-79.
- 145 Q. Y. Li, L. Chen and G. X. Lu, *J. Phys. Chem. C*, 2007, **111**, 11494-11499.
- 146 X. Q. Li, J. Zhang, S. Z. Kang, G. D. Li and J. Mu, *Ceram. Int.*, 2014, **40**, 10171-10176.
- 147 S. X. Min and G. X. Lu, *J. Phys. Chem. C*, 2011, **115**, 13938-13945.
- 148 S. X. Min and G. X. Lu, *Int. J. Hydrogen Energ.*, 2012, **37**, 10564-10574.
- 149 S. X. Min and G. X. Lu, *Int. J. Hydrogen Energ.*, 2013, **38**, 2106-2116.
- 150 C. Kong, S. X. Min and G. X. Lu, *Int. J. Hydrogen Energ.*, 2014, **39**, 4836-4844.

- 151 C. Kong, S. X. Min and G. X. Lu, *Chem. Commun.*, 2014, **50**, 5037-5039.
- 152 S. X. Min and G. X. Lu, *J. Phys. Chem. C*, 2012, **116**, 25415-25424.
- 153 S. X. Min, and G. X. Lu, *J. Phys. Chem. C*, 2012, **116**, 19644-19652.
- 154 J. Y. Xu, Y. X. Li, S. Q. Peng, G. X. Lu and S. B. Li, *Phys. Chem. Chem. Phys.*, 2013, **15**, 7657-7665.
- 155 X. J. Zhang, Z. L. Jin, Y. X. Li, S. B. Li and G. X. Lu, *J. Colloid. Interf. Sci.*, 2009, **333**, 285-293.
- 156 X. Liu, Y. X. Li, S. Q. Peng, G. X. Lu and S. B. Li, *Int. J. Hydrogen Energ.*, 2012, **37**, 12150-12157.
- 157 X. Liu, Y. X. Li, S. Q. Peng, G. X. Lu and S. B. Li, *Int. J. Hydrogen Energ.*, 2013, **38**, 11709-11719.
- 158 R. Abe, K. Hara, K. Sayama, K. Domen and H. Arakawa, *J. Photoch. Photobiol. A*, 2000, **137**, 63-69.
- 159 P. Chowdhury, H. Gomaa and A. K. Ray, *Chemosphere*, 2015, **121**, 54-61.
- 160 J. Fang, L. S. Yin, S. W. Cao, Y. S. Liao and C. Xue, *Beilstein J. Nanotech.*, 2014, **5**, 360-364.
- 161 T. T. Le, M. S. Akhtar, D. M. Park, J. C. Lee and O. B. Yang, *Appl. Catal. B: Environ.*, 2012, **111-112**, 397-401.
- 162 Z. T. Yan, X. X. Yu, Y. Y. Zhang, H. X. Jia, Z. J. Sun and P. W. Du, *Appl. Catal. B: Environ.*, 2014, **160-161**, 173-178.
- 163 S. Q. Peng, X. P. Zeng and Y. S. Li, *Int. J. Hydrogen Energ.*, 2015, **40**, 6038-6049.
- 164 T. Sreethawong, C. Junbua and S. Chavadej, *J. Power Sources*, 2009, **190**, 513-524.
- 165 T. Puangpetch, P. Sommakettarin, S. Chavadej and T. Sreethawong, *Int. J. Hydrogen Energ.*, 2010, **35**, 12428-12442.
- 166 N. Rungjaroentawon, S. Onsuratoom and S. Chavadej, *Int. J. Hydrogen Energ.*, 2012, **37**, 11061-11071.
- 167 T. Sreethawong and S. Yoshikawa, *Mater. Res. Bull.*, 2012, **47**, 1385-1395.
- 168 T. Sreethawong and S. Yoshikawa, *Chem. Eng. J.*, 2012, **197**, 272-282.
- 169 W. Zhang and R. Xu, *Int. J. Hydrogen Energ.*, 2012, **37**, 17899-17909.
- 170 J. Zhang and X. H. Liu, *Phys. Chem. Chem. Phys.*, 2014, **16**, 8655-8660.
- 171 Y. B. Wang, J. D. Hong, W. Zhang and R. Xu, *Catal. Sci. Technol.*, 2013, **3**, 1703-1711.
- 172 J. Y. Xu, Y. X. Li and S. Q. Peng, *Int. J. Hydrogen Energ.*, 2015, **40**, 353-362.
- 173 Z. G. Mou, Y. P. Dong, S. J. Li, Y. K. Du, X. M. Wang, P. Yang and S. D. Wang, *Int. J. Hydrogen Energ.*, 2011, **36**, 8885-8893.
- 174 H. W. Jeong and H. Park, *Catal. Today*, 2014, **230**, 15-19.
- 175 J. He, J. Q. Wang, Y. J. Chen, J. P. Zhang, D. L. Duan, Y. Wang and Z. Y. Yan, *Chem. Commun.*, 2014, **50**, 7063-7066.
- 176 Y. P. Yuan, L. S. Yin, S. W. Cao, G. S. Xu, C. H. Li and C. Xue, *Appl. Catal. B: Environ.*, 2015, **168-169**, 572-576.
- 177 X. L. Liu, R. Wang, M. Y. Zhang, Y. P. Yuan and C. Xue, *APL Mater.*, 2015, **3**, 104403-1-7.
- 178 W. Y. Zhang, Y. X. Li, X. P. Zeng and S. Q. Peng, *Sci. Rep.*, 2015, **5**, 10589-1-12.
- 179 M. C. Yin, S. Ma, C. J. Wu and Y. T. Fan, *RSC Adv.*, 2015, **5**, 1852-1858.
- 180 T. Kamegawa, S. Matsuura, H. Seto and H. Yamashita, *Angew. Chem. Int. Edit.*, 2013, **52**, 916-919.
- 181 D. Chatterjee, *Catal. Commun.*, 2010, **11**, 336-339.
- 182 D. L. S. Maia, I. Pepe, A. F. da Silva and L. A. Silva, *J. Photoch. Photobiol. A*, 2012, **243**, 61-64.
- 183 Y. Z. Wu and W. H. Zhu, *Chem. Soc. Rev.*, 2013, **42**, 2039-2058.
- 184 R. Abe, K. Shinmei, K. Hara and B. Ohtani, *Chem. Commun.*, 2009, 3577-3579.
- 185 R. Abe, K. Sayama and H. Arakawa, *J. Photoch. Photobiol. A*, 2004, **166**, 115-122.
- 186 R. Abe, K. Sayama and H. Arakawa, *Chem. Phys. Lett.*, 2003, **379**, 230-235.
- 187 R. Abe, K. Sayama and H. Arakawa, *Chem. Phys. Lett.*, 2002, **362**, 441-444.
- 188 S. H. Lee, Y. Park, K. R. Wee, H. J. Son, D. W. Cho, C. Pac, W. Choi and S. O. Kang, *Org. Lett.*, 2010, **12**, 460-463.

- 189 W. S. Han, K. R. Wee, H. Y. Kim, C. Pac, Y. Nabetani, D. Yamamoto, T. Shimada, H. Inoue, H. Choi, K. Cho and S. O. Kang, *Chem. Eur. J.*, 2012, **18**, 15368-15381.
- 190 S. K. Choi, H. S. Yang, J. H. Kim and H. Park, *Appl. Catal. B: Environ.*, 2012, **121-122**, 206-213.
- 191 Y. Park, W. Kim, D. Monllor-Satoca, T. Tachikawa, T. Majima and W. Choi, *J. Phys. Chem. Lett.*, 2013, **4**, 189-194.
- 192 Z. Li, Y. J. Chen, Y. K. Du, X. M. Wang, P. Yang and J. W. Zheng, *Int. J. Hydrogen Energ.*, 2012, **37**, 4880-4888.
- 193 J. Lee, J. Kwak, K. C. Ko, J. H. Park, J. H. Ko, N. Park, E. Kim, H. Ryu do, T. K. Ahn, J. Y. Lee and S. U. Son, *Chem. Commun.*, 2012, **48**, 11431-11433.
- 194 M. Watanabe, H. Hagiwara, A. Iribe, Y. Ogata, K. Shiomi, A. Staykov, S. Ida, K. Tanaka and T. Ishihara, *J. Mater. Chem. A*, 2014, **2**, 12952-12961.
- 195 X. H. Zhang, T. Y. Peng, L. J. Yu, R. J. Li, Q. Q. Li and Z. Li, *ACS Catal.*, 2015, **5**, 504–510.
- 196 U. Pal and I. Mondal, *New J. Chem.*, 2015, **39**, 6925-6934.
- 197 S. Chen, D. L. Jacobs, J. K. Xu, Y. X. Li, C. Y. Wang and L. Zang, *RSC Adv.*, 2014, **4**, 48486-48491.
- 198 S. Chen, Y. X. Li and C. Y. Wang, *RSC Adv.*, 2015, **5**, 15880-15885.
- 199 L. George, S. Sappati, P. Ghosh and R. N. Devi, *J. Phys. Chem. C*, 2015, **119**, 3060-3067.
- 200 G. Zhang, G. Kim and W. Choi, *Energ. Environ. Sci.*, 2014, **7**, 954-966.
- 201 T. Rajh, J. M. Nedeljkovic, L. X. Chen, O. Poluektov and M. C. Thurnauer, *J. Phys. Chem. B*, 1999, **103**, 3515-3519.
- 202 S. Ikeda, C. Abe, T. Torimoto and B. Ohtani, *J. Photoch. Photobio. A*, 2003, **160**, 61-67.
- 203 T. Lana-Villarreal, A. Rodes, J. M. Pérez and R. Gómez, *J. Am. Chem. Soc.*, 2005, **127**, 12601-12611.
- 204 Y. Park, N. Singh, K. S. Kim, T. Tachikawa, T. Majima and W. Choi, *Chem. Eur. J.*, 2009, **15**, 10843-10850.
- 205 G. Kim and W. Choi, *Appl. Catal. B: Environ.*, 2010, **100**, 77-83.
- 206 J. Kim and W. Choi, *Energ. Environ. Sci.*, 2010, **3**, 1042-1045.
- 207 G. Zhang and W. Choi, *Chem. Commun.*, 2012, **48**, 10621-10623.
- 208 H. J. Yan and Y. Huang, *Chem. Commun.*, 2011, **47**, 4168-4170.
- 209 Y. F. Zhang, F. Mao, H. J. Yan, K. W. Liu, H. M. Cao, J. G. Wu and D. Q. Xiao, *J. Mater. Chem. A*, 2015, **3**, 109-115.
- 210 X. H. Zhang, B. Peng, S. Zhang and T. Y. Peng, *ACS Sustain. Chem. Eng.*, 2015, **3**, 1501-1509.
- 211 K. He, M. T. Li and L. J. Guo, *Int. J. Hydrogen Energ.*, 2012, **37**, 755-759.
- 212 Y. Sui, J. H. Liu, Y. W. Zhang, X. K. Tian and W. Chen, *Nanoscale*, 2013, **5**, 9150-9155.
- 213 F. He, G. Chen, Y. G. Yu, S. Hao, Y. S. Zhou and Y. Zheng, *ACS Appl. Mater. Inter.*, 2014, **6**, 7171-7179.
- 214 C. L. Wang and D. Astruc, *Chem. Soc. Rev.*, 2014, **43**, 7188-7216.
- 215 R. B. Jiang, B. X. Li, C. H. Fang and J. F. Wang, *Adv. Mater.*, 2014, **31**, 5274-5309.
- 216 W. B. Hou and S. B. Cronin, *Adv. Funct. Mater.*, 2013, **23**, 1612-1619.
- 217 A. Tanaka, S. Sakaguchi, K. Hashimoto and H. Kominami, *Catal. Sci. Technol.*, 2012, **2**, 907-909.
- 218 A. Tanaka, S. Sakaguchi, K. Hashimoto and H. Kominami, *Catal. Sci. Technol.*, 2014, **4**, 1931-1938.
- 219 Z. W. Seh, S. H. Liu, M. Low, S. Y. Zhang, Z. H. Liu, A. Mlayah and M. Y. Han, *Adv. Mater.*, 2012, **24**, 2310-2314.
- 220 T. Torimoto, H. Horibe, T. Kameyama, K. Okazaki, S. Ikeda, M. Matsumura, A. Ishikawa and H. Ishihara, *J. Phys. Chem. Lett.*, 2011, **2**, 2057-2062.
- 222 J. Chen, J. C. S. Wu, P. C. Wu and D. P. Tsai, *J. Phys. Chem. C*, 2011, **11**, 210-216.
- 221 S. S. Rayalu, D. Jose, M. V. Joshi, P. A. Mangrulkar, K. Shrestha and K. Klabunde, *Appl. Catal. B*, 2013, **142**, 684-693.

- 223 J. S. DuChene, B. C. Sweeny, A. C. Johnston-Peck, D. Su, E. A. Stach and W. D. Wei, *Angew. Chem., Int. Ed.*, 2014, **53**, 7887-7891.
- 224 N. Fu and G. X. Lu, *Chem. Commun.*, 2009, 3591-3593.
- 225 N. Fu and G. X. Lu, *Catal. Lett.*, 2009, **127**, 319-322.
- 226 N. Fu and G. X. Lu, *Appl. Surf. Sci.*, 2009, **255**, 4378-4383.
- 227 C. Wang, K. E. deKrafft and W. B. Lin, *J. Am. Chem. Soc.*, 2012, **134**, 7211-7214.
- 228 J. He, Z. Y. Yan, J. Q. Wang, J. Xie, L. Jiang, Y. M. Shi, F. G. Yuan, F. Yu and Y. J. Sun, *Chem. Commun.*, 2013, **49**, 6761-6763.
- 229 J. R. Ran, J. Zhang, J. G. Yu,; M. Jaroniec and S. Z. Qiao, *Chem. Soc. Rev.*, 2014, **43**, 7787-7812.
- 230 J. H. Yang, D. E. Wang, H. X. Han and C. Li, *Acc. Chem. Res.*, 2013, **46**, 1900-1909.
- 231 X. X. Zou and Y. Zhang, *Chem. Soc. Rev.*, 2015, **44**, 5148-5180.
- 232 F. Y. Wen and C. Li, *Acc. Chem. Res.*, 2013, **46**, 2355-2364.
- 233 A. Reynal, F. Lakadamyali, M. A. Gross, E. Reisner and J. R. Durrant, *Energ. Environ. Sci.*, 2013, **6**, 3291-3300.

TOC graphic



This review especially focuses on the advances in the heterogeneous dye-sensitized semiconductors for H_2 production during the past 30 years.